POLITECNICO DI TORINO

Master's Degree in Biomedical Engineering

Master's Degree Thesis

Design and Implementation of a Personalized FES Protocol Toward Dexterous Hand Movements Rehabilitation

Supervisors

Prof. Danilo DEMARCHI

Ph.D. Fabio ROSSI

Ph.D. Andrea MONGARDI

M.Sc. Andrea PRESTIA

Candidate

Elena STEFANEL

March 2025

A nonno, che sono sicura stia dicendo '10 e lode'

Abstract

A significant number of pathologies, such as stroke or spinal cord injury, can lead to severe motor impairments and paralysis, drastically affecting a person's quality of life and autonomy. One of the most widely used rehabilitation techniques is Functional Electrical Stimulation (FES), a treatment that induces muscle contraction by delivering low-energy electrical pulses to the muscles through non-invasive electrodes. This approach, which has also been proven effective in improving muscle strength, alleviating pain, and reducing spasticity, enables patients to restore physiological muscle activity by leveraging the neuroplasticity of the central nervous system.

Despite extensive research over the past decades, applying FES to recover dexterous hand movements remains challenging. While surface electrodes allow for a simple and non-invasive approach, they limit the muscle selectivity of stimulation, which is crucial given the complexity of the muscles involved in hand movements. Moreover, the high inter-subject variability in response to electrical stimulation highlights the need for customized solutions.

In this thesis project, an experimental protocol to assess the feasibility of stimulating dexterous hand gestures and software to efficiently control the electrical stimulator were developed. A first experimental campaign was conducted on thirteen participants to evaluate the possibility of stimulating individual finger movements selectively. Specifically, eight movements were examined: thumb opposition and extension, flexion and extension of the index and middle fingers, and combined flexion and extension of the ring and little fingers. In this phase, particular attention was given to the customization of the stimulation, in terms of electrode placement and stimulation parameters, to enhance both movement effectiveness and subject comfort. Subsequently, in a separate session, a second test was carried out on five of the initial subjects to stimulate dexterous hand gestures. Seven specific hand movements were targeted: One, Two, Three, Four, Hand Open, Hand Close, and Thumb Up. This phase explored the feasibility of eliciting more complex hand movements by combining the finger motions identified in the first phase and allowed to assess the consistency of the stimulation parameters across sessions.

The results demonstrated that the proposed method allows for selective finger stimulation. Indeed, 69.23% of the participants exhibited at least five of the eight targeted motions. Considering also movements that were not entirely isolated or very limited, 76.92% of the participants achieved at least six out of eight motions, with three participants displaying all the targeted finger movements. The extension movements were more frequently elicited and better isolated than flexion movements, during which wrist flexion was often inadvertently elicited. Regarding the thumb, both opposition and extension were observed in all subjects, though extension was frequently limited. The final part of the protocol confirmed that achieving complex gestures by combining finger movements is feasible. However, the quality of the final gesture strongly depends on the precision of the individual finger movements and the use of multiple stimulation channels could result in unwanted wrist motions, resulting in suboptimal movements.

With further optimization, the proposed approach could contribute to a more effective and personalized therapy for hand motion recovery, ultimately improving patients' quality of life.

Acknowledgements

Table of Contents

List of Figures

List of Tables

Acronyms

ACh

  Acetylcholine

ADC

  Analog-to-Digital Converter

ADP

  Adenosine DiPhosphate

AFE

  Analog Front End

AI

  Artificial Intelligence

ANN

  Artificial Neural Network

API

  Application Programming Interface

ATC

  Average Threshold Crossing

ATP

  Adenosine TriPhosphate

BLE

  Bluetooth Low Energy

BMI

  Body Mass Index

CCLM

Continuous Channel List Mode

CFT

Constant Frequency Train

CMC

CarpoMetaCarpal

CMRR

Common-Mode Rejection Ratio

CNS

Central Nervous System

DAC

Digital-to-Analog Converter

DFT

Doublet Frequency Train

DIP

Distal InterPhalangeal

ECG

ElectroCardioGraphy

EMG

ElectroMyoGraphy

FES

Functional Electrical Stimulation

GUI

Graphical User Interface

IE

Index finger Extension

IF

Index finger Flexion

IP

InterPhalangeal

IR-UWB

Impulse-Radio Ultra-Wide Band

JSON

JavaScript Object Notation

LUT

LookUp Table

MCP

MetaCarpoPhalangeal

MCU

MicroController Unit

ME

Middle finger Extension

MF

Middle finger Flexion

MP

Motor Point

MU

Motor Unit

MUAP

Motor Unit Action Potential

MVC

Maximal Voluntary Contraction

NMES

NeuroMuscular Electrical Stimulation

OOP

Object-Oriented Programming

OSCLM

One Shot Channel List Mode

PCB

Printed Circuit Board

PGA

Programmable Gain Amplifier

PIP

Proximal InterPhalangeal

ReLU

Rectified Linear Unit

RLE

Ring and Little finger Extension

RLF

Ring and Little finger Flexion

RMS

Root Mean Square

SCI

Spinal Cord Injury

sEMG

surface ElectroMyoGraphy

SNR

Signal-to-Noise Ratio

SR

Sarcoplasmic Reticulum

SW

Software

TE

Thumb extension

TO

Thumb opposition

VFT

Variable Frequency Train

Chapter 1

Introduction

The human hand is one of the most sophisticated structures of the body, and it serves as an essential tool for countless daily activities. With a total of 21 degrees of freedom [1] and the capability to perform a wide range of motions, from the basic movements to the finest gestures, the human hand possesses a level of dexterity, precision, and versatility unmatched by any other species.

A relevant number of pathologies, such as stroke or Spinal Cord Injury (SCI), can lead to paralysis or severe motor impairments. Given the high incidence of those disorders, affecting millions of people worldwide [2, 3], different rehabilitation techniques have been introduced. Among those, one of the most common is non-invasive Functional Electrical Stimulation (FES), an active rehabilitation treatment that applies short electrical pulses to promote muscle contraction. Although the application of FES has been extensively investigated in the last decades, rehabilitation of fine hand movements still represents a challenge.

Since the loss or impairment of hand function can have an enormous impact on quality of life, significantly limiting a person's autonomy and ability to interact with the surrounding environment, the purpose of this thesis project is to investigate the application of an event-driven system for real-time FES control aimed at dexterous hand movements recovery. The idea is to allow the patient to replicate a movement performed by a therapist using a classifier that, based on the information extracted from the therapist's ElectroMyoGraphic (EMG) signal, can identify the specific gesture performed and determine the appropriate stimulation channels and parameters. Given the complexity of the muscles involved in hand movements and the significant variability between subjects in terms of optimal electrode placement and stimulation parameters, this thesis project primarily focuses on developing a protocol to customize the stimulation of finger movements, which are then combined to generate more complex hand gestures. This personalized approach is crucial to

effectively elicit the intended movements, ensuring successful rehabilitation while also enhancing patient comfort.

This introductory chapter provides an overview of the main topics of the project, beginning with the description of the hand anatomy and the skeletal muscle physiology. A description of the EMG signal and of the Average Threshold Crossing (ATC) technique applied to extract information about muscle activation is provided. Finally, an overview of FES and neural networks fundamentals is given.

1.1 Hand Anatomy

The remarkable functionality of the hand is reflected in its complex anatomy. The human hand is, indeed, composed of 27 bones, 29 joints, and 39 active muscles [4], all finely coordinated to perform a wide range of precise motions.

1.1.1 Wrist

The wrist, the distal joint of the upper limb, is formed by eight carpal bones, as shown in Figure 1.1. The carpal bones are organized in two rows: the proximal row, containing the scaphoid, lunate, triquetrum, and pisiform, and the distal row, comprising the trapezium, trapezoid, capitate, and hamate.
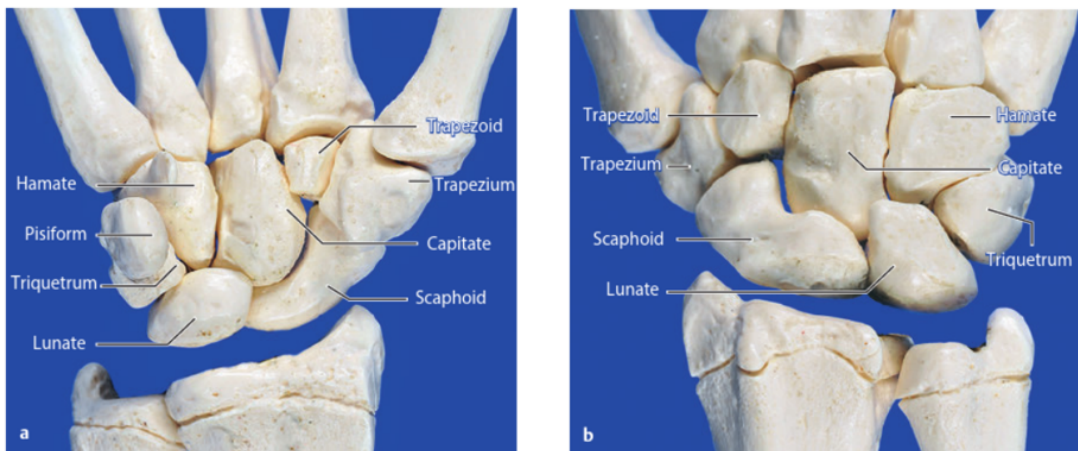
Figure 1.1: Carpal bones. Palmar **(a)** and dorsal **(b)** view of the right hand and palm [4].

Morphologically, the articular complex contains two separate joints:

- The *radio-carpal joint* is an ellipsoidal joint that connects the forearm bones, radius, and ulna to the proximal row of the carpal bones, with the involvement

of the ulnocarpal disc. The carpal aspect features two convexities: a transverse one, related to adduction/abduction movements, and an anteroposterior one, associated with movements of flexion and extension.

- The *mid-carpal joint*, located between the proximal and distal rows of the carpal bones, is composed of a lateral and a medial part. The former consists of two plane surfaces, creating a plane joint, while the medial part involves the capitate and the hamate bones, whose heads are convex in all planes and fit into the concavity of the three proximal carpal bones, forming a condyloid joint. Due to the involvement of stable ligament connections, this joint has limited mobility compared to the radio-carpal joint.

Movements of the Wrist

The wrist movements occur around two axes: the transverse axis and the antero-posterior axis.

Around the former axis, i.e., in the sagittal plane, flexion and extension movements occur. During flexion, the palmar surface of the hand moves towards the anterior aspect of the forearm, while during extension, the posterior surface of the hand moves towards the posterior aspect of the forearm.

About the anteroposterior axis, and therefore in the frontal plane, movements of abduction and adduction take place. During abduction or radial deviation, the radial border of the hand forms an obtuse angle with the lateral border of the forearm. In the adduction movements, or ulnar deviation, the ulnar border of the hand forms an obtuse angle with the medial border of the forearm. A clear representation of the axis and the movements is reported in Figure 1.2.
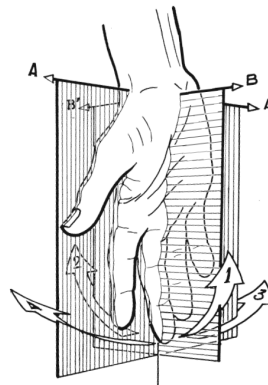
Figure 1.2: Wrist axis and movements. AA' represents the transverse axis, while BB' represents the antero-posterior axis. The numbered arrows indicate, respectively, the movements of flexion, extension, adduction and abduction [5].

The range of motion of these movements is measured from a reference position, which, for flexion and extension, is achieved when the posterior aspect of the hand is in line with the posterior surface of the forearm.

The range of flexion is 85°, as well as the range of extension, as reported in Figure 1.3a. Flexion and extension are maximal when the hand is in a neutral position, i.e., neither abducted nor adducted.

For abduction and adduction, the reference position is achieved when the hand and forearm axes are collinear. The range of abduction does not exceed 15°, while adduction has a range two to three times as great as that of abduction, depending on the anatomical line used for the measurement, as illustrated in Figure 1.3b. Generally, abduction and adduction are minimal when the wrist is fully flexed or extended.

(a)   (b)
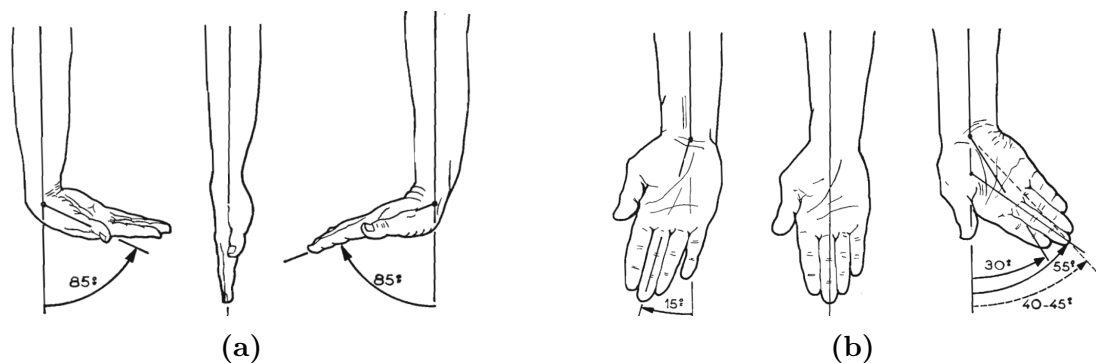
Figure 1.3: Wrist Range of Motions. In (a), from the left to the right, are illustrated flexion, neutral position and extension. In (b), from the left to the right, are represented abduction, neutral position and adduction [5].

Muscles of the Wrist

As shown in Figure 1.4, the muscles responsible for wrist movements are all extrinsic, meaning they are located in the forearm. These muscles are categorized into two groups: flexors and extensors.

- Wrist flexors:

    - *Flexor Carpi Ulnaris*: also involved in ulnar deviation, is the strongest wrist flexor
    - *Flexor Carpi Radialis*: responsible for wrist flexion in synergy with the Flexor Carpi Ulnaris, at the same time stabilizes the carpus
    - *Palmaris Longus*: absent in about 15% of the population [1], produces weak flexion and helps to stabilize the carpus

- Wrist extensors:

  - *Extensor Carpi Ulnaris*: involved in wrist extension and ulnar deviation, it also limits and stabilizes the radial deviation movement

  - *Extensor Carpi Radialis Longus*: responsible for wrist extension, is also involved in radial deviation

  - *Extensor Carpi Radialis Brevis*: along with the Extensor Carpi Radialis Longus, is the most important wrist extensor but, unlike the latter, is not involved in radial deviation
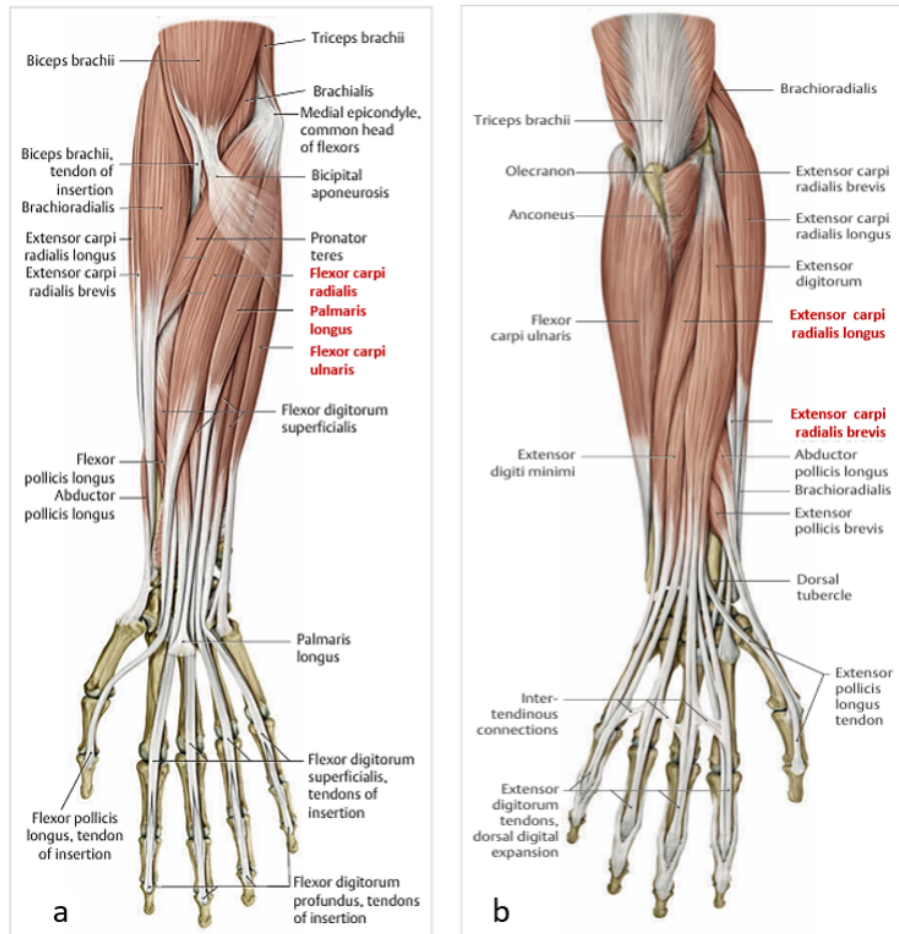
Figure 1.4: Forearm muscles. (a) Palmar view. (b) Dorsal view [4].

1.1.2 Palm

The anterior part of the hand contains five cylindrical bones known as the metacarpal bones, each consisting of a body and two extremities. The base, or carpal extremity, articulates with the carpus and the adjoining metacarpal bones, while the head, or digital extremity, articulates with the proximal phalanx [6], as shown in Figure 1.5.
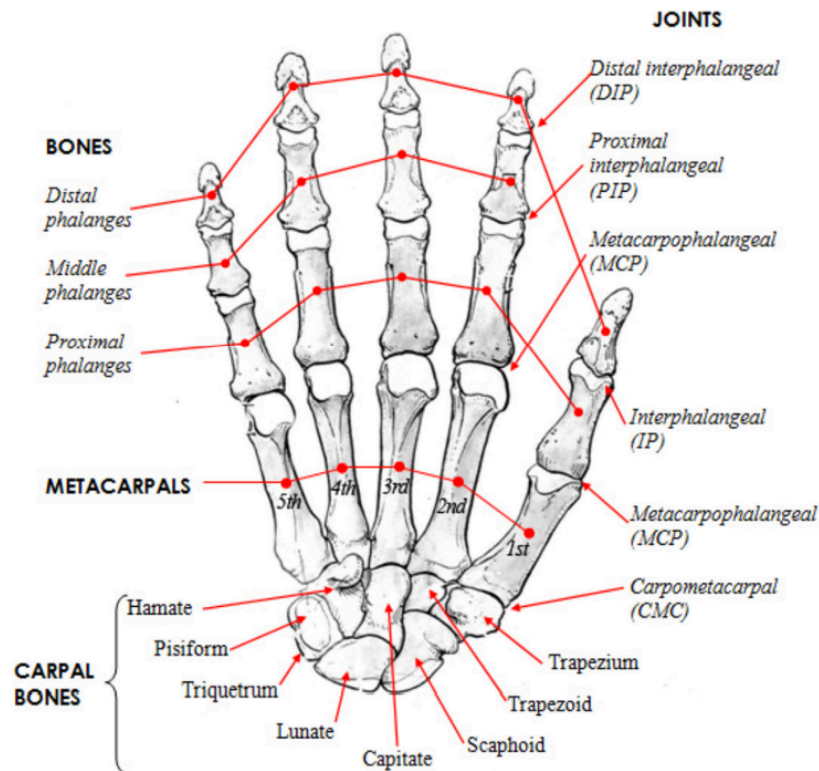
Figure 1.5: Human hand skeletal structure [7].

The metacarpal bones articulate with the distal row of the carpal bones, forming five *CarpoMetaCarpal (CMC) joints*. Due to the unique structure and placement of the first metacarpal bone (the metacarpal bone of the thumb), which is shorter, stouter, and with its volar surface oriented toward the palm, the first CMC joint differs significantly from the other four. In particular, the thumb CMC joint is a saddle joint, while the others are plane joints. This difference results in greater mobility for the first CMC joint, whereas the second and third have the most limited range of motion among the remaining four.

The mobility of the metacarpal joints enables the hand to adapt to the grasping requirements.

1.1.3   Thumb

One key feature that granted humans exceptional dexterity is the development of an opposable thumb. This adaptation marks one of the most significant distinctions between humans and other species, representing a major evolutionary leap.

The complexity of the thumb's role is, indeed, reflected in the brain area responsible for its movement, which is considerably more pronounced than that of the other fingers.

Anatomically, the thumb is composed of two phalanges and has three joints: the *CarpoMetaCarpal joint* (CMC), the *MetaCarpoPhalangeal joint* (MCP), and the *InterPhalangeal joint* (IP).

Thumb CMC joint

The thumb CMC joint, also known as the trapezo-metacarpal joint, is a saddle joint that gives rise to two degrees of freedom:

- Abduction and adduction movements occur around an axis that passes through the base of the first metacarpal and forms a 45° angle relative to the plane of the extended hand. Abduction movements can be further distinguished into palmar abduction and radial abduction.

- Flexion and extension take place around an axis that takes a radiopalmar to ulnodorsal course through the trapezium. The range of motion of flexion and extension is approximatively 25° and 45°, respectively.

In the typical opposition movement, the thumb, with the first metacarpal, is opposed to the other fingers; the inverse motion is called reposition. For these movements, the two degrees of freedom of the CMC joint work in coordination.

Thumb MCP and IP Joints

The metacarpophalangeal joint of the thumb is an ovoid joint with two degrees of freedom, allowing for flexion-extension with a range of motion of 80° and 0°, respectively, and abduction-adduction movements with a range of motion of 12° and 7°. In contrast, the thumb interphalangeal joint is a hinge joint with only one degree of freedom, permitting flexion and extension movements. The range of motion of these movements is 90° and 30°, respectively.

The MCP and IP joints play a crucial role, being involved in all the thumb movements, especially the opposition. This motion, indeed, would be impossible to achieve without a combination of extension, flexion, abduction, and adduction at the MCP joint, working in conjunction with the IP joint.

Figure 1.6 illustrates the wide range of thumb motions.
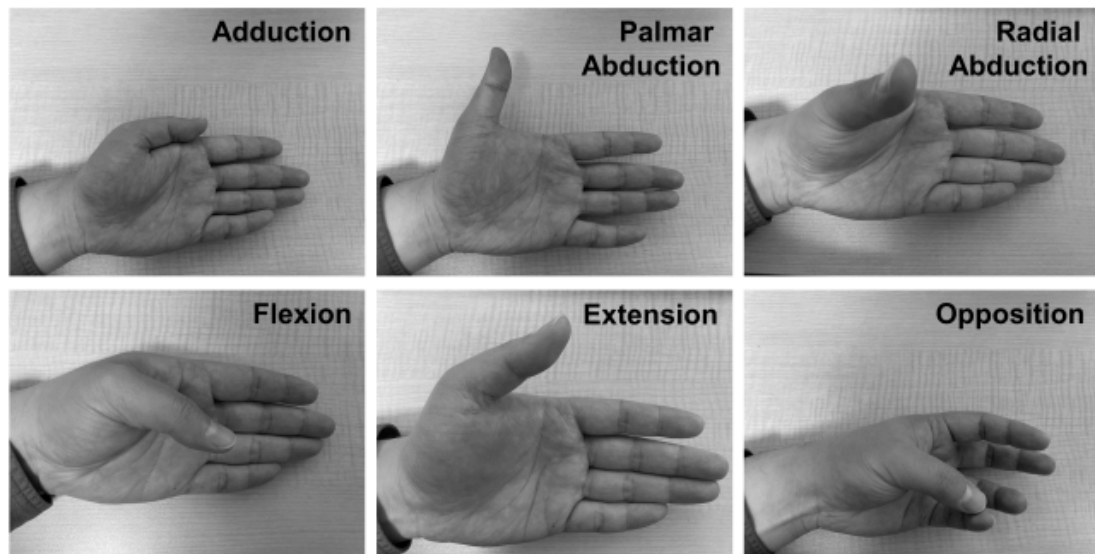
Figure 1.6: Thumb movements [8].

Muscles of the Thumb

The complex motions of the thumb are performed by nine extrinsic and intrinsic muscles.

- Extrinsic muscles:

  - *Abductor Pollicis Longus*: responsible of the thumb abduction and the stabilization the CMC joint, it is also involved in flexion and radial deviation of the wrist

  - *Extensor Pollicis Brevis*: together with the Abductor Pollicis Longus, extends and abducts the thumb

  - *Extensor Pollicis Longus*: also involved in radial deviation and wrist extension, serves as a primary extensor

  - *Flexor Pollicis Longus*: flexor of all thumb joints, supports radial deviation to a limited extent

- Intrinsic muscles:

  - *Flexor Pollicis Brevis*: also involved in opposition, it acts as a flexor, adductor and abductor

- *Abductor Pollicis Brevis*: primarily responsible for the abduction movement

- *Opponens Pollicis*: involved in opposition, as well as adduction and abduction movements

- *Adductor Pollicis*: responsible for adduction and opposition

- *First Dorsal Interosseous*: responsible for abduction

Abductor Pollicis Brevis, Flexor Pollicis Brevis, and Opponens Pollicis, located in the palm at the thumb base, form an intrinsic muscle group known as *Thenar Muscles*.

1.1.4 Fingers

The index, middle, ring, and little finger, in contrast to the thumb, are composed of three phalangeal bones. These bones are divided into proximal, medial, and distal and create three joints for each digit: the *MetaCarpoPhalangeal* (MCP), the *Proximal InterPhalangeal* (PIP) and the *Distal InterPhalangeal* (DIP).

Finger MCP Joints

The MCP joints of the fingers are of the condyloid type with two degrees of freedom. The movements occur about two axes: around the transverse axis, in the sagittal plane, take place flexion and extension, while around the anteroposterior axis, in the frontal plane, adduction and abduction movements occur.

Flexion has a range of about 90°: it falls short of 90° for the index but increases progressively with the other fingers. The extension range of motion is variable and can reach up to 30° or 40°.

Of all the fingers, except the thumb, the index finger has the greatest range of motion in terms of abduction and adduction (side-to-side movement).

Finger IP Joints

The interphalangeal joints of the fingers are hinge joints with one degree of freedom: in the sagittal plane, flexion and extension movements take place.

The range of flexion in the PIP joints is greater than 90°. As in the case of MPC joints, flexions increase in range from the second to the fifth finger to reach a maximum of 135° with the latter.

The range of flexion in the DIP joints is slightly less than 90° and increases from the second to the fifth finger to attain a maximum of 90° with the little finger.

The range of extension is nil at the PIP joints, while it is nil or trivial at the distal IP joints.

Figures 1.7 and 1.8 depict the movements of the finger MCP and IP joints, respectively.
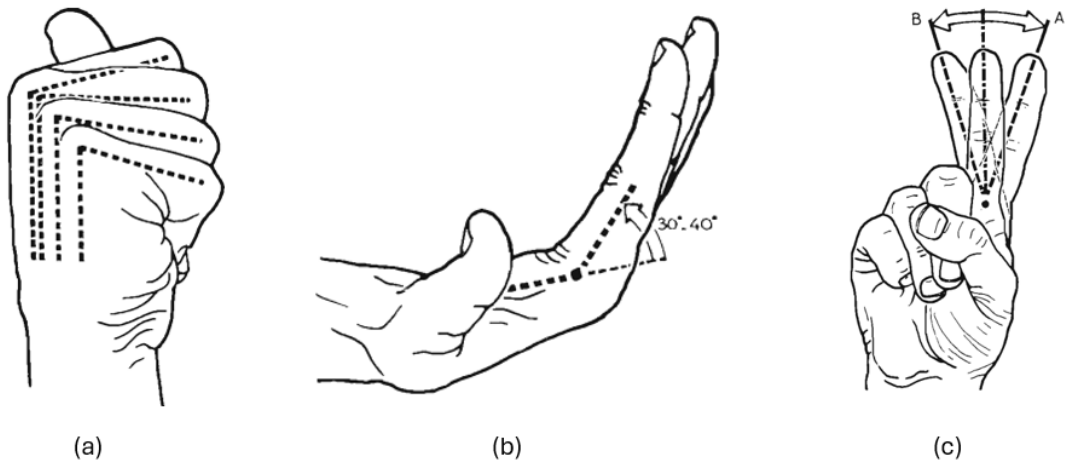
Figure 1.7: Finger MCP joint movements. (a) Flexion. (b) Extension. (c) Index finger adduction/abduction [5].
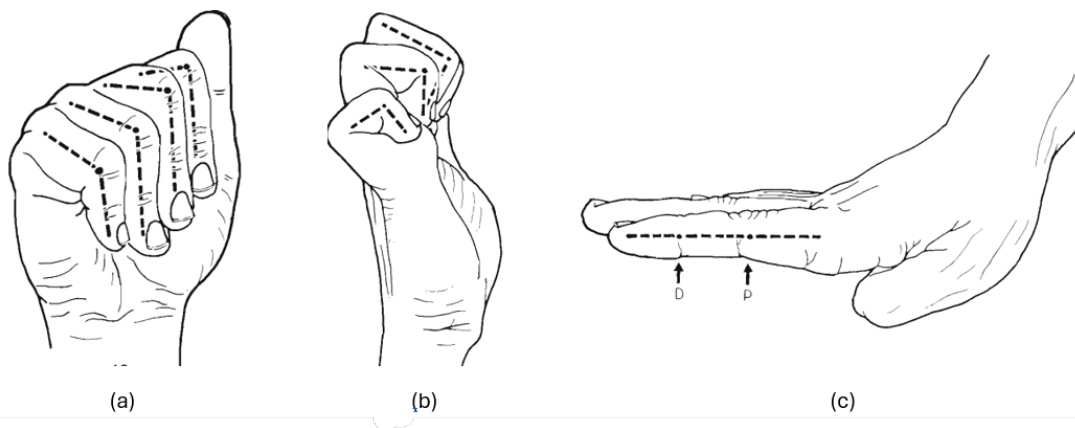
Figure 1.8: Finger IP joint movements. (a) PIP Joint Flexion. (b) DIP Joint Flexion. (c) PIP (P) and DIP (D) Joints Extension [5].

Muscles of the fingers

Fingers are moved by both extrinsic and intrinsic muscles; however, the extrinsic muscles can only exert their influence on the finger joints in interaction with the intrinsic muscles. A representation of the intrinsic muscles is reported in Figure 1.9.

- Extrinsic muscles:

  - *Extensor Digitorum Communis*: responsible for fingers extension and abduction, when the wrist is flexed can extend the fingers in the PIP and DIP joints. It is also involved in the wrist ulnar deviation and extension

  - *Proper Extensor Indicis*: also involved in wrist extension to a limited extent, produces isolated extension of the index finger

  - *Proper Extensor Digiti Minimi*: extends and abducts the little finger and is involved in ulnar deviation and wrist extension

  - *Flexor Digitorum Superficialis*: strong flexor of the MCP and PIP joints, it also provides support for wrist flexion

  - *Flexor Digitorum Profundus*: flexes all three joints of the fingers and it is involved in flexion and ulnar deviation of the wrist

- Intrinsic muscles:

  - *Dorsal and Palmar Interossei*: both contribute to flexion in the MCP joints and extension in the PIP and DIP joints when the MCP joints are in flexion. In addition, dorsal interossei abduct MCP joints while palmar interossei adduct them.

  - *Lumbricals*: lumbricals are four intrinsic muscles that produce slight flexions in the MCP joints and cooperate with the interossei to stabilize these joints and prevent the ulnar deviation of the fingers

  - *Abductor Digiti Minimi*: pure abductor for the little finger

  - *Flexor Digiti Minimi Brevis*: supports the little finger flexion at the MCP joint

  - *Opponens Digiti Minimi*: performs opposition of the little finger in synergy with the opposition of the thumb

Abductor Digiti Minimi, Flexor Digiti Minimi Brevis, and Opponens Digiti Minimi, the three intrinsic muscles responsible for little finger motions, form an intrinsic muscle group known as *Hypothenar Muscles*.

Abductor digiti minimi

Flexor digiti minimi brevis

Opponens pollicis

Abductor pollicis brevis

Flexor pollicis brevis

Adductor pollicis

Lumbricalis muscles

Pisometacarpal ligament

Opponens digiti minimi

Superficial muscles of left hand (palmar)

Deep muscles of left hand: (dorsal view)

Palmar interossei muscles

Dorsal interossei muscles

Interossei muscles of left hand (palmar view)

Interossei muscles of left hand (dorsal view)

Figure 1.9: Intrinsic muscles of the hand [9].

1.2 Skeletal Muscle

The human body presents three types of muscle tissue: skeletal, cardiac, and smooth. The skeletal muscles, comprising approximately 40% of total body weight [10], are often defined as voluntary muscles. Indeed, the main feature of skeletal muscle is its ability to contract and cause movement only in response to stimuli from the motoneurons.

1.2.1 Muscle Architecture

Skeletal muscle cells, commonly known as muscle fibers due to their cylindrical shape, are among the largest cells in the human body, with diameters of up to $100\,\mu$m and lengths reaching up to $30\,$cm [9]. The membrane of muscle fibers is called the *sarcolemma*, while the cytoplasm, containing glycogen and mitochondria, is called *sarcoplasm*. The *myofibrils*, highly organized filaments containing contractile proteins, form the primary intracellular structure. Additionally, muscle fibers contain the *Sarcoplasmic Reticulum* (SR), a specialized smooth endoplasmic reticulum that stores calcium ions (Ca^{2+}), essential for the contraction mechanism. As shown in Figure 1.10, the SR comprises enlarged regions, the *terminal cisternae*, that are closely associated with a network of transverse tubules, known as *T tubules*. These structures allow action potentials to rapidly propagate from the cellular surface to the fiber's interior. The arrangement of a T-tubule with the terminal cisternae on either side is called a *triad*.
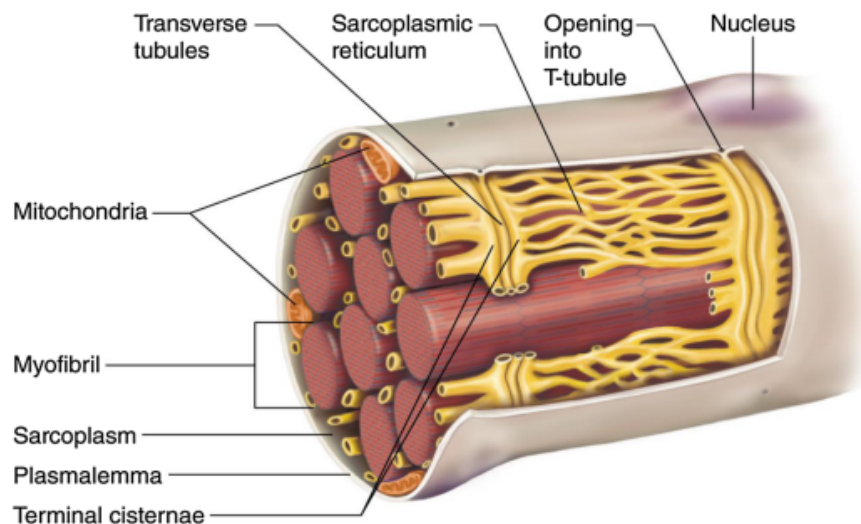
Figure 1.10: The transverse tubules and sarcoplasmic reticulum systems [11].

Each muscle fiber is encased in a thin layer of collagen connective tissue called the *endomysium.* The muscle fibers, aligned along their longitudinal axes, are grouped into parallel bundles called *fascicles*, surrounded by a middle layer of connective tissue known as the *perimysium.* Collagen, elastic fibers, blood vessels, and nerves are between the fascicles. The entire muscle is then wrapped in a sheath of dense, irregular connective tissue called the *epimysium.* Figure 1.11 displays the skeletal muscle architecture.
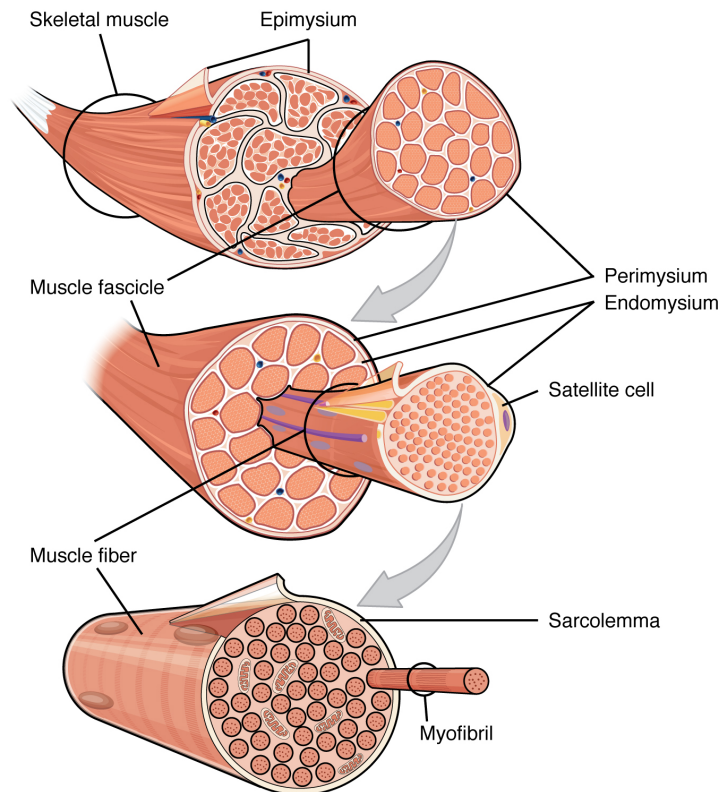
Figure 1.11: Skeletal Muscle Architecture [9].

1.2.2 Myofibrils

A single muscle fiber comprises thousands of myofibrils, which occupy most of the intracellular volume, leaving little space for cytoplasm and organelles. Each myofibril consists of various proteins organized into repeating contractile units called *sarcomeres.* The essential proteins in myofibrils include the motor protein *myosin*, which forms the thick filaments, and *actin*, which forms the thin filaments. Additionally, regulatory proteins, such as troponin and tropomyosin, and accessory proteins (titin and nebulin) are present.

14

Myosin is the muscle's motor, which can generate movement. The different isoforms of this protein differentiate the various types of muscle and characterize the contraction speed. Each myosin molecule consists of two intertwined protein chains forming a long tail with two globular heads. About 250 myosin molecules assemble in skeletal muscle to create a thick filament.

Actin is a globular protein (G-actin) that forms thin filaments of the muscle fiber. Many globular molecules of actin polymerize to form long chains called F-actin. In the skeletal muscle, two polymers of F-actin string together to form the thin filament of the myofibril.

Commonly, thick and thin filaments are connected using *crossbridges*, constituted of the myosin heads bound to the actin filament. Each G-actin has a binding site for the myosin, while each myosin head has two binding sites, one for actin and one for the Adenosine TriPhosphate (ATP). Figure 1.12 illustrates the structures of myosin and actin.

The arrangement of the thick and thin filaments gives rise to alternating light and dark bands repeated along the entire length of the myofibril. Each repetition of the bands constitutes a sarcomere, the functional unit of the skeletal muscle, composed of different elements:

- Z-line or disk: comprise proteins that create an attachment zone for the thin filaments. A sarcomere is constituted of the filaments between two successive Z-lines.

- I-band: light band, composed of thin filaments. A Z-disk crosses halfway through each I band, so the two halves of the band belong to different sarcomeres.

- A-band: dark band which covers the entire length of the thick filament. At the ends, thin and thick filaments overlap, while in the center there are only thick filaments.

- H-zone: central region of the A-bands, is occupied solely by myosin filaments.

- M-line: band constituted by proteins to which the thick filaments attach. Equivalent to the Z-line, it crosses halfway through the A-bands.
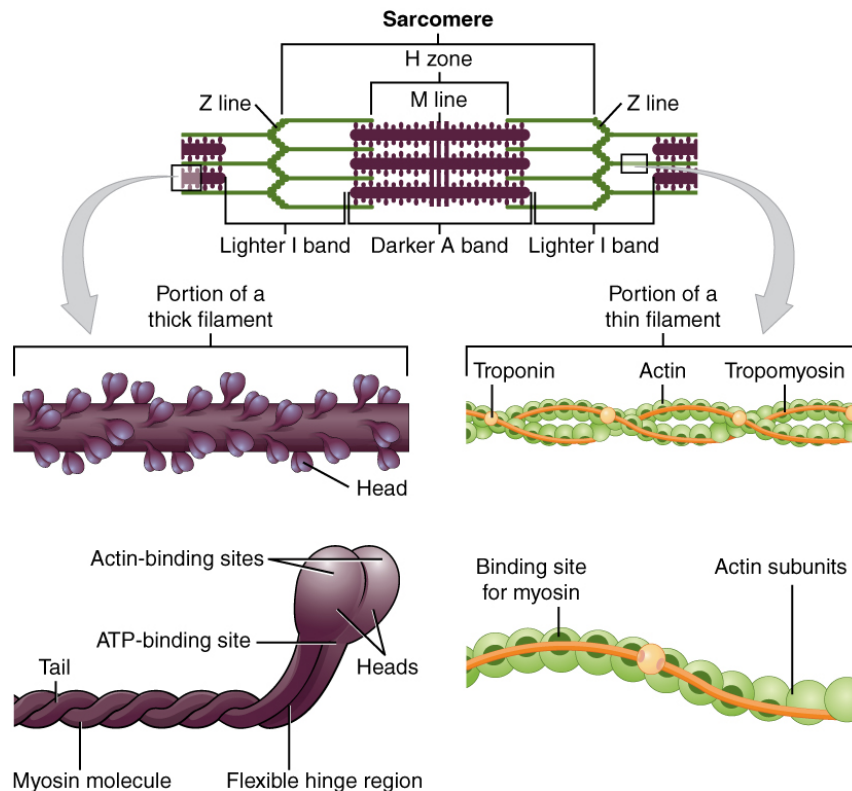
Figure 1.12: Sarcomere organization. The functional unit of the skeletal muscle fiber is the region of a myofibril between two successive Z-lines [9].

1.2.3 Contraction Mechanism

The muscle contraction begins at the neuromuscular junction level, where a motor neuron's terminal meets the muscle fiber. When a neuronal action potential reaches the motor neuron's axon terminal, acetylcholine (ACh) is released. This molecule diffuses across the synaptic cleft and binds to ACh receptors on the sarcolemma on the other side of the synapse. The opening of the ACh-gated channels allows sodium (Na^+) and potassium (K^+) to cross the sarcolemma. However, sodium flow is greater than potassium's outflow due to its electrochemical gradient. The addition of net positive charges to the muscle fiber depolarizes the membrane, triggering a muscle action potential that propagates along the sarcolemma and penetrates deep into the muscle fiber via the T-tubules. The depolarization of these structures stimulates the opening of calcium channels in the sarcoplasmic reticulum, releasing calcium ions into the muscle fiber's cytoplasm.

The process by which an action potential triggers an increase in intracellular calcium concentration is known as *excitation-contraction coupling*.

Muscular contraction is regulated by intracellular calcium, which interacts with troponin, a calcium-binding protein that controls the position of tropomyosin, an elongated polymer along the thin filament. In a resting muscle, tropomyosin is aligned within the groove of the filament, partially blocking the binding sites for myosin so that actin and myosin can weakly interact. When the calcium concentration increases, troponin binds with the calcium, shifting the tropomyosin and fully exposing the myosin-binding sites on actin.

At the molecular level, the events that lead to the skeletal muscle contraction are referred to as the *cross-bridge cycle*, illustrated in Figure 1.13:

1. Starting from the rigor state, meaning that myosin heads and G-actin are firmly bound, ATP binds to the myosin head, reducing its affinity for actin and allowing myosin to detach from the actin filament.

2. ATP is hydrolyzed into ADP (Adenosine DiPhosphate) and inorganic phosphate (Pi). The energy released allows the rotation of the myosin head, forming a 90° angle with the longitudinal axis of the filament. The myosin binds weakly with the actin; however, it has stored enough potential energy to initiate the contraction.

3. The power strokes initiate when calcium binds to troponin and the actin-binding sites are fully exposed: the myosin head releases the inorganic phosphate, increasing its binding strength with actin. The myosin head then rotates toward the M-line of the sarcomere, pulling the actin filament inward and shortening the sarcomere. The angle between the myosin head and the filament is reduced to 45°.

4. At the end of the power stroke, ADP is released, and the myosin head remains tightly bound to actin until a new ATP molecule binds, initiating another contraction cycle.
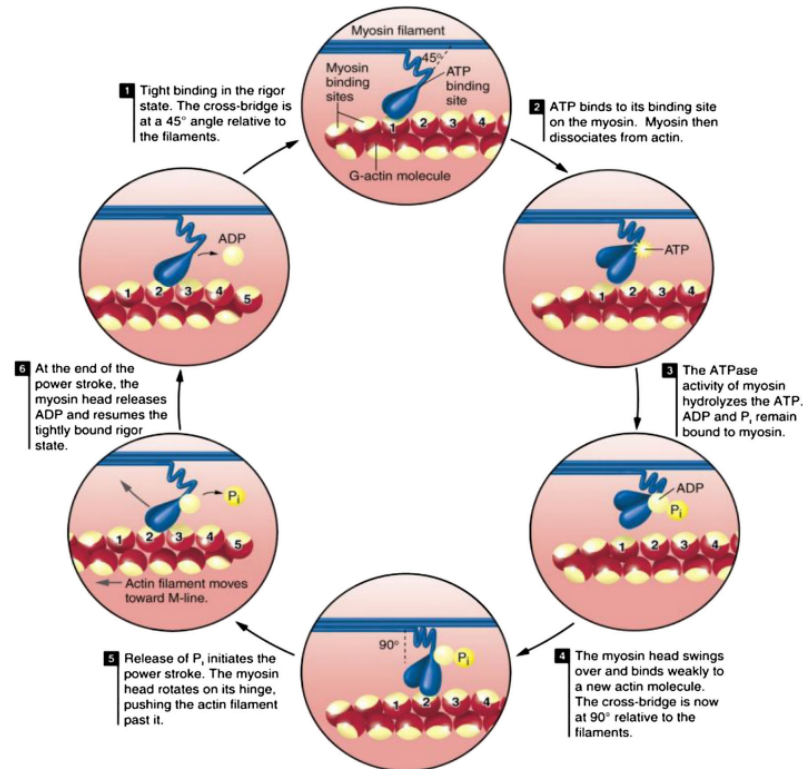
Figure 1.13: Cross-bridge Cycle phases [11].

The cross-bridge cycle is the mechanism underlying the sliding filament theory, proposed by Huxley and Niedergerke in 1954. According to this theory, actin and myosin filaments slide past each other, causing muscle contraction, while the A-band remains constant in length during the contraction process [10].

Types of Muscle Contraction

Muscle contraction generates a force known as muscle tension, able to overcome or resist a load. There are two main types of muscle contraction, *isotonic* and *isometric*:

- During isotonic contractions, the muscle produces a constant force and moves the load by changing its length. Isotonic contractions can be further divided into concentric contractions, where the muscle shortens, and eccentric contractions, where the muscle lengthens.

- During isometric contractions, the muscle generates tension without changing its length: despite the contraction, the load cannot be moved.

1.2.4   Muscle Fiber Classification

Muscle fibers are classified based on the specific myosin isoform expressed within each fiber. Muscle fiber types are not constant throughout life: muscles exhibit plasticity, meaning they can change fiber type in response to different activity levels.

The widely accepted classification of human muscle fiber types includes:

- Slow-twitch fibers (Type 1)

- Fast oxidative glycolytic fibers (Type 2A)

- Fast-twitch glycolytic fibers (Type 2X)

Human muscles contain varying proportions of these three fiber types, depending on the specific muscle and the individual's lifestyle.

Type 2 fibers (fast-twitch) develop tension two to three times faster than Type 1 fibers. That is because fast-twitch fibers break down ATP more rapidly and pump calcium ions into the sarcoplasmic reticulum faster than the Type 1 fibers, leading to faster twitches. Fast-twitch fibers generate contractions lasting only about 7.5 ms, making them ideal for rapid, delicate movements, while slow-twitch fibers produce contractions lasting up to 10 times longer.

Another distinction between fiber types is their ability to resist fatigue. Glycolytic fibers primarily rely on glycolysis to produce ATP; however, the accumulation of hydrogen ions (H^+) from this process leads to acidosis, a condition contributing to fatigue. Consequently, glycolytic fibers fatigue more easily than oxidative fibers (such as Type 1 and Type 2A), which use oxidative phosphorylation for ATP production. A factor that influences the efficiency with which muscle fibers obtain oxygen is the content of myoglobin, a protein similar to hemoglobin that binds oxygen and facilitates its rapid diffusion within the fiber. Oxidative fibers, also defined as red fibers, with their small diameters and high myoglobin content, allow oxygen to diffuse more efficiently toward the mitochondria. In contrast, Type 2X glycolytic fibers, also known as white fibers, with their lower myoglobin content and larger diameter, make oxygen diffusion less efficient, making them easily undergo conditions of limited oxygen availability during repetitive contractions.

The muscle fibers and the somatic motor neuron that innervates them form the *Motor Unit* (MU), the fundamental unit responsible for muscle contraction. The number of fibers within a MU varies: small motor units permit fine motor control, while larger MUs are involved in gross movements.

To achieve variations in muscle tension and contraction duration, the central nervous system (CNS) adjusts both the types of motor units (MUs) recruited and the number of MUs activated. When the stimulus intensity is low, only smaller motor units are engaged. As the stimulus intensity increases and greater tension is required, larger motor units are progressively recruited.

This orderly recruitment of MUs is known as the *size principle* [12].

1.2.5   Muscle Force

A single action potential of a muscle fiber produces an isolated contraction called a *twitch*. A muscle twitch is characterized by three phases, as shown in Figure 1.14. The *latent period* is the interval that elapses between the electrical stimulus and the onset of contraction, during which the action potential is propagated along the sarcolemma and calcium ions are released from the sarcoplasmic reticulum. After the latent period, the *contraction phase* occurs, where the muscle contracts and increases the level of tension. Finally, the last phase is the *relaxation phase*, where tension decreases, and the muscle fibers return to their resting state.
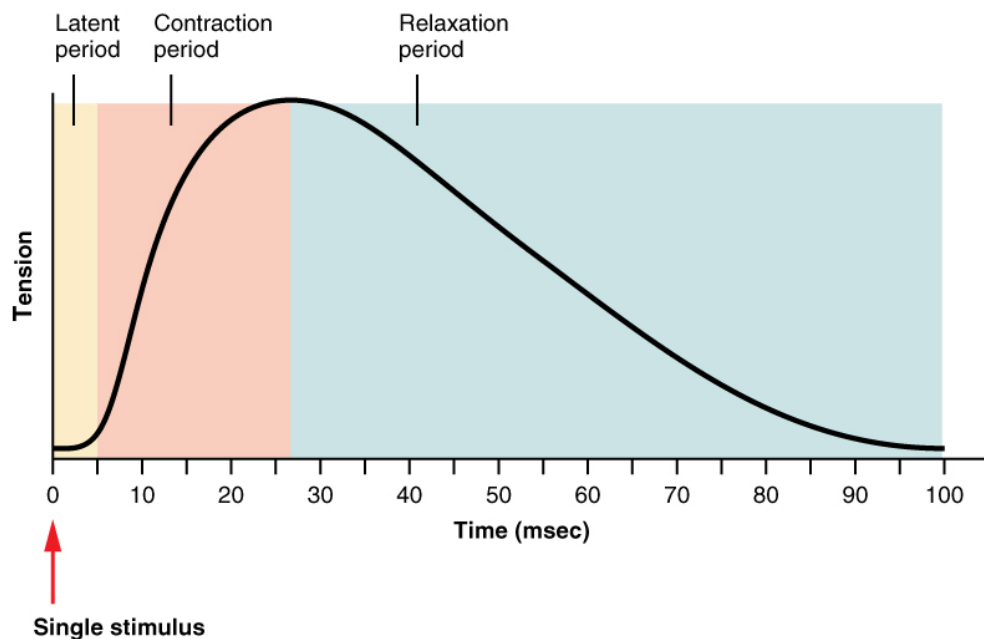
Figure 1.14: Muscle twitch. After the stimulus, a brief latent period preceeds the contraction and relaxation periods [9].

Depending on the muscle type, a single twitch can last up to $100\,\text{ms}$. If long intervals separate the action potentials, the muscle has time to relax completely between the stimuli. On the other hand, if the stimuli are close together, the

20

muscle fiber does not relax completely and develops a greater tension due to the summation of the responses. If the frequency of motor neuron signaling increases, the muscle tension generated rises until it reaches a peak point. During this state, called *incomplete (or unfused) tetanus*, the muscle goes through contraction cycles with short relaxation phases. Further increasing the frequency of the stimuli, the relaxation phases disappear completely, and the muscle generates a constant tension. This condition is called *complete tetanus*. Figure 1.15 highlights the muscle responses triggered by increasing action potential frequencies.
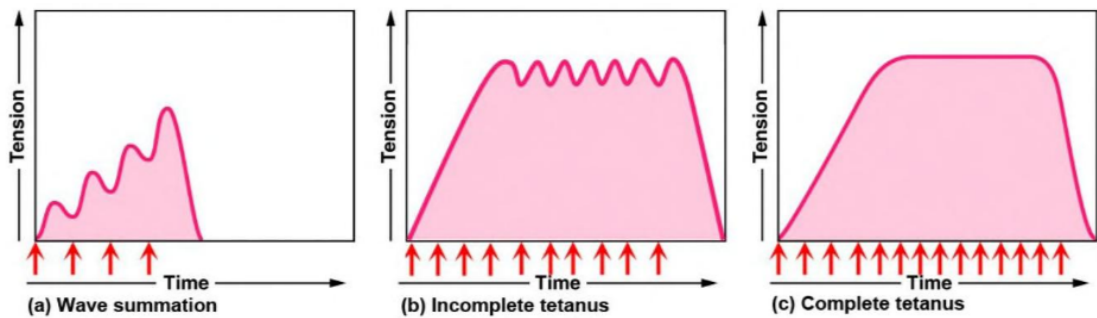
Figure 1.15: Wave Summation and Tetanus. Increasing the frequency of the action potential, the muscle cannot relax completely (incomplete tetanus). When the relaxation phase disappears completely, the condition of complete tetanus is reached [13].

1.3 Electromyography

Electromyography is a technique used to record and investigate the electrical activity produced by the skeletal muscle. The bioelectrical signal recorded, referred to as the *ElectroMyoGraphic (EMG) signal*, is the representation of the neuromuscular activity associated with muscular contractions.

EMG signal acquisition can be performed using either intramuscular or non-invasive detection systems. Intramuscular EMG involves the application of needle or wire electrodes into the muscle. Conversely, the non-invasive modality, called surface ElectroMyoGraphy (sEMG), applies surface electrodes on the skin above the investigated muscle.

Although intramuscular electromyography is characterized by greater selectivity and enables the recording of deep muscles, sEMG is preferred in rehabilitation due to its non-invasive nature and ease of repositioning. Moreover, the intramuscular recordings reflect only the activity of a small number of MUs close to the detection

site. In contrast, surface EMG gives a more global assessment of the muscle properties [14].

1.3.1 sEMG signal characteristics

As discussed in the previous section, a motor unit comprises a motor neuron and the muscle fibers it innervates. It is possible to activate a single motor unit during mild contractions, but as the force increases, more motor units are progressively recruited. Consequently, the recorded signal typically reflects the combined activity of multiple MUs.

As illustrated in Figure 1.16, the summated electrical activity of all muscle fibers activated within a single motor unit is referred to as the Motor Unit Action Potential (MUAP), and the overall EMG signal is the result of the spatiotemporal summation of the MUAPs of all the active motor units, producing what is referred to as an *interference pattern* [15, 16].
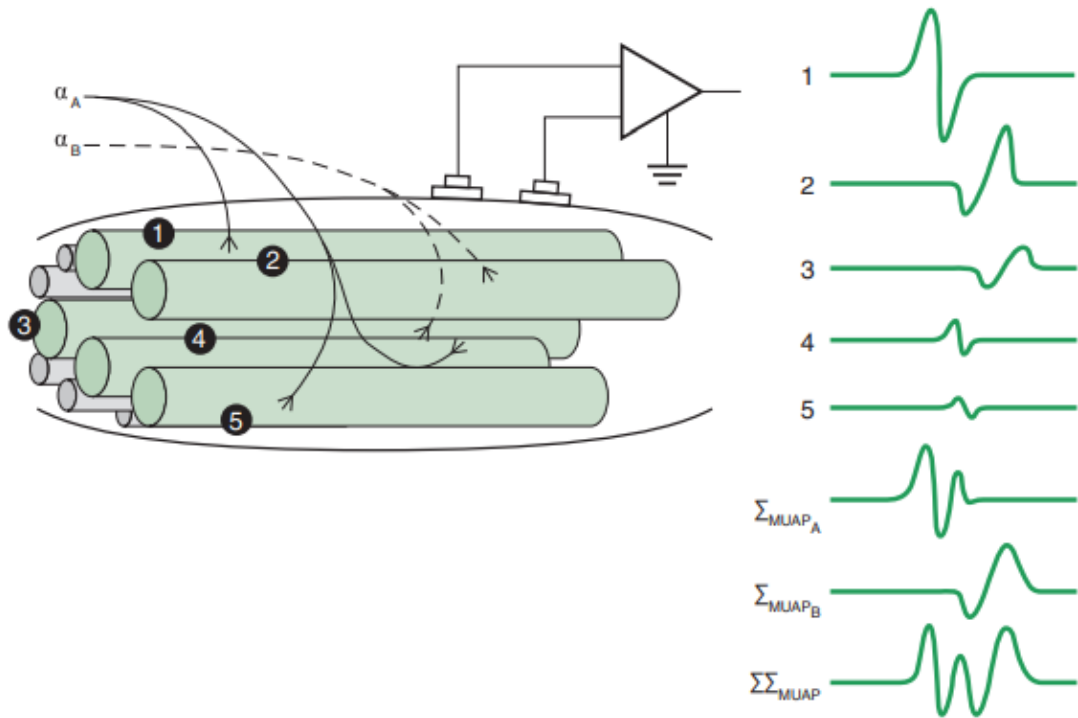
Figure 1.16: sEMG signal. Two motor units, innervating a total of five muscle fibers, are shown. Each motor unit is represented as the algebraic sum of the individual muscle fiber action potential ($\sum_{MUAP}$). The overall signal is the algebraic sum of all active motor units ($\sum \sum_{MUAP}$) [16].

As shown in Figure 1.17, surface electromyography exhibits lower amplitudes

than intramuscular signals, ranging from $0\,\mathrm{mV}$ to $10\,\mathrm{mV}$ peak-to-peak, while its frequency range is between $0\,\mathrm{Hz}$ and $500\,\mathrm{Hz}$. However, the majority of the significant energy is concentrated in the frequency range of $50\,\mathrm{Hz}$ to $150\,\mathrm{Hz}$ [17].
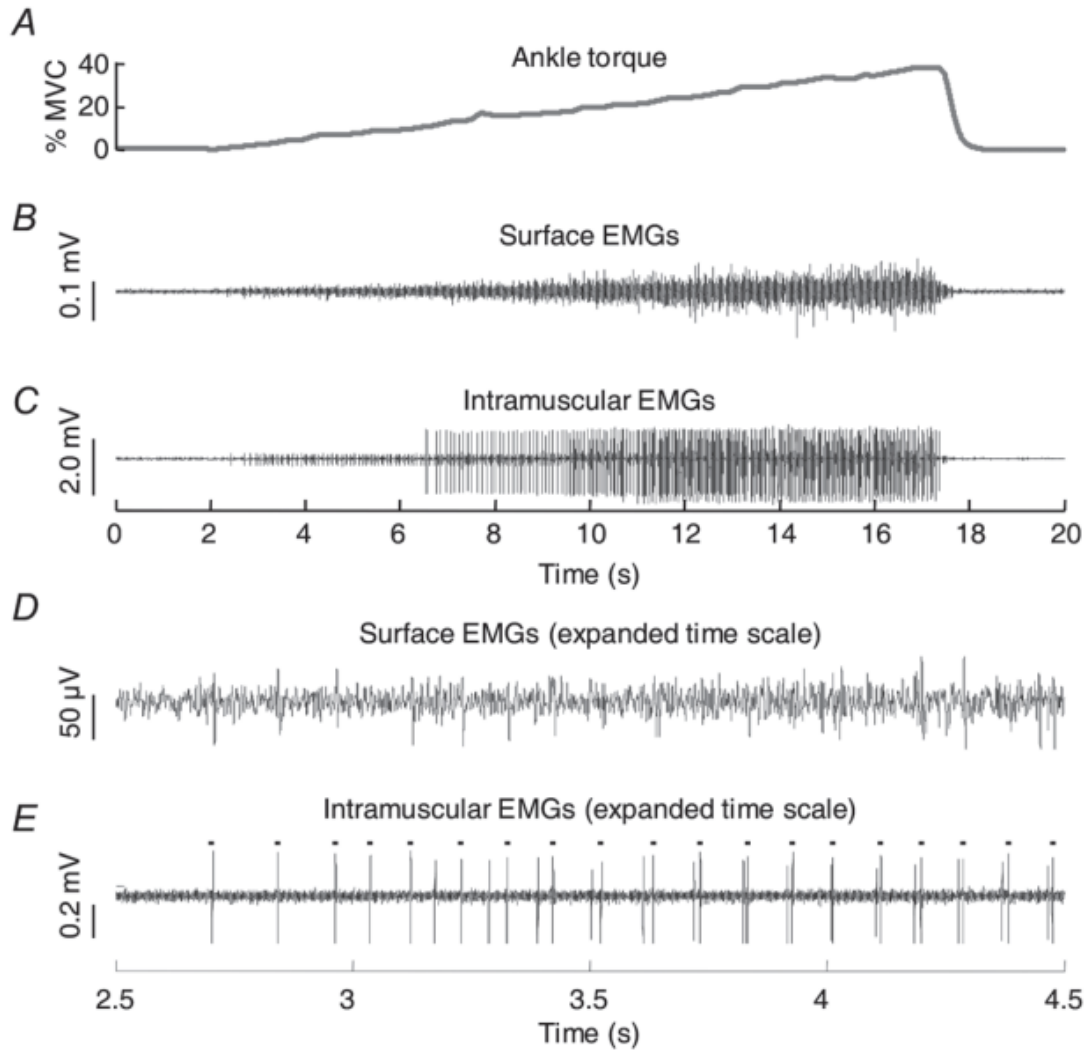
Figure 1.17: Example of electromyographic signals morphology. A) shows the plantar flexion torque during a isometric ramp contraction, from 0 to 40% MVC (Maximum Voluntary Contraction). Surface and intramuscular EMGs recorded from the medial gastrocnemius muscle are shown in B), D) and C), E), respectively. Spikes in the intramuscular EMG correspond to individual MUAPs, while they are not equally evident in the sEMG [12].

1.3.2 Surface electrodes

A biopotential electrode is a transducer that detects ionic currents within body tissues and converts them into electronic currents. There are different types of electrodes, commonly called dry electrodes, made from noble metals (such as gold, silver, or platinum), carbon, or silver/silver chloride. An electrode that includes a layer of conductive gel or a sponge saturated in an electrolyte solution is defined as a wet electrode.

One essential way to categorize sEMG electrodes is based on their electrochemical behavior. *Polarizable* electrodes exhibit a pronounced capacitive behavior due to the double layer of charges created at the metal-electrolyte interface. Gold and platinum electrodes exhibit a quasi-ideal polarizable behavior. These electrodes are unsuitable for sEMG recordings, as any movement between the metal surface and the electrolyte solution or skin can alter the surface potential, generating motion artifacts around 20 Hz that interfere with the signal and lead to data loss.

Conversely, *non-polarizable* electrodes display an ohmic behavior, allowing a free flow of charge across the interface. The Ag-AgCl electrode is the most suitable example of a non-polarizable electrode [18].

When biopotentials are recorded from the skin surface, the interface between the electrode and the skin has to be considered. The electrode-skin interface, comprising the electrolyte-electrode interface and the electrolyte-skin interface, can be modeled by a non-linear RC time, current, and frequency-dependent circuit, as shown in Figure 1.18.

Specifically, the electrolyte-electrode interface is represented by a voltage source representing the half-cell potential at the metal-electrolyte junction, a parallel RC circuit that takes into account the polarizability and the capacitive behavior, and a series resistance that represents the interface effects and the resistance of the electrolyte. A similar model is employed for the electrolyte-skin interface: the half-cell potential is relative to the differences in the ionic concentrations between the gel and the superficial layer of the skin, the RC parallel describes the impedance of the epidermal layer and the dermis and subcutaneous layer resistive behavior is represented by a series resistance [18, 19].

The global impedance of the electrode-skin interface ranges from a few kΩ to a few MΩ, depending on the electrode and the condition of the skin [18]. Careful skin preparation, such as removing oils and body hair, can help minimize impedance [12].
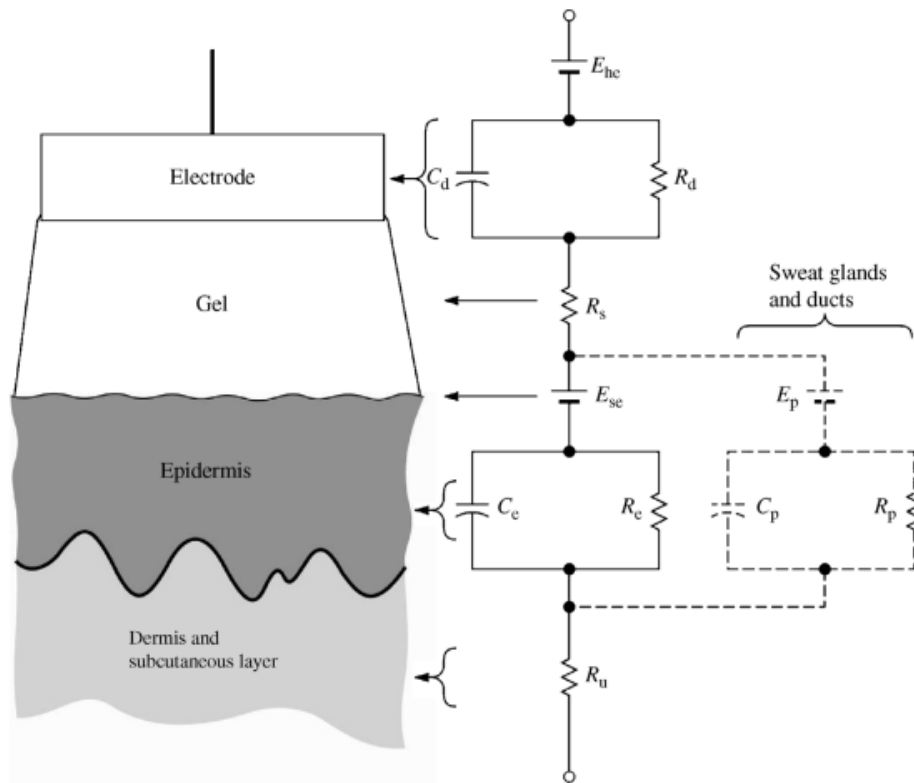
Figure 1.18: The electrode-skin interface model. E_{he} and E_{se} represent the half-cell potentials of the electrolyte-electrode and the electrolyte-skin interfaces, respectively. The parallel R_dC_d and R_eC_e circuits describe the behavior of the two interfaces while the two series resistances (Rs and Ru) represent, respectively, the resistance of the electrolyte and the dermis and subcutaneous layer [19].

Electrode configuration

The electromyographic activity can be recorded using different electrode configurations [12, 16], illustrated in Figure 1.19:

- The monopolar configuration consists of one electrode placed directly over the muscle and a second electrode placed at an electrically neutral site. This configuration allows the recording of all the information on the detection volume. However, it might also record interferences from outside sources.

- The bipolar or single differential configuration is more common. It utilizes two electrodes placed on the skin above the investigated muscle, while a third electrode is placed at an electrically neutral site. This configuration uses a differential amplifier that records the electrical difference between the two

25

monopolar EMG, attenuating any signal common to the two inputs. The degree of this attenuation depends on the Common-Mode Rejection Ratio (CMRR), a characteristic of differential amplifiers.

- The double differential configuration applies three equally spaced electrodes parallel to the direction of the muscle fibers. The resulting signal is the difference between the two single differential signals referred to the signal of the middle electrode. This configuration is characterized by an enhanced CMRR with respect to the single differential modality.
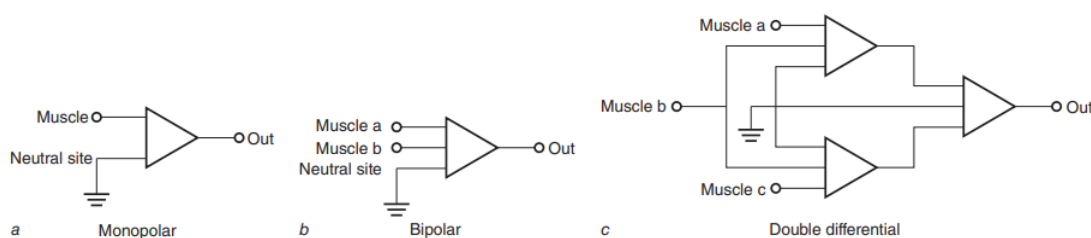
Figure 1.19: EMG electrode configuration. Electromyographic signals can be acquired using either a monopolar (a), bipolar (b) or double differential (c) configuration [16].

1.3.3 Noise sources

An EMG signal contains inevitable noise as it travels through different tissues. The sources of EMG signal contamination can be grouped into three main categories [20]:

- *Baseline noise* (or inherent noise) refers to the signal detected in the absence of muscle contraction. It is composed of thermal noise, introduced by the instrumentation system, and electrochemical noise, originating from the electrode-skin interface.

- *Interference noise* consists of unwanted signals recorded by the equipment, typically manifesting as periodic signals. This interference can come from other physiological signals, such as the electrocardiogram (ECG), crosstalk from other muscles, or ambient noise. The ECG signal appears as a superimposed periodic signal with a frequency spectrum extending up to $100\,\mathrm{Hz}$. Crosstalk, being the EMG signal of other muscles, shares the same frequency spectrum as the EMG. Finally, ambient noise is caused by electromagnetic radiation and is unavoidable. The most problematic source of ambient noise is power line interference, originating from differences in electrode impedance and displacement currents in the cables or the patient's body. This interference

matches the power line frequency and may include harmonics of this frequency (50 Hz in Europe, 60 Hz in North America).

- *Artifacts* are perturbations that cause irregularities in the signal. The most common type is the motion artifact, caused by body movement during recordings. These artifacts typically result from changes in skin-electrode impedance and occur in the frequency range between 0 Hz and 20 Hz. Motion artifacts can also arise from the motion of the cables; in this case, they can be up to 50 Hz. Another potential source of artifacts is the electrical current used for muscle stimulation.

1.4   Average Threshold Crossing

The Average Threshold Crossing (ATC) is an event-driven technique applied to the electromyographic signal that allows for the reduction of power consumption and wireless transmission, as well as the miniaturization of the acquisition channel [21].

At the base of the technique, there are three design paradigms [22]:

- Bio-inspired: the sEMG information is converted in the form of digital pulses to mimic the neural spikes communication

- Event-based: the system acts only in response to an event, limiting the power consumption

- Information synthesis: the feature extraction is performed on the sensor node to lower the transmission payload and to provide higher-level information instead of raw data

The ATC technique applies a static or dynamic threshold to the amplified and filtered sEMG signal. An informative event is generated whenever the signal overcomes the threshold, creating the TC (Threshold Crossing) signal. The TC signal exhibits quasi-digital characteristics, presenting a digital signal shape and carrying analog timing information. The ATC parameter is then computed as the ratio between the number of TC events during an observation window and the length of the window itself (Eq. 1.1). As demonstrated in [23], this parameter is highly correlated to the muscle force generated.

$$ATC = \frac{\#TC_{events}}{T_{window}} \tag{1.1}$$

Typically, the window is set to 130 ms as a compromise between the time resolution needed to capture muscle activation and the ability to distinguish

different levels of muscle force [24]. An overview of the ATC technique is provided in Figure 1.20.
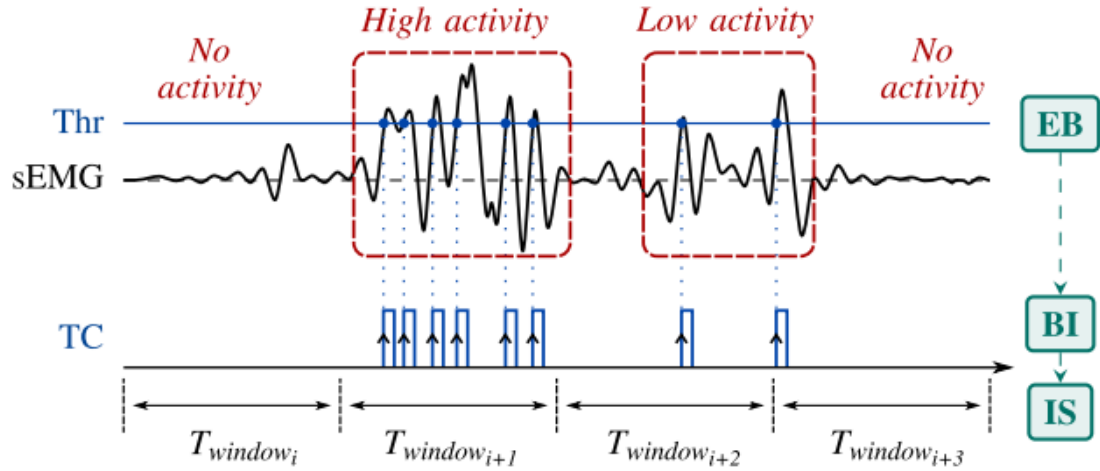
Figure 1.20: ATC technique. Following the Event-Based (EB) paradigm, the TC (Threshold Crossing) points are identified as the events carrying the information of muscle activation. A time distribution of electrical spikes represents them as it happens in the biological communication among neuron cells (Bio-Inspired process). The Information Synthesis (IS) is achieved by applying a time-window approach on the distribution in order to compute the ATC parameter [25].

An advantage of the ATC technique is that the feature extraction process is performed in the hardware domain, limiting the power consumption and the computational effort. In fact, the TC signal can be generated using a voltage comparator on the amplified signal, and thanks to its quasi-digital properties, it can be directly interpreted by digital electronics, eliminating the need for an analog-to-digital converter. Therefore, the event counting can be performed by connecting the TC signal directly to a microcontroller.

A critical point of the ATC technique is the choice of the threshold value, as it should detect as many events as possible while maintaining robustness to environmental noises and artifacts. The ideal value is just above the signal baseline. Indeed, if the threshold value is too high, not all muscle activations are detected, while with low values, spurious noise spikes would be detected erroneously as muscular contractions. Therefore, a threshold calibration has to be performed to find the proper threshold value [25].

1.5 Functional Electrical Stimulation

Electrical stimulation is a technique that delivers short electrical stimuli to the muscles in order to elicit action potentials that result in muscle contractions. One of the primary rehabilitation applications is NeuroMuscular Electrical Stimulation (NMES), which is used on muscles that are still innervated but have impaired voluntary control due to central nervous system (CNS) injuries. When NMES is applied aiming at the realization of purposeful movements, it is called functional electrical stimulation (FES).

During electrical stimulation, the impulses propagate bidirectionally along the motor axon: orthodromically toward the muscle to generate contractions and antidromically toward the CNS. This bidirectional propagation does not occur during voluntary contractions and is hypothesized it plays a role in neuroplasticity, i.e., the CNS's ability to modify its synaptic connectivity to reorganize itself and acquire new motor abilities during electrical stimulation. Moreover, different studies hypothesized that neuroplasticity is also induced by the patient's voluntary intent when performing movements [26].

FES has been shown to enhance muscle control, leading to the restoration of independent movement (carry-over effect) [27]. Beyond motor recovery, FES is also used to restore bladder, bowel, and respiratory functions, preserve bone mass, reduce spasticity, improve muscle strength, reduce edema, decrease atrophy, and alleviate pain [28, 29].

1.5.1 FES technology

Electrical impulses are generated by a stimulator and delivered through individual stimulation channels, each consisting of a pair of electrodes (cathode and anode). Stimulation electrodes are categorized based on their invasiveness into implanted, percutaneous, and transcutaneous. Typically, for FES and NEMS applications, the stimulation occurs through transcutaneous (superficial) electrodes. A primary advantage of this electrode type is their ease of repositioning, which is crucial to adapting the stimulation to the individual's needs. At the same time, a limitation is represented by their reduced effectiveness in stimulating deeper muscles, as this would require higher intensities that could activate unintended muscles.

In NMES, two standard stimulation configurations [30] are used:

- In the *monopolar configuration*, two electrodes of different sizes are applied. The stimulation occurs only near the smaller, active electrode (usually the anode) placed over the target muscle. The larger electrode, known as the

reference (or return) electrode, is positioned over the antagonist muscle or opposite the active electrode. The large dimensions of the reference electrode ensure that, in its proximity, the current density remains below the excitation threshold of the axonal branches, while the current density in the proximity of the active electrode may exceed the excitation level, allowing the stimulation of localized populations of superficial motor units.

- In the *bipolar configuration*, two electrodes of similar size are applied directly over the muscle, confining the current distribution to a smaller area and providing a more uniform current density along the stimulation path.

Crucial aspects of electrical stimulation, both in terms of selectivity and comfort, are the placement and size of the electrodes. Electrode placement determines the current pathway and its relative density across anatomical structures, including peripheral nerve sensory and motor branches. Non-optimal positioning requires higher current levels to activate both motor branches and pain afferent fibers, leading to increased discomfort. The optimal placement is at the muscle's *Motor Point* (MP), i.e., the area on the skin above the muscle where the motor threshold is lowest for a given electrical input. Stimulating over the MP primarily excites the motor branch, reducing the need for high currents and minimizing discomfort. The motor point is defined electrophysiologically and differs from the anatomical motor entry point, where the motor nerve enters the muscle belly [31]. A significant limitation of MP stimulation is represented by the high inter-subject variability in MP location, which makes the research of the optimal electrode placement for each subject time-consuming and challenging.

The electrode size depends on the target muscle. Small electrodes are more precise, allowing for selective activation of small muscles or specific muscle parts, unlike larger electrodes. However, smaller electrodes require more accurate placement, as they are more sensitive to deviations in their positioning [32].

1.5.2 Stimulation parameters

The impulses used during electrical stimulation can be *regulated-current* or *regulated-voltage* [33]. The first type of impulse provides a reproducible applied electric field. On the other hand, voltage-regulated impulses are less reproducible, as the current intensity depends on the electrode impedance. For this reason, although less safe, regulated-current impulses are generally more used. A regulated-current rectangular stimulus delivers a fixed total charge Q per stimulus, calculated as the product of the current intensity and the pulse width: $Q = I * t$.

Electrical impulses can be delivered using various waveforms, with the rectangular shape being the most common. The pulses can be distinguished into monophasic

or biphasic [27]. During biphasic pulses, anode and cathode are alternated, ensuring that all residual charge left in the tissue is removed. In contrast, during monophasic pulses, an electric charge could accumulate between pulses and damage the stimulated tissue. Biphasic pulses can be further classified as symmetric and asymmetric. Symmetric biphasic pulses consist of two identical pulses of opposite polarity, while asymmetric pulses are composed of two opposite polarity pulses of different amplitude or duration. Balanced asymmetric pulses have different pulses, but the total electrical charge delivered to the body is the same as the total charge removed.

The main parameters of the stimulation impulse are frequency, pulse width and pulse amplitude, as shown in Figure 1.21.
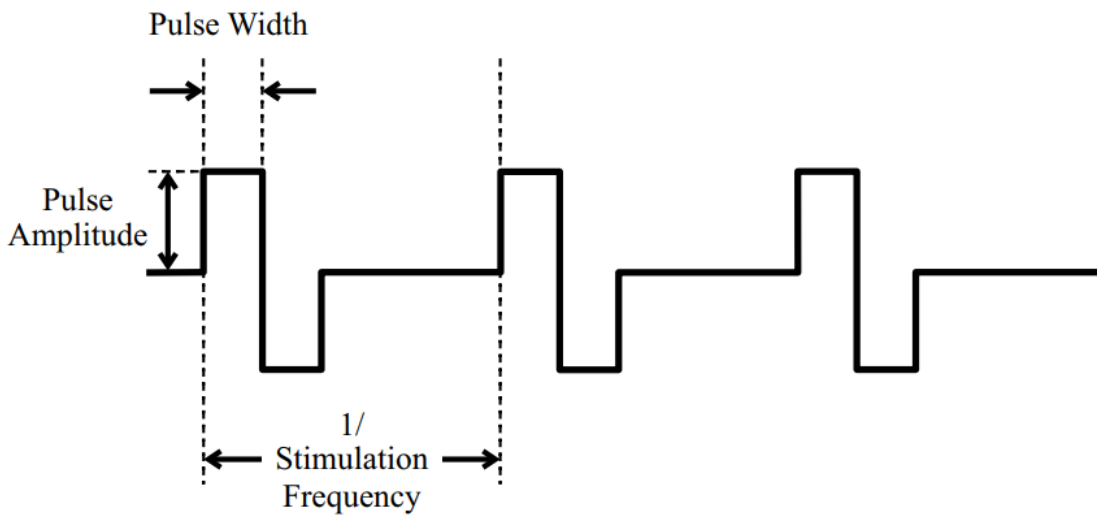
Figure 1.21: Stimulation Parameters. Crucial parameters of the stimulation pulse are frequency, pulse width and amplitude. In the figure, a biphasic symmetric pulse is reported [27].

Frequency

Frequency refers to the rate at which stimulation pulses are delivered. During volitional movements, tetanic contractions are obtained for low frequencies, normally around 6 Hz to 8 Hz. However, in FES applications, typical frequencies range between 20 Hz and 50 Hz. The reason of these higher frequencies lies in the synchronous recruitment performed by the electrical stimulation. Indeed, when applying an electrical impulse, all of the motor units are activated at the same time (synchronous recruitment). For this reason, FES stimulation requires higher frequencies to obtain a tetanic contraction [34].

Pulse Width

Pulse width is the time span of a stimulating pulse. Typical values in FES applications range between 200 µs and 500 µs. Larger pulse durations lead to stronger contractions and can penetrate deeper in the subcutaneous tissue [26].

Current Amplitude

The amplitude is the current intensity by which the stimulation is delivered. Typical FES pulses do not overcome 100 mA. The exact level of intensity depends on the muscle properties, electrode size, and pulse width. High intensities lead to more fatigue and discomfort. In addition, it has been suggested that lower intensities are more effective in inducing central changes in the CNS. Indeed, at high NMES amplitudes, antidromic transmission in motor axons blocks the orthodromic transmission, reducing the extent to which the central recruitment of motor units can contribute to electrically evoked contractions [35].

1.5.3 Stimulation patterns

Different stimulation patterns have been investigated, as shown in Figure 1.22. Commonly, the stimulation is delivered in form of constant frequency train (CFTs), during which the frequency remains constant. However, other patterns have been proposed such as variable frequency trains (VFTs) and doublet frequency trains (DFTs). VFTs are trains that begin with an initial doublet (two closely spaced pulses 5 µs - 10 µs apart) followed by pulses at a constant frequency. DFTs are composed by regularly spaced doublets throughout the train. The idea behind this patterns comes from the *catchlike property* of the muscles, i.e., the force augmentation that occurs when an initial, brief, high-frequency burst of two to four pulses is included at the onset of a subtetanic low-frequency stimulation train. The catchlike property is an inherent property of skeletal muscle cells [36].

Different studies tried to determine which of the mentioned patterns was the optimal one, both in terms of force produced and fatigue onset, and their finding suggests that the ideal pattern depends on the task, the population studied and the muscle investigated [29].
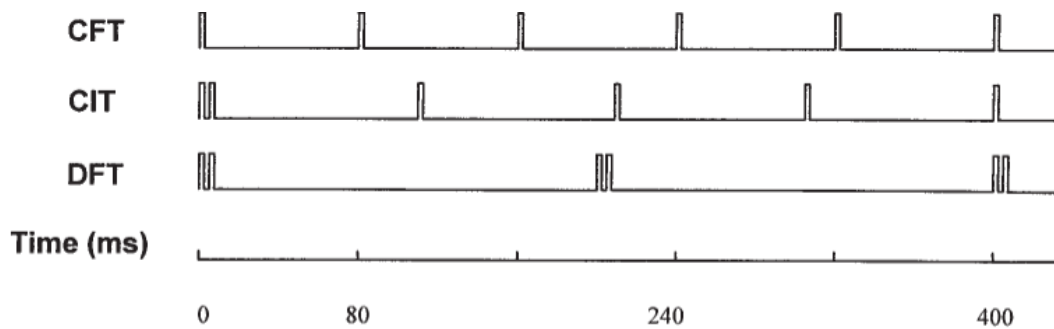
Figure 1.22: Representation of different stimulation patterns. CFTs contain regularly spaced single pulses. Catchlike-inducing trains (CITs), also called variable frequency trains, contain a high-frequency doublet at the start of each train. DFTs consists of regularly spaced doublets [36].

1.5.4 Muscle Fatigue

Excessive neuromuscular fatigue is one of the most significant limitations of functional electrical stimulation. The first cause of augmented fatigue during FES is stimulation frequency. As mentioned before, electrical stimulation synchronously recruits all the motor units instead of rotating through the motor units, as done by the nervous system. For this reason, tetanic contraction is reached with higher frequencies than the physiological ones, leading to an increased rate of fatigue.

Furthermore, FES alters the normal motor unit recruitment order. Usually, the smaller fatigue-resistant motor units are activated first (*Henneman's size principle*), while this order is reversed when stimulating. This non-physiological recruitment order happens because the fast-twitch fibers are innervated by axons with larger diameters than slow-twitch fibers. These axons couple more of the electric field, responding to FES at lower stimulation levels. Since fast-twitch fibers fatigue more quickly, this recruitment order contributes to the fatigue onset.

Due to the impossibility of avoiding the synchronous activation of the motor units and the non-physiological recruitment order, fatigue can be reduced by modulating the stimulation parameters, mainly the frequency, using optimal stimulation patterns. Another possibility is to increase the fatigue resistance of the muscles by intensive muscle training using FES.

33

1.6 Neural Networks

Artificial Intelligence (AI) is a machine's ability to simulate human capabilities such as reasoning, learning, and problem-solving. As illustrated in Figure 1.23, AI is a broad field that comprises machine learning, deep learning, and neural networks.

Machine learning relies on human intervention to identify the key features needed for categorizing different elements. In contrast, deep learning methods require less human intervention, as they can automatically determine the functions necessary to distinguish between different categories of data [37].
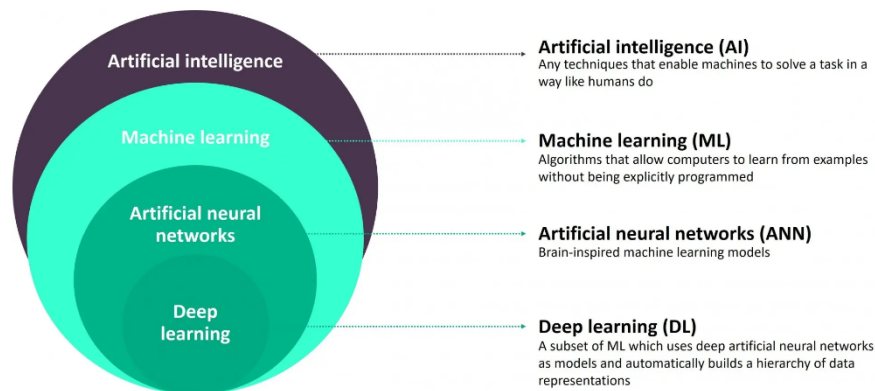
Figure 1.23: Subsets of Artificial Intelligence [38].

In machine learning, the primary goal is to predict an outcome using available data. The prediction task is called a classification problem when this outcome represents different classes. Commonly, the task involves only two possible classes (binary classification), although there may be more than two. When this happens, the task is called multi-class classification [39].

One method for implementing a classifier in machine learning is through Artificial Neural Networks (ANNs). An ANN is a network structure consisting of connected artificial neurons that replicate how the information is processed in the human brain.

1.6.1 Artificial Neuron

In biological neurons, inputs are received through dendrites, processed in the cell body, and transmitted to other neurons via axons. Similarly, in an ANN, each artificial neuron receives inputs from other neurons. Each input has an associated weight, indicating its importance. The neuron computes a linear combination of the inputs with their respective weights and applies an activation function to produce an output. The most elementary activation function is the step function, which

outputs one if the input exceeds the threshold and zero otherwise. This function mimics the behavior of the biological neuron firing when its activation threshold is reached [40]. However, non-linear functions are typically more representative of the biological neuron processes. Non-linearity is provided by activation functions such as Rectified Linear Unit (ReLU), sigmoid, or hyperbolic tangent [41]. Among these, the most common is the ReLU function, which outputs 0 for negative inputs and leaves positive inputs unchanged.

Figure 1.24 provides a visual comparison of biological and artificial neurons.
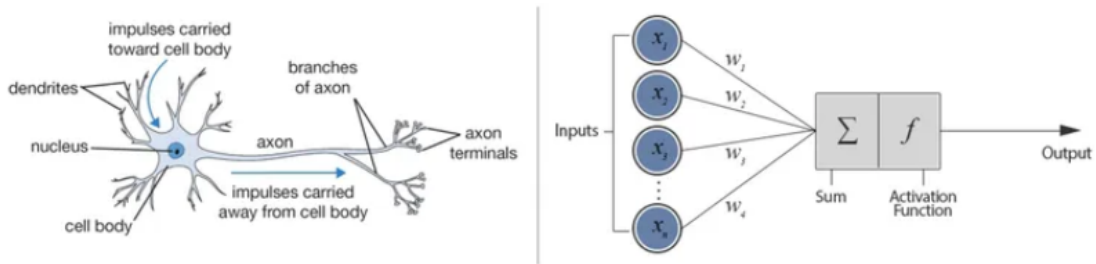
Figure 1.24: Comparison between biological and artificial neurons [40].

1.6.2 Neural Networks Architecture

The Perceptron, the simplest neural network model, was proposed by Rosenblatt in 1958. Also known as a single-layer neural network, the Perceptron aims to classify multiple inputs into two classes (binary classifier). The Perceptron greatly impacted the artificial intelligence field, as it showed that a simple algorithm could adapt its parameters based on input data to improve its performance [40].

More complex neural networks, known as Multilayer Perceptrons, consist of at least three layers, as shown in Figure 1.25:

- The input layer receives the raw data from the external environment.

- The output layer, which transmits the final prediction of the network

- The hidden layers, placed between the input and the output layers, are responsible for the data processing. Increasing the number of hidden layers increases the model's complexity.
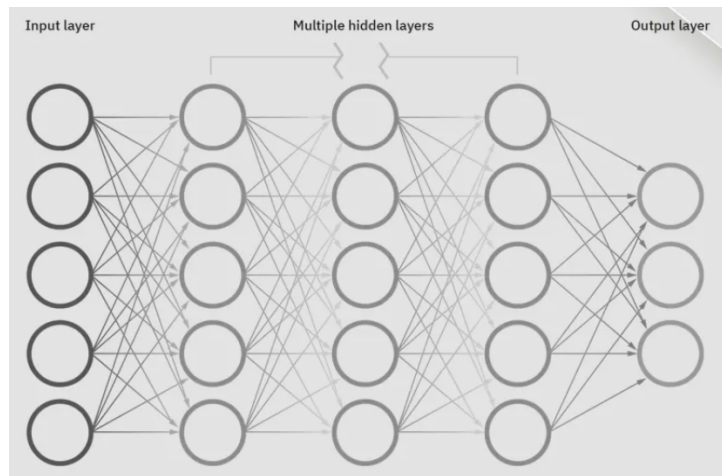
Figure 1.25: Neural Network Structure [41].

Two essential phases of neural network operation are *feedforward* and *backpropagation*. Feedforward is the process during which data is passed through the network layers, and a prediction is generated. On the other hand, backpropagation is the learning algorithm that allows the network to optimize the model's weights. To do this, the backpropagation uses a loss function, i.e., a metric that compares the intended to the actual output. The result is a cost value that the backpropagation uses to modify the weights, using different optimization algorithms such as the stochastic gradient descent. The error decreases for each iteration as the weights are adjusted and the performance improves. This process continues until the network's output closely matches the intended output; at this point, the model is considered fully trained.

Chapter 2

State of Art

The main focus of this project is the customization of stimulation to achieve complex hand gestures, in order to develop a system capable of identifying the movement performed by a therapist and appropriately delivering stimulation to a patient to replicate the gesture.

Due to the system's complexity, multiple aspects must be integrated, including signal acquisition, feature extraction, gesture classification, and stimulation delivery. In particular, acquiring electromyographic signals from the therapist's forearm during movement requires compact and wearable systems to avoid obstructing motion. Once the signals are obtained, the relevant features must be identified and extracted, in order to train a classifier capable of recognizing the gesture performed. Finally, based on the classification, real-time personalized stimulation must be delivered to the patient, enabling gesture replication.

This chapter provides an overview of the state of the art related to these key elements. Specifically, Section 2.1 reviews commercially available wearable sEMG acquisition systems, while Section 2.2 presents the evolution of the ATC technique used to extract information from sEMG signals. Section 2.3 explores studies that implemented artificial neural networks for hand gesture classification. Finally, Sections 2.4 and 2.5 discuss the application of functional electrical stimulation for hand and fine finger movement rehabilitation.

2.1 sEMG acquisition systems

Electromyographic signals represent a fundamental resource in diagnosis and as control signals in rehabilitation. As discussed in Section 1.3, sEMG signals typically have amplitudes within the $\pm 10\,\mathrm{mV}$ range and are prone to contamination from various noise sources. Therefore, before being transmitted to a computer, the signal

detected by surface electrodes must undergo amplification and filtering. Typically, the signal is amplified by a factor of 1000 V/V and then passed through two analog filters: a high-pass filter that removes movement artifacts and a low-pass filter to limit the useful bandwidth. To be processed by a computer, the analog signal is then sampled and digitalized by an Analog-to-Digital Converter (ADC). The resulting signal is transmitted to a computer using wired or wireless connections. The presence of cables could represent an obstacle to the patient's movement, besides being a potential source of noise. For these reasons, wireless wearable systems represent an ideal solution. This technology's main constraints are miniaturization, since signal acquisition and conditioning have to be performed on-board, and power consumption, as a power supply is needed [42].

Several wearable EMG acquisition systems are commercially available, as shown in Figure 2.1.

The Pico EMG of Cometa Systems, Inc. [43], with a dimension of $41.0\,\mathrm{mm}$ x $15.5\,\mathrm{mm}$ x $11.3\,\mathrm{mm}$ and a total weight of $7\,\mathrm{g}$, is the smallest EMG sensor on the market. This device, shown in Figure 2.1a, includes a memory on board for synchronous data logging and an integrated accelerometer with a battery life of up to ten hours. In addition, integrated clip connections allow for easy attachment of pre-gelled electrodes. The Pico EMG can achieve a transmission range of up to $30\,\mathrm{m}$ indoors. Another product by Cometa Systems, Inc., the MiniWave device, is slightly larger than the Pico EMG but offers more flexible placement and a transmission range of up to $40\,\mathrm{m}$. However, its battery life is limited to eight hours. The MiniWave device is depicted in Figure 2.1b.

The Trigno Avanti Wireless Biofeedback System [44], developed by Delsys and displayed in Figure 2.1c, is a device that records the EMG signal, along with complementary biofeedback data. The device is $27\,\mathrm{mm}$ x $37\,\mathrm{mm}$ x $13\,\mathrm{mm}$ and is equipped with a rechargeable lithium-polymer battery with an expected duration between four to eigth hours. This device uses Bluetooth Low Energy (BLE) 4.2 to communicate with host devices and features a LED indicator able to convey different status, such as charging, power on, and data collection. With an inter-electrode distance of $10\,\mathrm{mm}$, Trigno Systems are supplied with adhesive interfaces to facilitate sensor attachment and promote a high-quality electrical connection between the sensor bars and the skin.

The DataLITE Wireless EMG Sensor of Biometrics Ltd [45], in Figure 2.1d, measures $42\,\mathrm{mm}$ x $24\,\mathrm{mm}$ x $14\,\mathrm{mm}$ and weighs $17\,\mathrm{g}$. Its high input impedance greater than $100\,\mathrm{M\Omega}$ allows for signal recording with minimal skin preparation, making it convenient for users. Data transmission is handled via the DataLITE PIONEER dongle, ensuring reliable communication over distances of up to $30\,\mathrm{m}$.

The sensor is powered by a rechargeable Li-Ion polymer battery, offering up to eight hours of continuous operation.

(a) Cometa Pico EMG [43].

(b) Cometa MiniWave [43].

(c) Delsys Trigno Avanti [44].

(d) Biometrics Ltd DataLITE [45].

Figure 2.1: State of art wearable sEMG acquisition systems.

2.2   ATC technique evolution

As mentioned above, miniaturization and power consumption represent the main challenges related to wearable sEMG acquisition. The ATC technique, discussed in Section 1.4, represents an ideal solution to these problems. Indeed, the power consumption associated with the digitalization of the analog sEMG signal is reduced, as the TC signal generated has a quasi-digital shape that the electronics can directly interpret without needing an Analog-to-Digital Converter. Moreover, miniaturization often leads to a simplification of the circuitry and, therefore, a loss in terms of signal quality. However, the generation of the TC signal can be achieved by using a simple voltage comparator on the sEMG signal, reducing the need for complex circuitry [25].

The ATC technique was first proposed by Crepaldi *et al.* [23] to extract only valuable information from the sEMG signal, aiming at reducing the amount of data to be processed. The proposed system was based on the Impulse-Radio Ultra-Wide Band (IR-UWB) transmission. This wireless technology is based on short pulses (in the order of nanoseconds) that allow ultra-low power transmission. The idea was to use an event-driven transmission, where the pulse is generated only when the signal overcomes a given threshold. Once the receiver received the data, the ATC count was performed by a laptop. Besides demonstrating the advantages of the ATC technique in terms of power consumption reduction, this work also showed the high correlation between the ATC parameter and the force generated during the contraction, obtaining an average correlation equal to 0.95±0.02.

In a subsequent study [46], the previous work was extended to a multi-channel system using an address-event representation protocol for data transmission. In this study, the ATC approach was tested in three different noise conditions, artificially modifying the data: 1) adding noise at different Signal-to-Noise Ratios (SNR), 2) distorting the signal to account for non-linear, saturating amplifiers, and 3) randomly losing ATC events. These tests demonstrated the robustness of the ATC technique, showing that it can tolerate $5\,\mathrm{dB}$-$6\,\mathrm{dB}$ of signal-to-noise ratios and up to 70% event loss.

In [47], Sapienza *et al.* designed a low-complexity, compact prototype featuring a $23\,\mathrm{mm}$ x $34\,\mathrm{mm}$ wearable printed circuit board (PCB) capable of acquiring differential sEMG signals, generating TC events, and triggering IR-UWB transmission. In-vivo experiments demonstrated that the increase in the force applied during isometric and isotonic contractions was reflected in an increase in the TC events. Thanks to this correlation between ATC and muscle activity, the prototype achieved a 0% error rate in distinguishing between a rest state and two different levels of force.

In [48], Guzman *et al.* developed an ATC acquisition system using Commercial Off-the-Shelf components, proving that the benefits of the ATC approach are not exclusively due to customized microelectronics. This work also explored employing a static threshold rather than a dynamic one to reduce system complexity.

In [21], for the first time, Rossi *et al.* implemented the ATC technique as a control mechanism for functional electrical stimulation (FES). Based on Guzman *et al.*'s design, the acquisition board included a microcontroller unit, four detachable analog front-end channels, and a BLE module for data transmission to a computer. In a follow-up paper [24], Rossi et al. introduced a new version of the sEMG(ATC)-controlled FES system, replacing the previous software architecture with an embedded version running on a Raspberry Pi to address performance

limitations associated with general-purpose computers.

In [25], Rossi *et al.* developed a wearable system, designed to overcome key challenges such as robustness, miniaturization, versatility, and power efficiency. The resulting prototype, measuring $57.8\,\text{mm} \times 25.2\,\text{mm} \times 22.1\,\text{mm}$, consists of an Analog Front-End (AFE) responsible for sEMG signal detection and processing, along with a digital component dedicated to ATC evaluation and wireless communication. This device supports both sEMG and ATC transmission and successfully addresses major issues related to wearable acquisition systems. It achieves a consistent signal-to-noise ratio exceeding $15\,\text{dB}$ and offers an average operating time of $80\,\text{h}$ for high-resolution sEMG sampling, which increases to $230\,\text{h}$ when used exclusively for ATC acquisition.

2.3 sEMG-based hand motion classification using ANNs

Different works have previously implemented Artificial Neural Networks (ANNs) to recognize different hand motions starting from the electromyographic signals.

In [49], Tenore et al. demonstrated that twelve distinct finger movements from a single subject can be decoded with an accuracy exceeding 98%. Precisely, 32 surface electrodes were placed on the forearm of a healthy subject to record electromyographic signals during individual finger movements. These movements included the flexion and extension of each finger individually and combined movements of the middle, ring, and little fingers. The recorded signals were processed to extract four relevant time-domain features, which were then fed into a feedforward multilayer artificial neural network. The network employed two different activation functions for the hidden and the output layers and a scaled conjugate gradient algorithm was used as the learning method. The network assigned a probability for each movement, outputting the movement with the highest value.

In another study [50], an artificial neural network was employed to classify EMG signals into four movements (left, right, up, down), achieving an average success rate of 88.4%. Electromyographic signals were recorded from three able-bodied subjects, with electrodes placed on the brachioradialis and flexor carpi ulnaris muscles and a reference electrode on the wrist. Seven features were extracted from the sEMG signals and fed into the neural network. The ANN used was a multilayer architecture with nonlinear differentiable activation functions. The backpropagation was implemented using the Widrow-Hoff learning rule, also known as the Least Mean Squares algorithm.

In a more recent study [51], Briouza *et al.* implemented an automatic neural network where the number of layers and the parameters are selected with a trial-and-error approach. The basic structure of the network comprises five dense layers, with only the first layer always present in the architecture. After each dense layer, the algorithm optionally includes a dropout layer. The parameters that change in the architecture are the number of units for each layer, the activation function, and the learning rate. This ANN was applied to the Ninapro DB2 dataset, which contains preprocessed data from 40 subjects performing 49 different hand motions. These motions are divided into three types of exercise: Exercise B includes 17 basic movements of the finger and the wrist, Exercise C comprises 23 gestures that use external objects (such as grasping), and Exercise D contains nine motions with different force patterns. When tested on ten subjects, the ANN proposed showed an accuracy of 81.18% for exercise of type B, 77.76% for exercise of type C, and 91.70% for exercise of type D.

In [52], Lee *et al.* developed four classifiers based on different machine learning methods, one of which was an ANN-based classifier. These classifiers were tested on ten healthy subjects performing various hand gestures. EMG signals were recorded using surface electrodes placed on the flexor carpi radialis, flexor carpi ulnaris, and brachioradialis muscles. Six time-domain features were extracted from the signals to distinguish between ten different motions (rock, scissors, paper, one, three, four, good, okay, finger gun, and rest). The study achieved a mean classification accuracy of 94% using the ANN-based classifier, which also demonstrated the lowest inter-subject variance in accuracy.

2.4   FES for hand rehabilitation

The significance of hand movements in daily life has driven extensive research on Functional Electrical Stimulation (FES) for hand rehabilitation in individuals with motor impairments. Much of this research focuses on grasping, a fundamental action in everyday tasks. Several devices and systems have been developed to aid in rehabilitating grasping movements using FES.

The Bionic Glove [53] is a fingerless glove that allows hand opening and grasping through wrist movements. The glove has conductive areas that align with self-adhesive electrodes placed on the skin beforehand. A displacement transducer senses wrist movements, triggering stimulation through three channels targeting finger and thumb flexors and extensors. Wrist flexion initiates hand opening, while wrist extension triggers hand grasping, as shown in Figure 2.2.
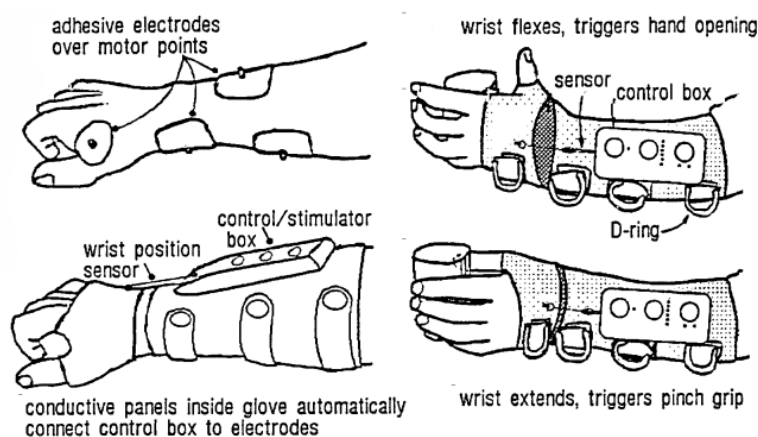
Figure 2.2: Bionic Glove. Self-adhesive electrodes are positioned over the target muscles for stimulation. The glove is then worn, making electrical contact with the electrodes. The images on the right show the neuroprosthesis functionality: voluntary wrist flexion activates stimulation to open the hand, while wrist extension triggers stimulation to initiate a grasping motion [53].

The Handmaster by NESS [54], depicted in Figure 2.3, consists of a splint with five integrated surface electrodes and a control unit. Within the splint, the electrodes are positioned to target the Flexor Digitorum Superficialis, Extensor Pollicis Brevis, Flexor Pollicis Longus, Extensor Digitorum Communis, and the thenar muscles. The Handmaster offers two exercise modes (cyclic hand opening/relaxation and cyclic hand open/grasp) and three functional modes (hand open, grasp, and key-grip), controlled by a simple push-button interface.

Figure 2.3: Handmaster system. The Handmaster consists of an external control unit connected via cable to a splint with integrated surface electrodes [55].

The Belgrade Grasping-Reaching System [56] expands on grasping by incorporating a reaching function. This neuroprosthesis includes three channels for grasping and a fourth for stimulating the triceps brachii to extend the elbow. The grasping function involves prehension, relaxation to get in contact with the object, and hand closing, while the release function includes hand opening and resting. The reaching component uses a goniometer to measure shoulder velocity and generate a synergistic elbow motion by stimulating the triceps brachii.

Recent advancements focus on controlling FES using electromyographic signals. For instance, Zhou *et al.* [57] developed a sEMG bias-driven FES system for upper limb rehabilitation. This system computes the Root Mean Square (RMS) value of EMG signals for each channel, using the difference between affected and unaffected sides to adjust FES intensity in real-time. This type of control provides the muscle of the affected side only the needed assistance: the lower the EMG signal recorded in the affected side, the higher the FES intensity of the stimulation delivered.

In [58], Camilo *et al.* developed an FES controller using contralateral sEMG, enabling continuous control of hand opening and power grasp movements. The controller uses an envelope of the EMG signal derived from the RMS value and a median filter. Electrical stimulation is delivered via the RehaStim 2 stimulator, and the system incorporates a movement classification algorithm along with proportional mapping of sEMG signals to FES amplitude. However, the performance of the implemented algorithm posed a challenge in this study.

Similarly, Chen *et al.* [59] created a portable FES system integrated with an EMG-based real-time motor intention classification system. Four electrode pairs on the unaffected side record sEMG signals, which are processed to extract time-domain features. A Support Vector Machine classifier identifies six distinct hand motions, and stimulation is delivered through four FES channels. The system switches between electrode pairs to classify and stimulate multiple motions, though this limits simultaneous movement execution.

2.5   FES for Individual Finger Control

Recent studies have increasingly focused on finer hand movements, particularly individual finger control.

In a 2018 study [60], Bao *et al.* investigated the feasibility of stimulating single-digit movements and identified several challenges and limitations. Specifically,

Bao *et al.* designed a customized grid with over 400 points distributed across the participants' forearms and tried to determine the optimal stimulation points for each subject. In his setup, one electrode (4 cm × 4 cm) was fixed on the elbow olecranon, while the second electrode (⌀2.2 cm) was moved across the grid to identify the most effective stimulation points. In order to do this, each point was tested using fixed stimulation parameters (8 mA, 50 Hz, 400 µs) to determine the corresponding finger flexion and extension movements. The results revealed significant variability in the optimal stimulation points among subjects since the same grid points sometimes produced different movements across individuals. Moreover, not all finger movements could be consistently elicited in every participant.

The study also aimed to determine the activation thresholds for different stimulation points and to assess whether the posture of the forearm influenced them. Bao found that current intensity requirements varied between subjects and depending on the specific stimulation point. However, slight variations in electrode positioning or forearm posture had minimal impact on the activation thresholds. Figure 2.4 illustrates the variability between different subjects in terms of stimulation points and parameters, in line with the findings reported in the study.
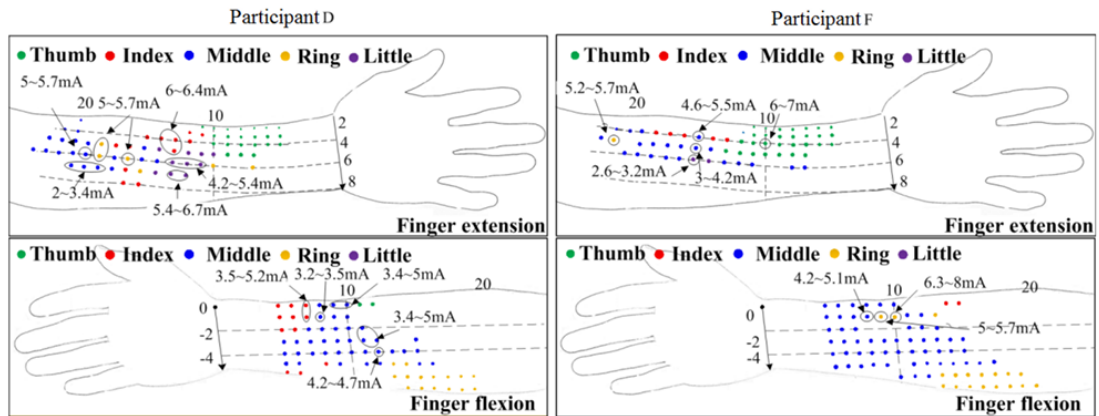
Figure 2.4: Stimulation points variability. The figure represent a comparison between two different subjects. Bao *et al.* observed significant inter-subject heterogeneity in both the position of stimulation points and the movements achieved. Additionally, the figure reports the current ranges required to achieve selective finger movements, which also exhibit high variability [60].

In another study [61], Usman *et al.* developed a system capable of automatically determining the optimal stimulation parameters and locations to achieve isolated finger flexions. The system featured a flexible electrode array with 32 pads (1.2 cm x 1.5 cm) placed on the ventral side of the forearm, while a reference electrode

(5 cm x 9 cm) was positioned near the wrist. Stimulation was delivered with a fixed pulse width of 250 µs and frequency of 25 Hz, while the current amplitude ranged from 5 to 15 mA, adjusted based on subject feedback. Figure 2.5 illustrates an example of the electrode array placement on the forearm.
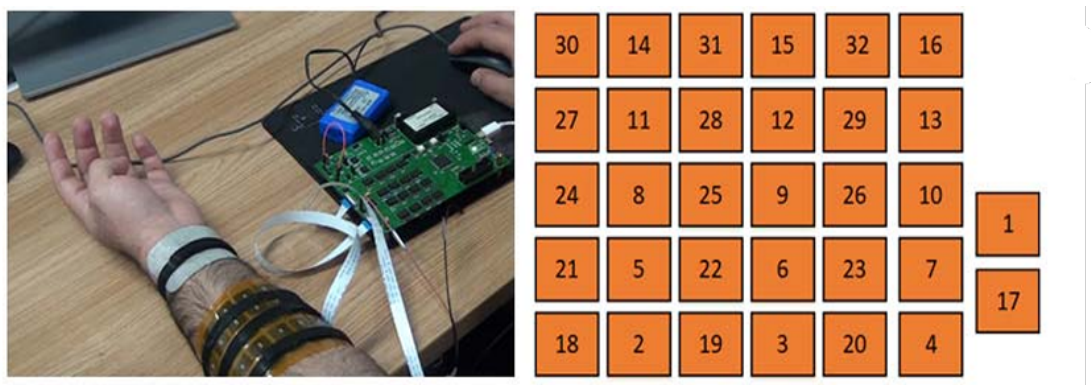
Figure 2.5: Electrode array placement. The figure demonstrates the positioning of the 32 pads that form the electrode array on the forearm. To ensure the sequential recruitment of a diverse set of motor neurons and prevent charge distribution to neighboring muscles during stimulation, each pad was numbered such that no two consecutive electrode pads were adjacent to each other in terms of their numbering [61].

The system successfully identified optimal electrode pads for at least three fingers in six out of eight subjects, significantly reducing the time required to determine ideal parameters and stimulation sites. Usman *et al.* found that current intensities were generally consistent across subjects, except for index finger flexion, which consistently required higher intensities (> 11 mA).

Among the tested movements, the index and little fingers were the most challenging to stimulate selectively, whereas ring finger flexion was successfully achieved in all subjects. Additionally, the authors observed considerable variability in the placement of active electrode pads between individuals, emphasizing the importance of personalized stimulation strategies. Figure 2.6 shows the variability in the optimal stimulation points across the tested subjects.
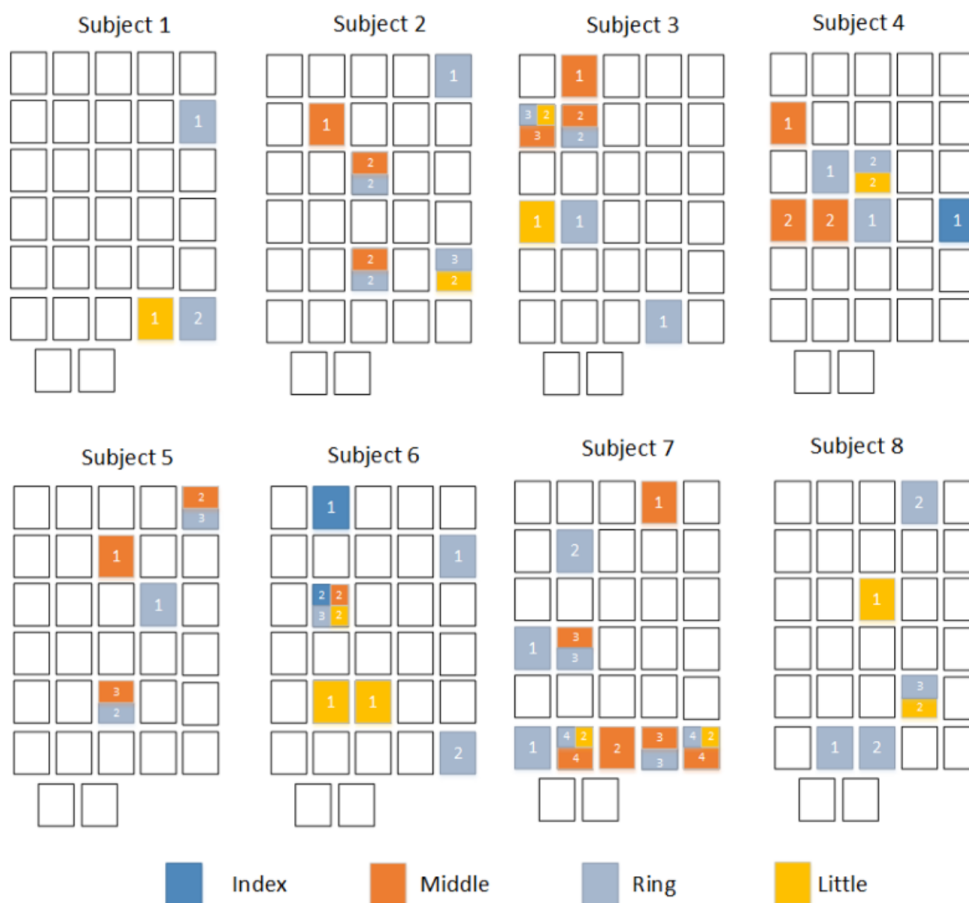
Figure 2.6: Electrode array mapping of the tested subjects. The figure shows the active electrodes capable of selectively activating a finger, highlighted in their respective colors. The numbers represent the selectivity and strength of the achieved flexion, with 1 indicating a strong isolated flexion, while 2 or higher correspond to weaker or shared movements [61].

In a 2021 study [62], Takahashi et al. proposed an innovative method to overcome the time-consuming process of identifying optimal stimulation points and parameters for finger flexions. Instead of stimulating the forearm, they targeted the interossei and lumbrical muscles in the palm, which are smaller than the extrinsic finger flexors and therefore allow for a more efficient search for optimal stimulation points. In this study, 1 cm x 3 cm electrodes were placed on the back of the hand, while a 3 cm x 3 cm ground electrode was positioned at the wrist. The optimal stimulation parameters were determined through a calibration process, in which the current amplitude was incrementally increased in 1 mA steps while maintaining

47

a fixed pulse width of 200 µs until the movement was fully executed.

The study demonstrated that this method reduced electrode placement and calibration times while enabling greater movement selectivity compared to the traditional electrode placement. Although the achieved flexions are limited to the metacarpophalangeal joint, Takahashi *et al.* demonstrated the validity of this approach for various applications, such as playing drums, guitar, or piano, which require a high level of dexterity. Figure 2.7 represents a comparison between the flexions obtained with the traditional electrode placement and the proposed approach.
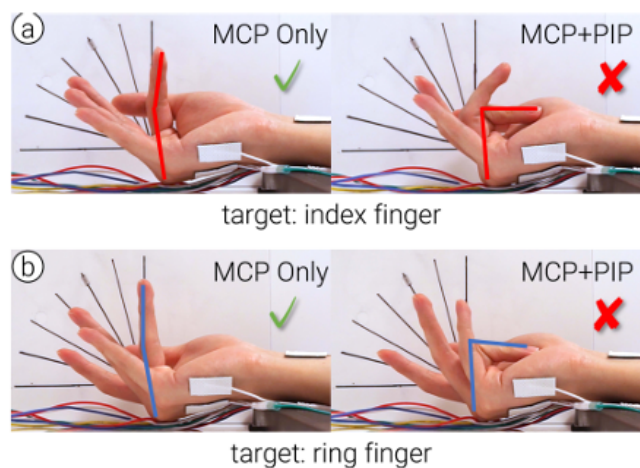
Figure 2.7: Comparison of flexions between forearm and back of the hand stimulation. The proposed approach enables more isolated flexions compared to traditional forearm stimulation. A key difference is that back of the hand stimulation is limited to the MCP joint, whereas forearm stimulation also flexes the IP joints [62].

Due to the significant intersubject variability in electrode placement for generating isolated finger movements, a 2020 study by RaviChandran *et al.* [63] aimed to identify the motor points of muscles responsible for wrist and individual finger flexion and extension to create a generalized map. To achieve this, a 60 mm x 60 mm grid was defined on the forearm's surface, with the number of points varying according to the forearm's length. A motor point pen, used as a tracing electrode, delivered stimulation at each point with a fixed pulse width of 280 µs, a frequency of 50 Hz, and a current intensity optimized for a balance between subject comfort and effective muscle contraction. The experiment was performed on nine subjects, and the identified motor points were subsequently grouped into clusters using machine learning-based clustering algorithms. The study also explored the displacement of motor points during pronation and supination, focusing on the shifts

in the centroids of these points. Based on these findings, the authors developed a map of stimulation zones tailored to forearm anthropometry. These maps allow for the generalization of optimal stimulation point identification across different subjects, therefore facilitating the development of dexterous hand control through customized electrode array designs and reducing the calibration time required for each individual. Figure 2.8 shows the maps of the stimulation zones obtained, generalized to accommodate any forearm anthropometry.
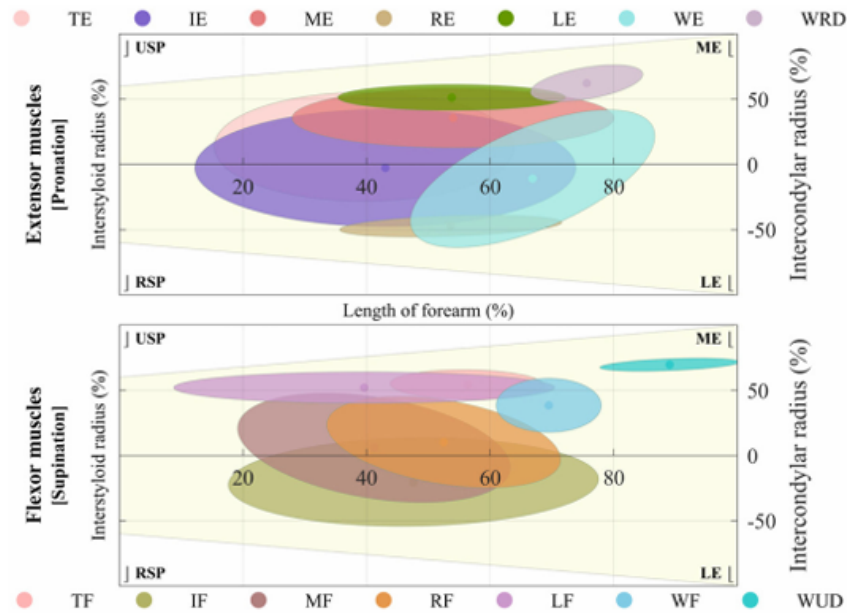
Figure 2.8: Stimulation zones for flexor and extensor muscle groups. Each ellipse represents the confidence region covering the experimentally identified motor point locations for flexion of the thumb (TF), index (IF), middle (MF), ring (RF), and little (LF) fingers, wrist flexion (WF) with ulnar deviation (WUD), and extension of the thumb (TE), index (IE), middle (ME), ring (RE), little (LE) fingers, wrist extension (WE) with radial deviation (WRD) [63].

49

Chapter 3

System Description

Since this thesis project mainly focuses on the application of functional electrical stimulation for dexterous hand movement rehabilitation, this chapter provides an overview of the electrical stimulator used and the Software (SW) previously developed by the eLiONS Laboratory research group for controlling the device.

3.1 Electrical stimulator

For the electrical stimulation, the device used is the RehaStim2, manufactured by HASOMED®. The RehaStim2 is classified as a Class IIa medical device under EU guidelines MDD 93/42/EWG, certified in compliance with international standards EN 60601-1 and EN 60601-2-10 for medical devices and systems [64].

The RehaStim2, equipped with an integrated battery, is a portable device with two independent current sources capable of generating impulses on up to 8 channels simultaneously. User control of stimulation parameters can be achieved through a display interface integrated in the device or through the ScienceMode2 serial communication protocol [65], which enables the interface with a PC via USB connection.

To assure user safety, the device performs a skin resistance check with a small test impulse before stimulation. If the resistance value is not within the normal range, the stimulation stops. In addition, an emergency stop button is also provided, allowing the stimulation to be stopped immediately when pressed. Figure 3.1 presents the device along with its accessories.
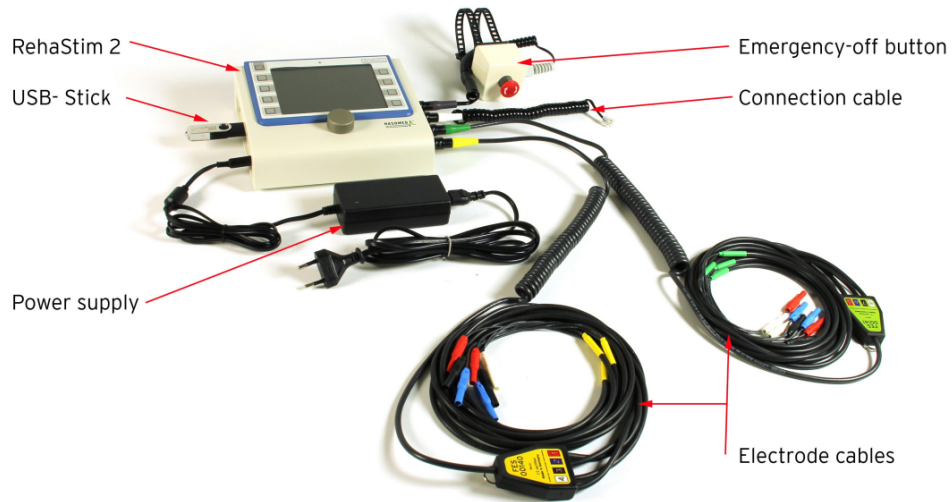
Figure 3.1: RehaStim2 by HASOMED®. The device is provided with an emergency stop button, a connection cable and two electrode cables [64].

The stimulator produces biphasic rectangular pulses with balanced electrical charge, as shown in Figure 3.2. While a fixed pause of 100 µs separates the positive and negative phases, other stimulation parameters, such as frequency, current amplitude, and pulse width, are user-adjustable. In addition, the RehaStim2 allows the selection of the pulse mode to be used, choosing between single, doublet, or triplet. For doublet and triplet stimulation modes, the interpulse interval is also user-adjustable, allowing control over the time between two consecutive pulses within the group. Table 3.1 summarizes the user-adjustable parameters and other technical specifications of the RehaStim2 device.
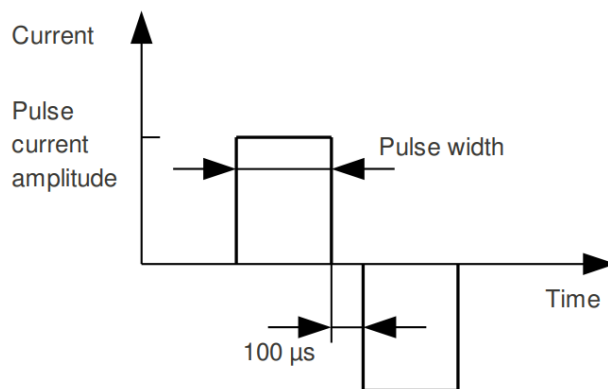
Figure 3.2: RehaStim2 pulse waveform [65].

51

Table 3.1: RehaStim2 technical details

Feature	Details
Current	[0-130] mA in 2 mA steps
Pulse Width	[20-500] µs in 10 µs steps
Frequency	[10-50] Hz in 5 Hz steps
Pulse form	Biphasic rectangular impulses with balanced electric charge
Channels	8 (2 current sources)

The RehaStim2 provides three modes for the pulse generation:

- Continuous Channel List Mode (CCLM): this mode enables the generation of complex stimulation patterns by repeatedly delivering pulses or pulse groups (e.g., doublets or triplets). The list is processed cyclically with the main stimulation period $t_1 = 1/frequency$. Pulses are generated on the selected channels according to the pulse group configuration: the channel list is processed once, twice, or three times (corresponding to single, doublet, or triplet modes) using the interpulse interval t_2. Since a time slot of 1.5 ms is reserved for each selected channel, the minimum interpulse interval is calculated as 4x1.5 ms + 2 ms (to account for a communication buffer), resulting in a minimum of 8 ms. As regards the main stimulation interval, the condition $t_1 \geq nPgr \cdot t_2$ (where n_{Pgr}=1 for single, n_{Pgr}=2 for doublets and n_{Pgr}=3 for triplets) must be respected. An illustrative example is shown in Figure 3.3.

- One Shot Channel List Mode (OSCLM): as in the CCLM mode, pulses or pulse groups are generated, although the channel list is processed once and not automatically repeated. The user is allowed to set the main interval, while the stimulator realizes the interpulse interval selection for doublets and triplets.

- Single pulse: after processing the command, the stimulator immediately generates a single pulse on a specified channel with the desired parameters.

In this thesis project, the RehaStim2 is used in CCLM mode.
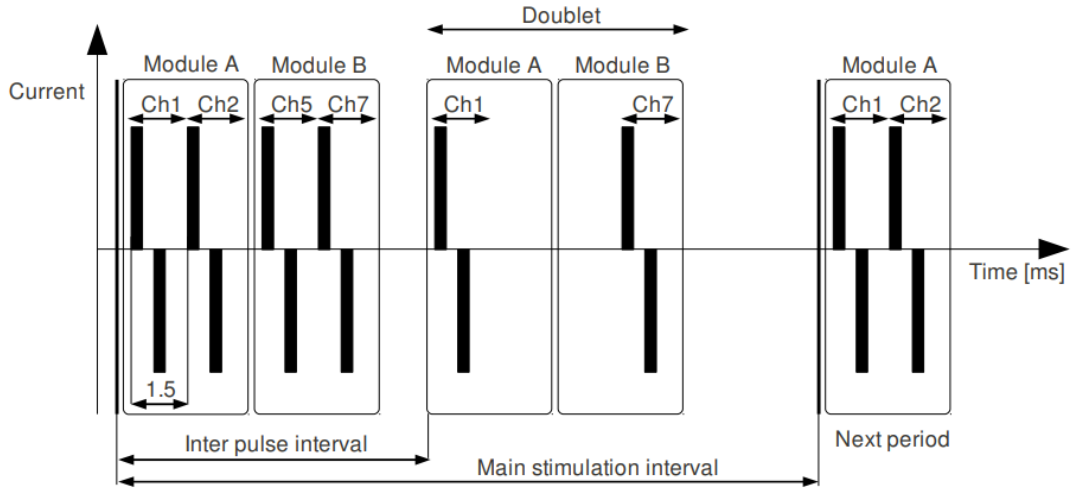
Figure 3.3: Example of Continuous Channel List Mode. Stimulation pulses are depicted as black bars. The channel list includes channels 1, 2, 5, and 7: channels 2 and 5 operate in single mode, while channels 1 and 7 illustrate the use of doublets [65].

3.2 Software overview

To meet the objectives of this thesis, a Software (SW) capable of efficiently controlling the electrical stimulator is required. This project builds upon software previously developed by the eLiONS Laboratory research group to control the RehaStim2 device and generate pyramidal stimulation profiles.

In the following subsections, an overview of the SW architecture and the original Graphical User Interface (GUI) is provided. The modifications and enhancements made to this software, aimed at addressing the specific requirements of the project, are detailed in Chapter 5.

3.2.1 Software architecture

Developed in Python® following the Object-Oriented Programming (OOP) paradigm, the control software is designed with modularity as its key feature. Indeed, the software is structured into independent modules that communicate through the implementation of Application Programming Interfaces (APIs).

The initial version of the software consisted of two layers: a top layer responsible for the user interactions and the core operations, and a bottom layer for the

communication with the electrical stimulator. In order to achieve a more organized architecture, the first modification made to the SW involved the separation of the top layer into two distinct components: System, responsible for all core operations, and GUI, dedicated to graphical functionalities. Therefore, the final SW architecture, illustrated in Figure 3.4, is composed of three layers:

- The top layer, GUI, is coupled with a frontend developed with the Kivy Python-compatible framework and handles all user interactions and graphical functionalities;

- The middle layer, System, oversees all the core operations and allows the communication between the top and bottom layers;

- The bottom layer, RehaStim2, contains the objects for connecting to and communicate with the electrical stimulator through the ScienceMode2 communication protocol.
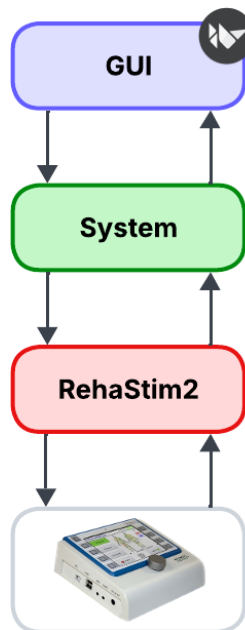
Figure 3.4: Software architecture. The software is composed of three layers. GUI handles the user interactions, while RehaStim2 is responsible for the communication with the electrical stimulator. The System layer oversees all core operations, interfacing the top and bottom layers.

3.2.2 Previous Graphical User Interface

As mentioned above, the starting point of the software development was a SW designed to generate pyramidal profiles for the RehaStim2 device. In this subsection, the main features of the original software are described. Figure 3.5 shows the original graphical user interface.
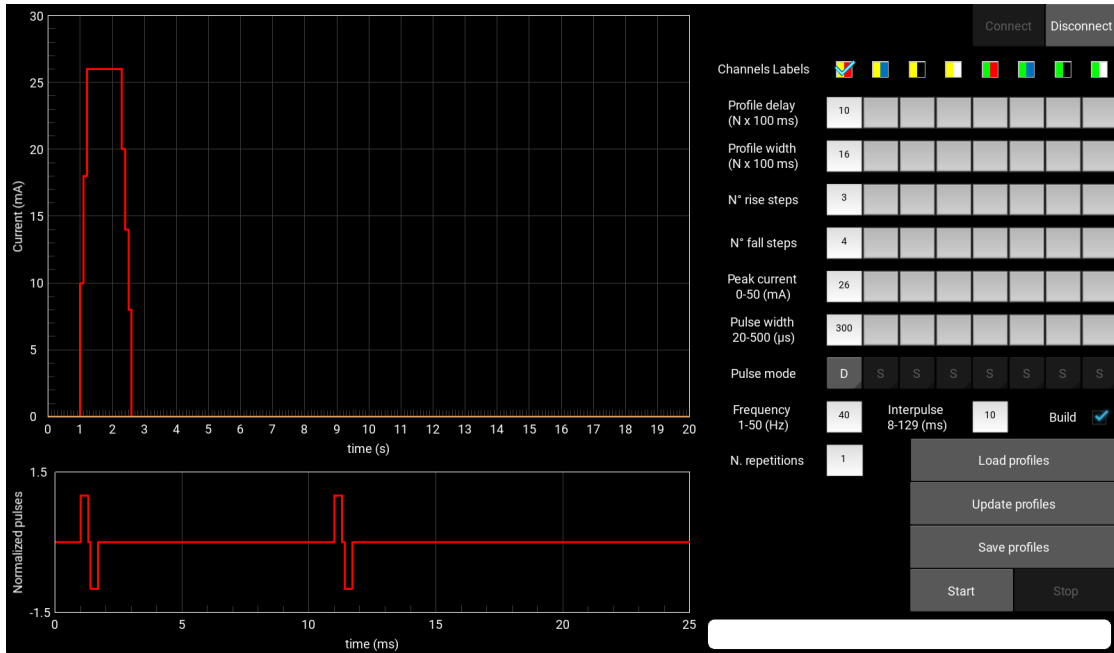
Figure 3.5: Previous GUI. On the left side, two graphs display the generated profile and the selected pulse mode. On the right, various input fields, buttons, and checkboxes allow modification of the profile and management of the stimulation.

As shown in the figure, the original GUI featured a variety of widgets, providing users with great flexibility in managing stimulation profiles. On the left side of the screen, two graphs display the created stimulation profile (top) and the selected pulse mode (bottom).

On the right side of the screen, several parameters could be adjusted to create the desired profile:

- *Channels Labels*: allow the user to select which stimulator channel is in use;

- *Profile Delay*: the value entered, multiplied by 100 ms, sets the delay between pressing the start button and the beginning of the stimulation;

- *Profile Width*: determines the duration of the stimulation profile. The value entered is multiplied by 100 ms, similar to the profile delay;

55

- *N° rise/fall steps*: indicates the number of steps required to reach the desired current and to descend to zero;

- *Peak Current*: defines the maximum current value reached by the profile (in mA);

- *Pulse Width*: sets the duration of a single pulse (in µs);

- *Pulse Mode*: allows the selection of the pulse mode (single, doublet, triplet);

- *Frequency*: sets the stimulation frequency (in Hz);

- *Interpulse*: defines the delay between two successive pulses in doublet or triplet modes (in ms);

- *N. Repetitions*: specifies the number of times the profile should be repeated.

To manage the stimulation, various buttons are available. On the top, the *Connect/Disconnect* buttons handle the connection to the electrical stimulator. Under the input fields, the *Start/Stop* buttons allow the user to begin and terminate the stimulation directly from the interface. For safety reasons, the stimulation can also be immediately terminated by pressing a physical emergency button connected to the stimulator. The *Update profiles* adjusts the profile based on the inputs entered. Finally, the *Save profiles* button saves the generated profile as a .json file for future sessions, and the *Load profiles* button allows one of the previously saved profiles to be uploaded.

Although the software was developed to generate pyramidal profiles, it also allows for the creation of typical rectangular shapes. If the Build checkbox is active, pyramidal profiles are generated. However, if the Build checkbox is unchecked, the user can only adjust the essential stimulation parameters, such as current amplitude, pulse width, frequency, interpulse interval, pulse mode, and number of repetitions.

Different checks are performed on the input values to ensure the software is functioning correctly. Specifically:

- The frequency, interpulse interval, and pulse width values must fall within the range supported by the stimulator;

- The current amplitude value, for safety reasons, must be smaller than $50\,\text{mA}$;

- The number of repetitions must be at least 1;

- The number of pulses (1, 2, or 3, depending on the selected pulse mode), multiplied by the interpulse interval, must be smaller than the main interval (1/frequency);

- The sum of the rise and fall steps must be less than the value entered for the profile width.

If any of these conditions are not met, an error message will appear in the screen's white panel on the bottom right. Additionally, error messages related to the stimulator, such as *Rehastim2 not connected*, *Electrode error*, and *Emergency switch activated*, will also be displayed in this panel.

Chapter 4

Preliminary Setup for Protocol Definition

This chapter provides a description of the preparatory steps undertaken before defining the final experimental protocol. Section 4.1 outlines the gestures selected for the experiment and the stimulation patterns defined for each gesture. On Section 4.2 a description of the electrodes used in the study is provided. Finally, Section 4.3 presents the design of a grid, which was developed and employed in the final protocol to customize the stimulation points for each subject.

4.1 Selection of gestures and stimulation patterns

Since the final objective of this thesis project is the stimulation of dexterous hand gestures, the first step involved identifying fine motor movements to target for stimulation. While many studies focus exclusively on grasping and basic hand opening/closing motions, this experimental study selected seven movements, shown in Figure 4.1: *One*, *Two*, *Three*, *Four*, *Hand Open*, *Hand Close*, and *Thumb Up*.

These complex movements require a stimulation approach that enables isolated flexion and extension of individual fingers and thumb extension and opposition, resulting in ten potential sub-movements. However, the electrical stimulator used in this study has only eight available channels, meaning that not all sub-movements can be stimulated individually. To overcome this limitation, the interdependence between the ring and little fingers was considered. Since these two digits are strongly dependent and their isolated movements are not required for the selected gestures, their flexion and extension were grouped, reducing the total number of sub-movements to eight. This allows for the optimal use of the stimulator, assigning one channel to each movement:

- Thumb Opposition (TO)

- Thumb Extension (TE)

- Index finger Flexion (IF)

- Index finger Extension (IE)

- Middle finger Flexion (MF)

- Middle finger Extension (ME)

- Ring finger and Little finger Flexion (RLF)

- Ring finger and Little finger Extension (RLE)

| One | Two | Three | Four |

| Hand open | Hand close | Thumb up |
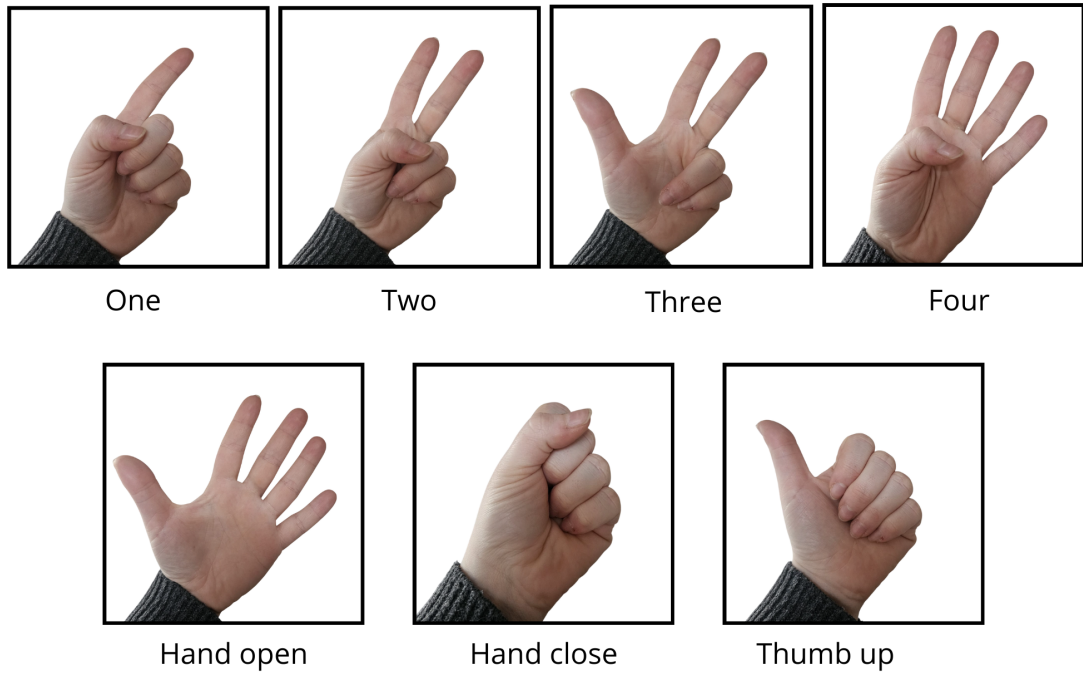
Figure 4.1: Selected gestures.

Since the eight sub-movements can be paired into four opposite movements, only four channels are necessary to achieve all the selected gestures.

The stimulation patterns for all the gestures last one second. However, while the *Three*, *Four*, and *Hand Open* gestures follow simple patterns, with simultaneous stimulation across all four involved channels, the *One*, *Two*, *Hand Close*, and

Thumb Up gestures feature a slightly more complex pattern, with the thumb's movement stimulation slightly delayed to avoid interference with the other digits. This delay is set at 200 ms.

Table 4.1 summarizes the channels required to perform the different gestures and their stimulation patterns.

Table 4.1: Channels and Stimulation Patterns for the Selected Gestures

Gesture	Channels	Pattern
One	TO, IE, MF, RLF	Thumb opposition delayed of 200 ms
Two	TO, IE, ME, RLF	Thumb opposition delayed of 200 ms
Three	TE, IE, ME, RLF	All movements stimulated simultaneously
Four	TO, IE, ME, RLE	All movements stimulated simultaneously
Hand Open	TE, IE, ME, RLE	All movements stimulated simultaneously
Hand Close	TO, IF, MF, RLF	Thumb opposition delayed of 200 ms
Thumb Up	TE, IF, MF, RLF	Thumb opposition delayed of 200 ms

4.2 Electrode design

One of the key aspects of this thesis project is to achieve selective stimulation of the fingers. To this end, particular attention was given to the choice of electrodes. The size of the electrodes is crucial for selectivity, as smaller electrodes can more precisely target specific muscles or muscle parts compared to larger ones [32].

The commercially available electrodes were too large to meet the selectivity requirements of this project. Therefore, they were modified to match the sizes reported in the literature for similar works. Specifically, FIAB PG479/32W electrodes with a diameter of 32 mm were reduced to 1.9 cm x 1.6 cm. To ensure uniform and

precise electrode cuts, an appropriate cutting tool was initially designed. This device consists of a base and an upper component. The base includes a guide matching the original electrode's dimensions, where the electrode is placed. The guide also features a space for positioning the electrode's cable, ensuring the electrode is held in the correct position without risking damage to the cable during the cutting process. The upper component contains the cutting part of the tool, which was shaped to match the desired electrode dimensions. The non-round shape was chosen to ensure minimal damage to the electrode cable.

The tool was designed in SolidWorks and fabricated using a 3D filament printer with PLA (PolyLactic Acid) material. Once printed, two springs were inserted between the base and upper components to raise the upper part. In Figure 4.2 is provided an overview of the designed tool.
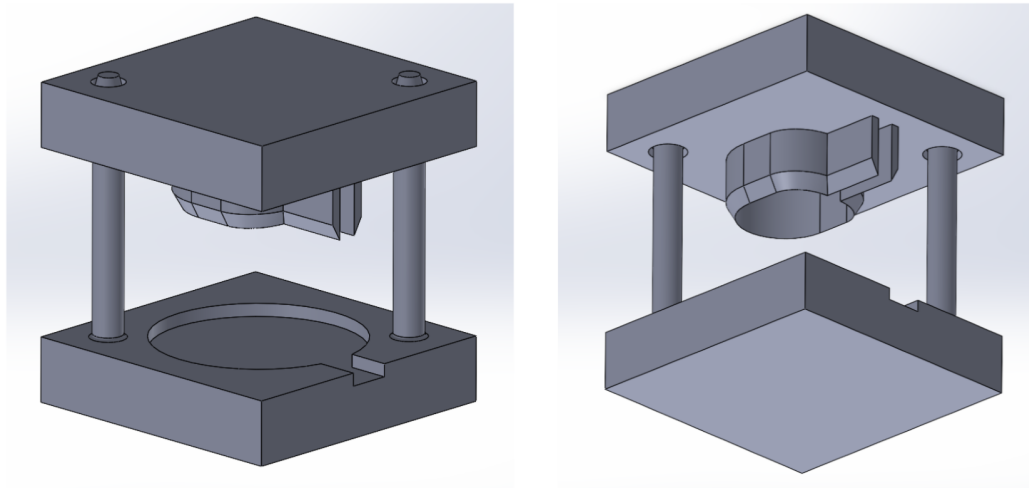
Figure 4.2: 3D design of the electrode cutting tool. The base ensures precise electrode placement through a guide, while the upper component performs the cutting.

Although the tool was intended to cut the electrodes directly, it proved ineffective as a result of its material and the electrode's. Instead, it was repurposed as a guide to imprint the desired shape onto the electrode, which was then manually cut with scissors. Figure 4.3a illustrates the complete tool and the correct electrode positioning, whereas Figure 4.3b provides a comparison between the original and cut electrode.
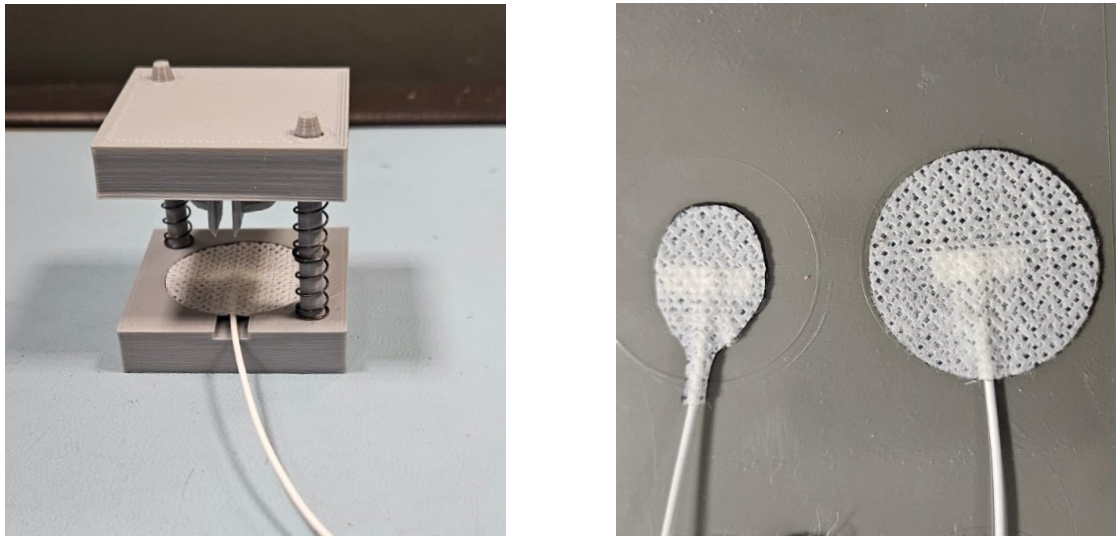
(a) Complete cutting tool.

(b) Cut and original electrode.

Figure 4.3: Electrode cutting process. (a) Displays the complete cutting tool, highlighting the proper positioning of the electrode. (b) Presents a comparison between the cut electrode and its original form.

4.3 Grid design for stimulation point customization

One of the major challenges of this project is the high intersubject variability, not only in terms of stimulation parameters but also in terms of optimal stimulation points. Since the electrodes employed are relatively small, precise placement is crucial to achieve the desired movements. To address this, the first step was to identify the main muscles responsible for the eight sub-movements outlined in Section 4.1. Specifically:

- Flexion movements involve the *Flexor Digitorum Superficialis* and *Flexor Digitorum Profundus*;

- Extension movements are controlled by the *Extensor Digitorum Communis* (which governs all finger extensions), the *Extensor Indicis* (specific to index finger extension), and the *Extensor Pollicis Longus* (responsible for thumb extension);

- Thumb opposition is driven by the *Opponens Pollicis*.

While the Opponens Pollicis is an intrinsic muscle located in the radial aspect of the hand, the other muscles are extrinsic muscles situated on the forearm. Due to

the small size of the Opponens Pollicis, electrode placement for thumb opposition is relatively straightforward. In contrast, electrode positioning for the forearm muscles is more complex, given the intricate anatomy of the muscles involved.

To ensure a precise, customized, and consistent electrode placement across sessions, a grid system was designed. In this way, it is possible to identify the correct placement for each sub-movement, moving one of the electrodes along the grid while maintaining the other fixed. The grid must meet three essential requirements: cover the skin above the targeted muscles for effective stimulation, be quick and easy to replicate across different sessions, and be adaptable to various subjects.

Since the forearm lacks prominent anatomical landmarks, three anatomical measurements were used to ensure accurate grid placement: wrist circumference, elbow circumference, and forearm length. While the initial approach aimed to create a single grid for the entire forearm, due to the forearm's complex shape, the final design consists of two separate grids: one for the anterior side and one for the posterior side. The grid construction process, which is performed with an appropriate dermatograph pencil, is identical for both sides and follows these steps, as illustrated in Figure 4.4:

- After completing the anatomical measurements, the center of the forearm surface must be identified at both the wrist and elbow levels. Due to the lack of anatomical reference points, these centers were determined by aligning with the direction of the middle finger. These points serve as the starting points for grid construction.

- Four marks are placed from the identified center at the wrist: one in the radial direction and three in the ulnar direction. The spacing between these marks is set at 1.5 cm, ensuring complete coverage of the available surface, as the smallest electrode dimension is 1.6 cm. The same process is repeated at the elbow level. However, to accommodate the shape of the forearm, which is approximated as a truncated cone, the spacing between the marks is adjusted using the proportion: $d = \frac{e_c \cdot d_w}{w_c}$, where w_c is the wrist circumference, e_c is the elbow circumference, and d_w is the corresponding wrist-level spacing.

- Once all the marks have been traced, five lines connecting them are drawn.

- To define the starting point of the grid at the wrist, a reference line is drawn at 15% of the forearm length, measured from the natural wrist line. From this reference line, parallel lines are drawn at 2 cm intervals until the grid extends over approximately 60% of the forearm length. The remaining spaces outside the grid are designated for placing fixed electrodes.

While this approach meets all three key requirements, its main limitation lies in the definition of starting points. Although the grid may not be identical between

sessions, it significantly speeds up the identification of optimal stimulation points for each subject.

| **(a)** | **(b)** | **(c)** | **(d)** |
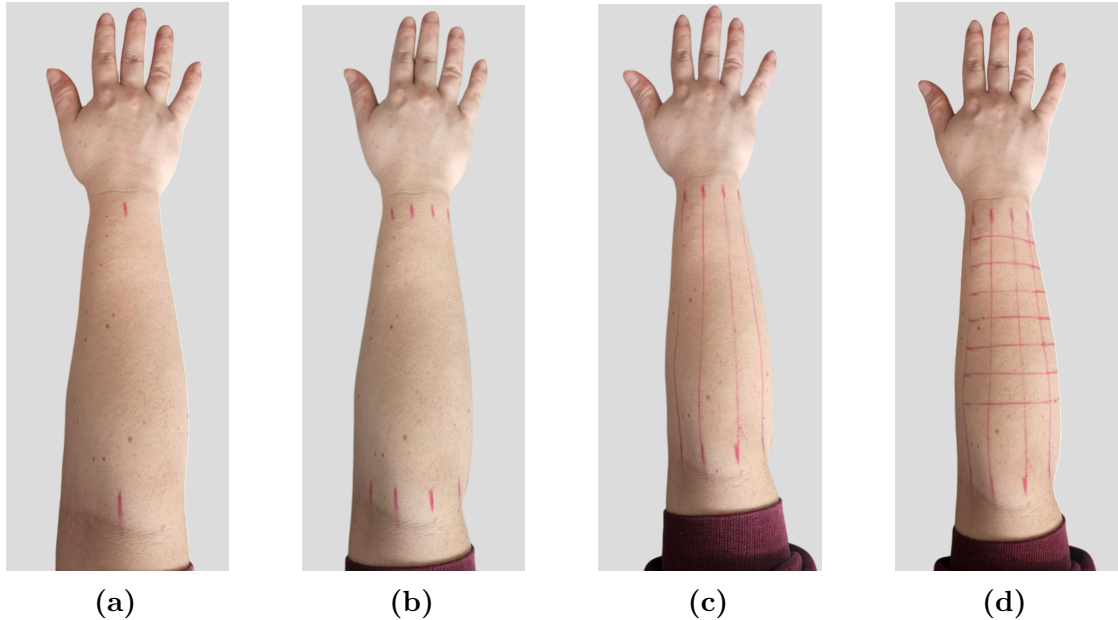
Figure 4.4: Grid construction process. The grid is constructed in four steps for both the anterior and posterior sides of the forearm. The figure illustrates an example of the grid construction for the posterior side. (a) The centers at the wrist and elbow levels are defined, following the direction of the middle finger. (b) Equidistant marks are placed along the centerline—spaced 1.5 cm apart at the wrist and 2.5 cm apart at the elbow—extending once in the radial direction and three times in the ulnar direction. (c) The marks are connected to form the grid's columns. (d) The final grid is completed by tracing rows equidistantly, with a spacing of 2 cm, starting at 15% of the forearm length from the wrist and extending until 60% of the forearm length is covered.

The defined grid is always composed of four columns following the forearm's longitudinal axis. The number of rows in the transverse direction depends on the forearm's length and thus may vary between subjects. Since the primary purpose of the grid is to identify optimal stimulation points across different sessions, a coordinate system was essential. Therefore, each section is labeled with a combination of a letter and a number to identify each area uniquely. Specifically, the columns are represented by letters, while numbers represent the rows. On the anterior side of the forearm, where the flexors are located, the columns range from A to D, moving from radial to ulnar. On the posterior side, the columns range from E to H, moving from ulnar to radial. For the rows, the numbering starts at

the wrist and increases toward the elbow. An illustration of the grid coordinates is provided in Figure 4.5.

(a) (b)
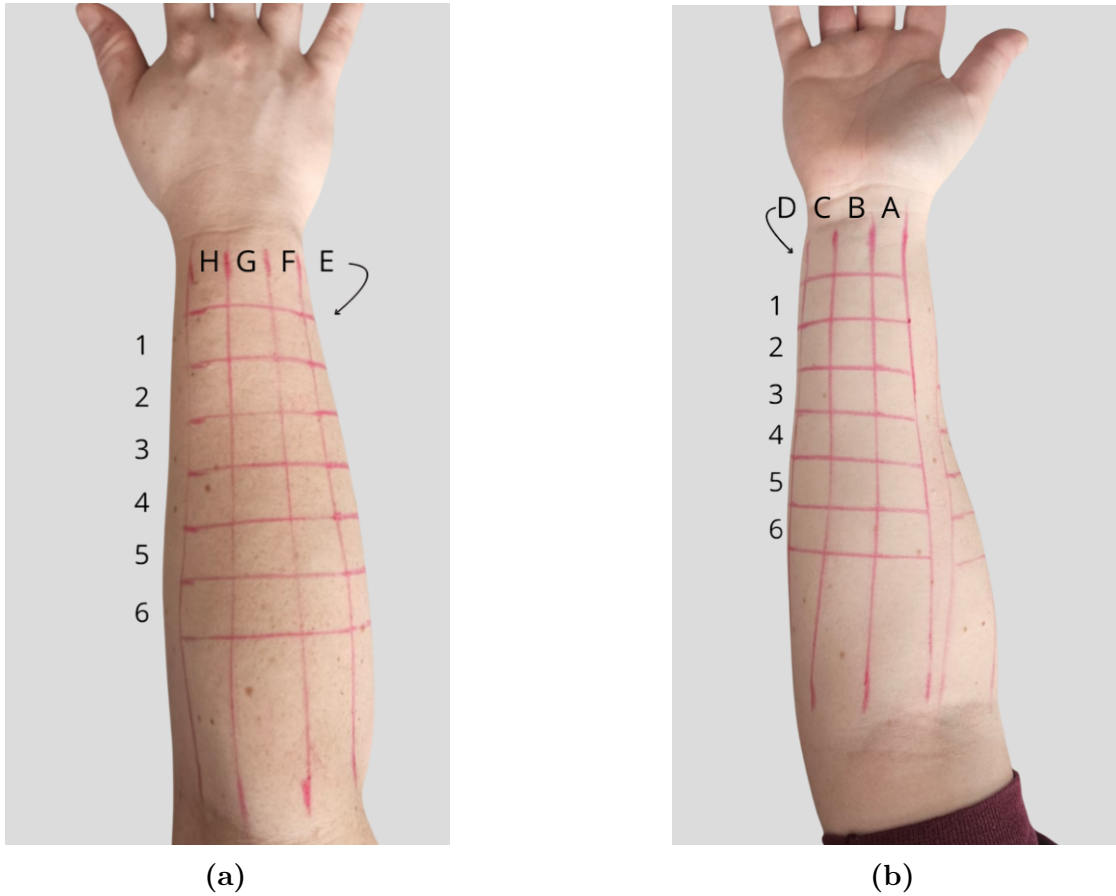
Figure 4.5: Grid coordinate system. The figure illustrates the coordinate system used for the (a) posterior and (b) anterior sides of the forearm.

Chapter 5

Software Enhancement

As mentioned in Section 3.2, the previous control software for the RehaStim2 device was designed to generate pyramidal stimulation profiles. In order to meet the objectives of this thesis project, both the software and the graphical user interface were modified to achieve greater flexibility in profile creation and to simplify the experimental process. In particular, beyond the addition of various functionalities to the main screen, the most significant modification made was the implementation of a second screen, referred to as the Calibration Screen, which facilitates the calibration of stimulation parameters, as described in Section 6.2, making the process more intuitive and efficient.

This chapter outlines the key modifications. Specifically, Section 5.1 describes the enhancements made to the original screen, now referred to as the Main Screen, which was previously introduced in Section 3.2.2. Section 5.2 then details the newly added Calibration Screen and its functionalities.

5.1   Main Screen modifications

Although the previous software effectively controlled the electrical stimulator and allowed for the creation of pyramidal stimulation profiles with precise parameter adjustments, its flexibility in pattern customization was limited. Since the ability to design flexible, customized stimulation patterns is crucial for replicating complex gestures, several modifications were made to enhance this aspect. These improvements are clearly reflected in the updated graphical user interface, as shown in Figure 5.1, and are detailed in this section.
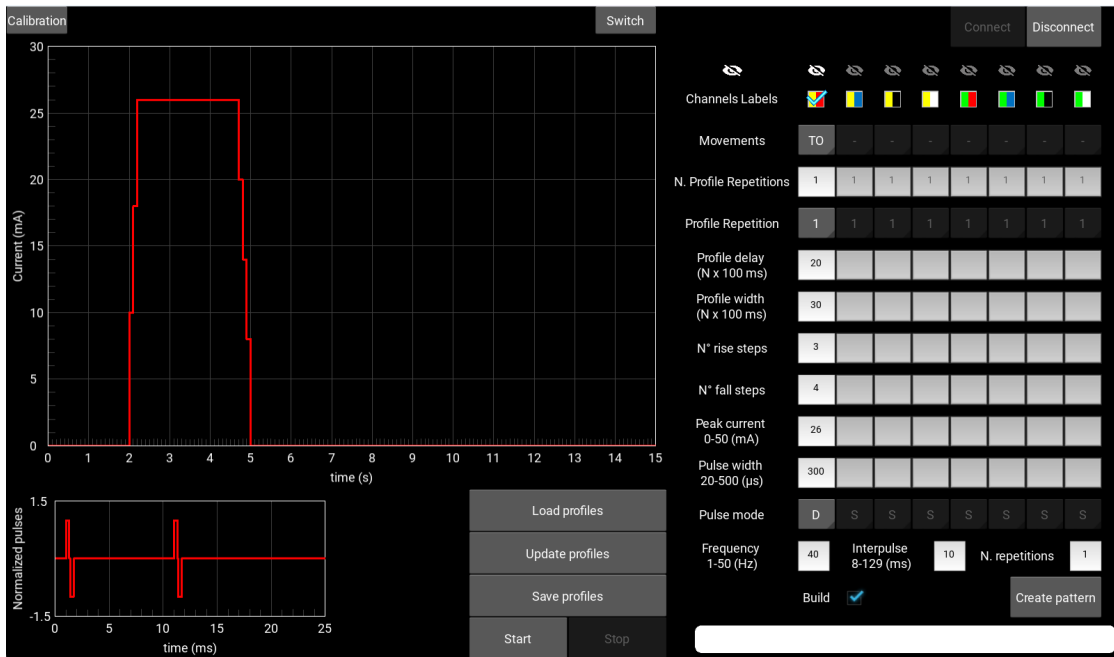
Figure 5.1: Actual GUI. This version of the interface introduces several new input fields and functionalities, including the ability to create complex and customized stimulation patterns.

5.1.1 Input parameters

The first modification made to the software was the addition of various input fields to increase flexibility in pattern creation. Specifically, the main limitation of the previous software was that the profile generated for a single channel could not be executed more than once per repetition, representing a significant obstacle when designing complex patterns.

To address this issue, the input field *N. Profile Repetitions* was introduced, allowing users to specify the number of times a profile repeats within a single repetition. Initially, the profile could only repeat identically. To further increase flexibility, a drop-down menu *Profile Repetition* with the same number of options as the selected repetitions was added. When a specific repetition is chosen from the menu, all input fields below become specific to that repetition, meaning the profile can be repeated with different shapes and values across repetitions. The only parameters that must remain consistent throughout all repetitions are pulse mode, frequency, and interpulse interval. This implementation significantly improves flexibility, enabling the creation of virtually any pattern, as illustrated in Figure 5.2.
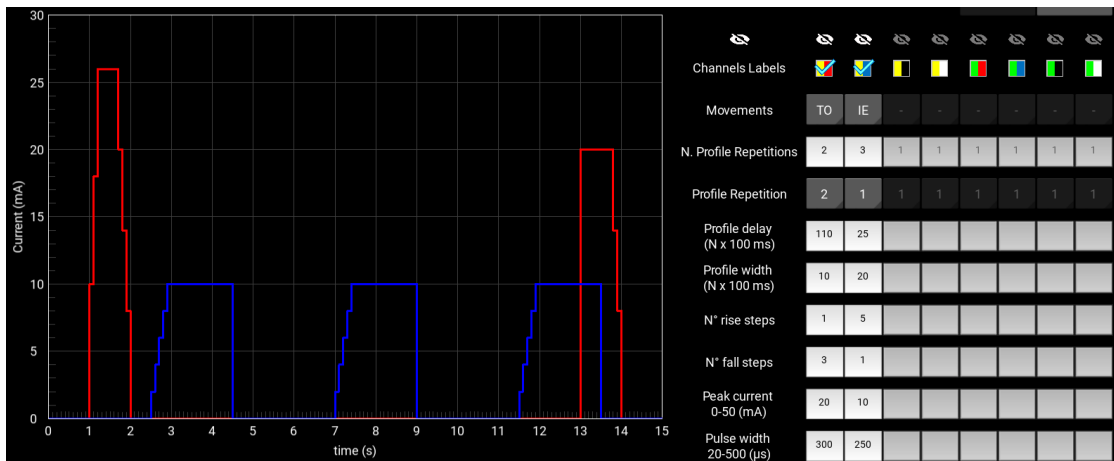
Figure 5.2: Example of complex stimulation pattern. The developed software allows the profile to be repeated multiple times within a single repetition. The profile can either repeat identically, as shown in the blue profile, or vary in shape with each repetition, as seen in the red profile.

To simplify parameter configuration, if the first repetition is selected and the other repetitions parameters have not been modified, the changes automatically apply to all repetitions. In this way, creating patterns with identical repetitions is greatly facilitated, eliminating the need to enter the same parameters more than once. However, once parameters for other repetitions are modified, further changes to the first repetition will only apply to that specific repetition.

All input values undergo the same validation checks as in the previous software. Additionally, a check on the total pattern duration ensures that it does not exceed the graph limit, set at fifteen seconds.

Finally, a drop-down menu labeled *Movements* was added for each channel to provide a clear and organized overview of the executed movement, improving clarity and usability. In addition to the sub-movements defined in Section 4.1, the menu also includes Wrist Extension (WE) and Wrist Flexion (WF).

5.1.2 Graph display enhancements

When creating complex stimulation patterns that involve multiple channels, the profile graph can become difficult to interpret. Although each channel is represented by a unique color, overlapping profiles can obscure each other, making it challenging to distinguish individual channel contributions, especially when multiple channels share the same parameters. Therefore, two key modifications were introduced to improve the readability of the profile graph.

The first enhancement allows the main graph to be divided into eight separate graphs, one for each channel. Users can switch between the combined and separated views by pressing the *Switch* button on the graph top right. A comparison between the single combined graph and the eight distinct subplots is illustrated in Figure 5.3.

(a) Single-graph.

(b) Graph subdivision into eight separate plots.
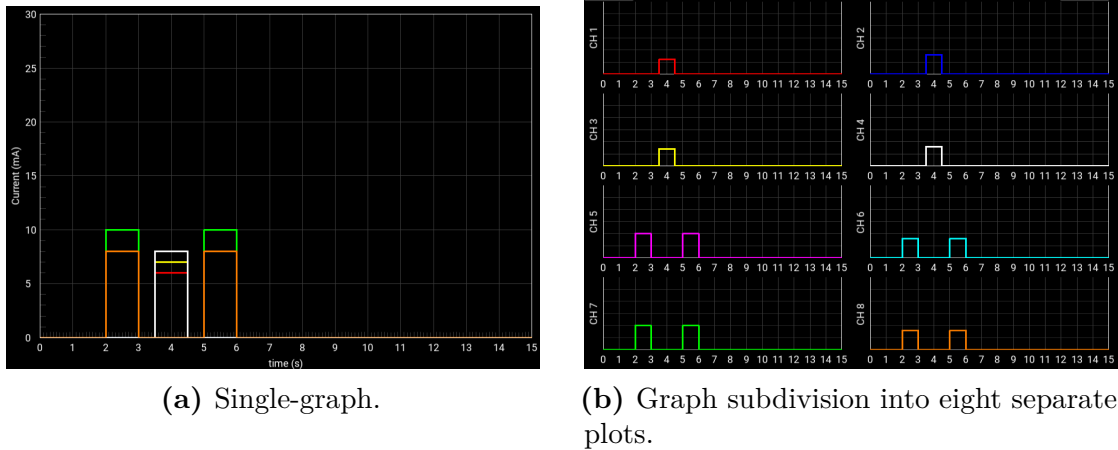
Figure 5.3: Profile graph separation. In (a), an example of complex stimulation pattern is shown, with the eight channels overlapping, causing some to be hidden. By pressing the Switch button, the graph can be divided into eight subplots, one for each channel. As shown in (b), this functionality improves the comprehension of the overall pattern, making it easier to visualize profiles that were otherwise hidden by others, such as the fuchsia profile, or partially hidden, like the red and yellow profiles.

The second modification introduces the ability to show or hide individual channel profiles within the graph. In order to do this, each channel was associated with an eye icon that users could click on to toggle its visibility, allowing users to focus on specific channels while temporarily hiding others. On the left side of these icons, a larger eye button provides global control over the channels' visibility, allowing all profiles to be shown or hidden simultaneously with a single action. This functionality is illustrated in Figure 5.4.

By implementing these modifications, the visualization of stimulation patterns has been significantly improved, making the profile graph more intuitive.
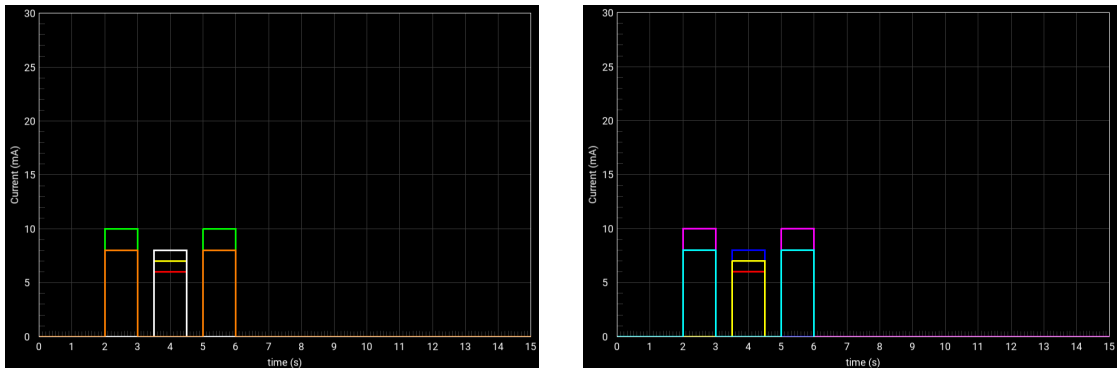
(a) Complex pattern with all channels visible.

(b) Complex pattern hiding three channels.

Figure 5.4: Channel visibility in the profile graph. In (b), the fuchsia, yellow and light blue profiles, which were completely hidden in (a), become visible by removing the visibility of the green, orange, and white profiles.

5.1.3 Pattern Creation

Since the stimulation points and parameters differ for each subject, it is essential to create customized patterns to stimulate complex gestures.

During the calibration process, later explained in Section 6.2, the sub-movements found and the associated parameters are saved in a specific file for each subject. Once the sub-movements are defined, the pattern creation could be time consuming as it involves manually defining each channel parameter. In order to facilitate this process, a *Create Pattern* button was added on the bottom right side of the Main Screen. Pressing this button opens a popup, illustrated in Figure 5.5, where a first drop-down menu allows the user to select a subject from those saved during the calibration process. Once the subject is selected, a second drop-down menu automatically updates, showing as options the available gestures for the selected subject, depending on the sub-movements present in his file, according to what was described in Section 4.1.

Once the gesture is selected, a message communicates the number of channels necessary to perform the movement. At the same time, the channels checkboxes appear and allow the user to select which channels to use. Once the channels are selected, the button Create Pattern on the bottom side of the popup becomes active, allowing the popup to be closed.

Once the popup closes, on the profile graph the complete pattern appears, while on the right side of the interface the input fields automatically adjust, as seen in Figure 5.6.
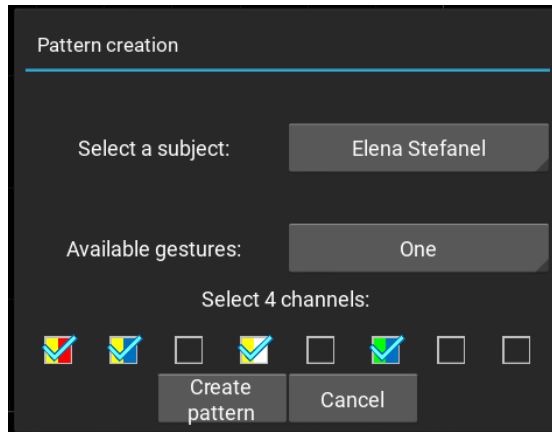
Figure 5.5: Pattern creation popup. The first drop-down menu allows the user to select subject, while the second displays the available gestures. Upon selecting a gesture, a message indicates the required channels, and checkboxes allow selection. In this example, the selected gesture *One* requires four channels: thumb opposition, index extension, middle finger flexion, and ring and little finger flexion.
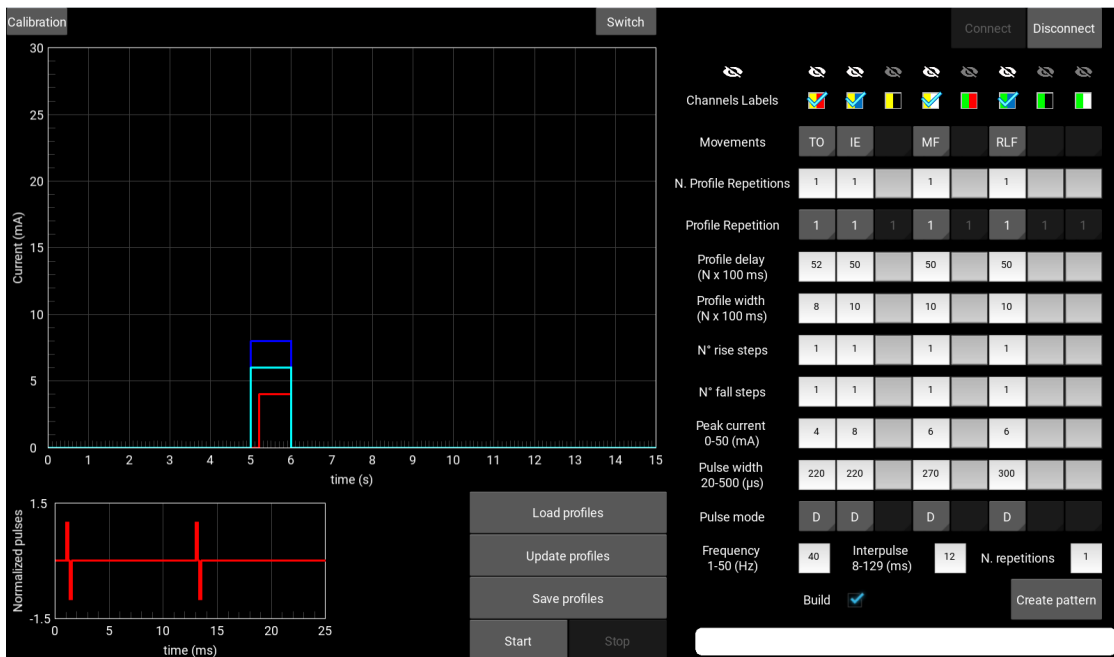
Figure 5.6: Customized pattern example. Once the popup closes, the customized pattern is displayed on the graph. The inputs on the right update to show the selected channels, associated sub-movements, and their parameters.

71

This implementation eliminates the need to manually configure channel parameters each time a different subject or gesture is selected, allowing for more efficient and rapid pattern creation.

5.2 Calibration Screen

As mentioned before, a second screen has been added to facilitate the execution of the calibration process, which aims to find the optimal stimulation points and parameters to achieve the eight sub-movements previously defined. The Main and Calibration screens are part of the same interface, but their functions are independent. The "Calibration" button on the top left of the Main Screen allows to switch to the Calibration Screen, shown in Figure 5.7.
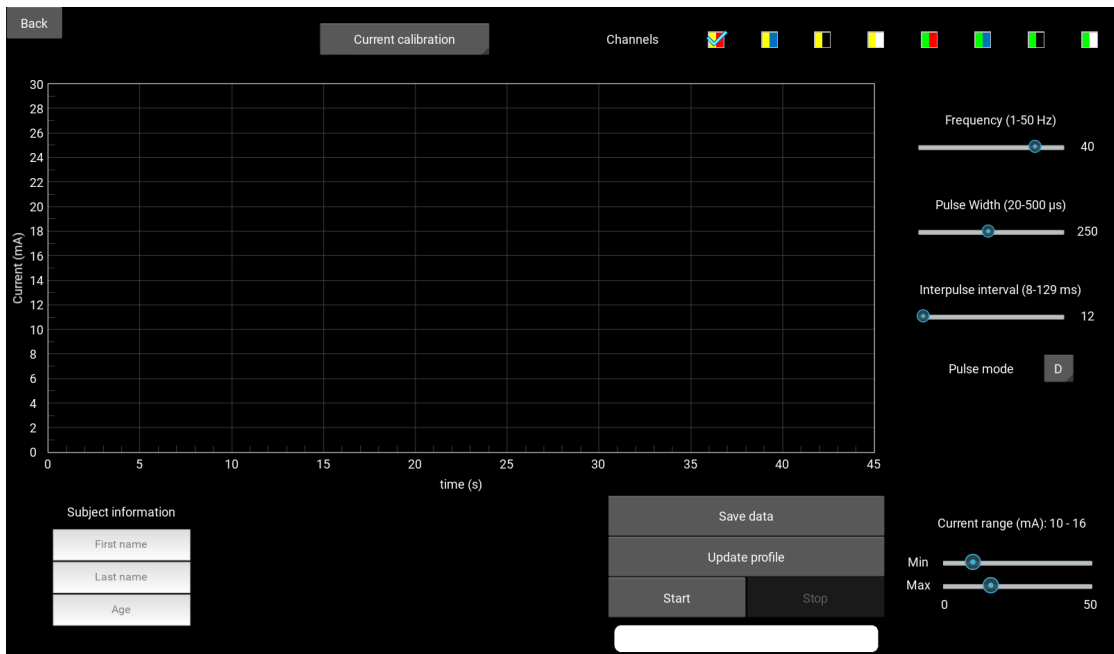
Figure 5.7: Calibration Screen.

5.2.1 Stimulation parameters calibration

As later discussed in Chapter 6, to customize the stimulation two main steps are performed: optimal stimulation point identification and calibration of the stimulation parameters. The second phase, for which this screen was specifically designed, is further divided into two sub-phases: current amplitude calibration and pulse width calibration.

During the first sub-phase, the previously identified stimulation point is stimulated using a stimulation profile with increasing current amplitude values. As soon as the desired movement is achieved, the current value is fixed, and the pulse width calibration begins. In this phase, the stimulation profile consists of seven stimulations, where the pulse width value varies from -30% to +30 % in 10% increments relative to the initial value used during current calibration. The calibration screen was designed to facilitate this parameter adjustment.

Above the graph, where the stimulation profiles are plotted, a drop-down menu allows the user to select the current step of the calibration process: current calibration or pulse width calibration.

On the right side, checkboxes allow the user to select the active channel, while a set of sliders provides control over the stimulation parameters. Specifically, the sliders remain active during the current calibration step, enabling the selection of the stimulation frequency, interpulse interval, and initial pulse width. Additionally, a drop-down menu allows the selection of the pulse mode (single, doublet, or triplet). At the bottom, two sliders define the range where the current amplitude gradually increases. By pressing the *Update Profile* button, the corresponding stimulation profile is displayed on the graph. Figure 5.8 illustrates an example of a stimulation profile for this phase.
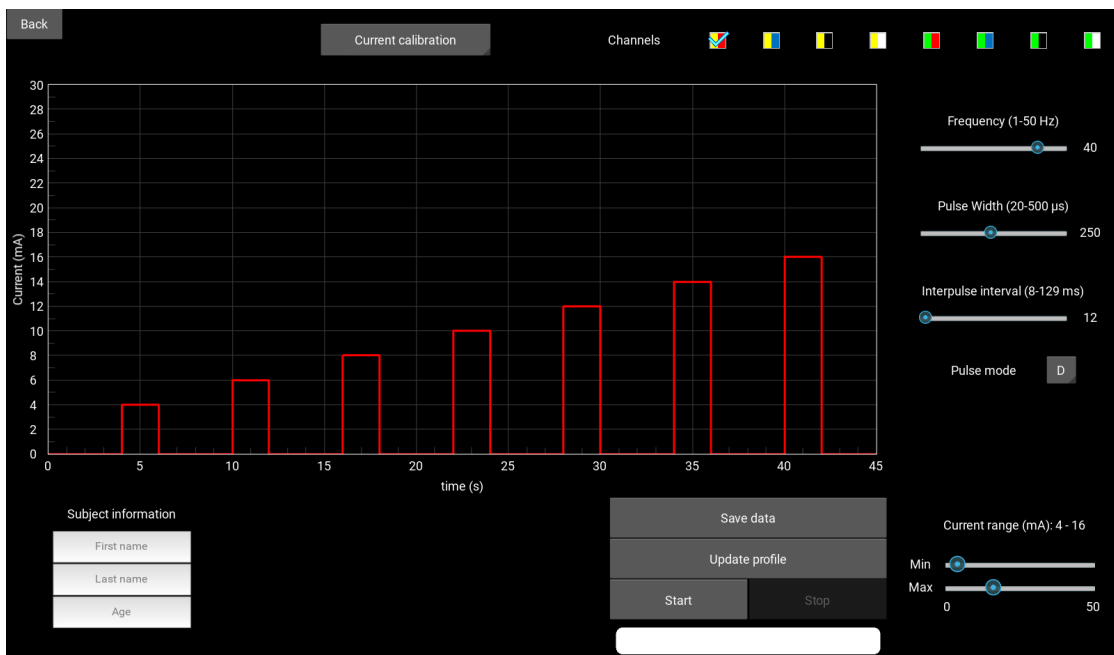
Figure 5.8: Current calibration profile. The sliders in the bottom right allow to select the range within the current values increase.

73

Once the current calibration stimulation profile is defined, stimulation is applied to the previously identified location. As soon as the desired movement is achieved, the stimulation is stopped. At this point, the second phase of the calibration process can begin. When the drop-down menu is set to pulse width calibration, the software automatically saves the last recorded current amplitude value, and a confirmation message appears in the white panel below the buttons. To ensure consistency with the previous step, all sliders and the pulse mode selection menu are disabled. By pressing *Update Profile*, the stimulation profile for this phase is displayed, as shown in Figure 5.9. Since pulse width variations are not distinguishable on the graph, real-time tested values are displayed on the white panel during stimulation. Once the desired movement is achieved, the stimulation can be stopped and the data can be saved.
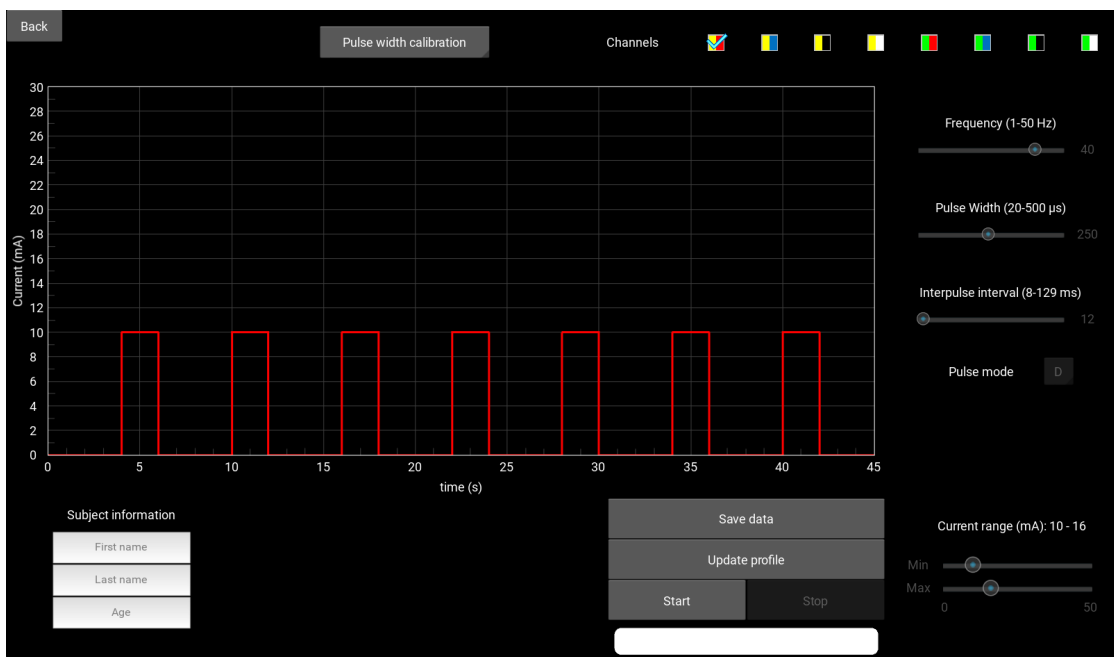
Figure 5.9: Pulse width calibration profile. During this phase, the profile consists of seven stimulations with a fixed current intensity and increasing pulse width.

5.2.2   Calibration data

Since the calibration process is time-consuming and the stimulation points and parameters may be required for future sessions, it is essential to save the obtained data. On the bottom left side of the Calibration Screen, three input fields under the *Subject Information* section allow the user to enter the subject's name, last name, and age. Once this information is provided, pressing the *Save Data* button

opens a popup, shown in Figure 5.10a.

In the popup, a drop-down menu displays the last tested pulse width value, while previously tested values are available as alternative options and can be selected if needed. Below this menu, two input fields allow the user to specify which movement was achieved and in which grid cell. Once all information has been entered, pressing *Save* stores the calibration data. The data is saved in a JSON (JavaScript Object Notation) file named LastName_Name_Age within an appropriate folder. The file contains a dictionary of dictionaries, where each dictionary's key corresponds to an achieved movement, and its values store the calibration results: current amplitude, pulse width, and grid location. Additionally, the file includes frequency, pulse mode, and interpulse interval for each movement. Figure 5.10b illustrates an example of the saved data.
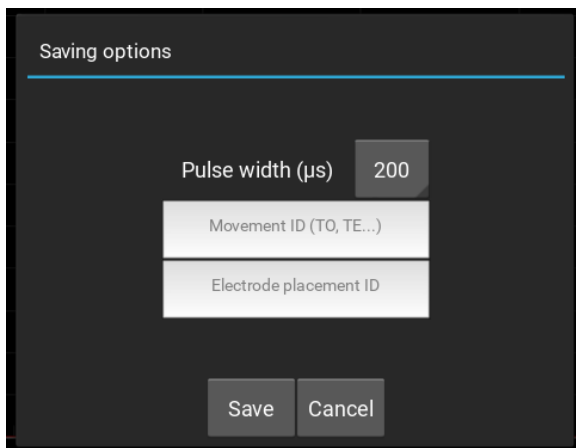
(a) Calibration data saving popup.
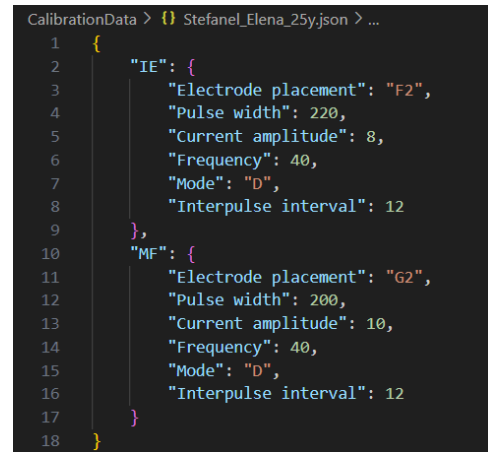
(b) Calibration data example.

Figure 5.10: Calibration data saving. a) Shows the popup for saving the recorded movement along with its electrode placement on the grid. A drop-down menu enables selection of the optimal pulse width value. (b) Provides an example of the saved data. The .json file is stored in a designated folder and contains the optimal stimulation parameters for each recorded movement.

Chapter 6

Experimental Protocol Description

In this chapter, a detailed description of the experimental protocol is provided. This thesis project aims to stimulate complex gestures by combining eight sub-movements, as defined in Section 4.1. In order to do that, the experimental process is structured into three main phases. The first phase aims to identify the optimal stimulation points that allow to achieve the desired finger movements, as described in Section 6.1. Once the stimulation points are defined, the stimulation parameters are calibrated to achieve a more efficient and comfortable stimulation. This phase is described in Section 6.2. The final phase, illustrated in Section 6.3, aims to stimulate complex gestures based on the data saved in the previous phases. As the desired sub-movements cannot always be obtained, the last phase was performed only on a subset of participants for whom at least six of the eight finger movements were identified. This last phase was performed in a separate session from the previous two to ensure the accuracy of the grid definition and the consistency of the previously saved parameters.

In all phases, the only variable parameters were the current amplitude and pulse width. In contrast, the stimulation frequency was fixed at $40\,\mathrm{Hz}$, while the selected pulse mode was the doublet, with an interpulse interval of $12\,\mathrm{ms}$. This modality was preferred as it is more comfortable compared to single-pulse stimulation, where individual pulses can be distinctly perceived. Due to the small size of the electrodes, biomedical tape was applied to all of them to ensure secure adhesion to the skin and prevent painful detachment.

The first two phases of the experimental protocol were conducted on thirteen participants, consisting of seven males and six females, aged between 24 and 61 years. Five of these participants were subsequently recalled to perform the phase

involving complex gesture stimulation. For each individual, the experiment was conducted on their dominant forearm, which was consistently the right side.

Table 6.1 summarizes the participants' information. In this table, in addition to the grid size, the Body Mass Index (BMI) is also reported. BMI, calculated as the ratio of weight (in kilograms) to height (in centimeters) squared, is taken into account as it can influence the distribution of electrical current in tissues, the depth of the target muscle and the response to stimulation.

Table 6.1: Subjects' information.

Subject	Gender	Age	BMI	Grid size
1	M	29	24.97	7x4
2*	M	32	22.49	7x4
3*	F	26	22.20	7x4
4	F	59	25.78	6x4
5	M	24	25.50	8x4
6*	M	25	22.55	8x4
7	M	25	25.95	7x4
8	M	61	30.12	6x4
9*	F	25	25.39	6x4
10	M	24	27.78	7x4
11*	F	24	20.83	6x4
12	F	42	27.69	6x4
13	F	29	37.20	6x4

*subjects recalled for complex gesture stimulation

Before the experiment, each participant received detailed information about the objectives of the project and the procedure's safety. All participants provided their informed consent for the testing protocol, which the Bioethical Committee of the Università degli Studi di Torino approved. Additionally, at the end of the tests, each subject completed a survey to provide feedback on their experience.

6.1 Optimal stimulation points identification

Given the high inter-subject variability in stimulation points demonstrated by previous studies, this initial phase of the protocol focuses on identifying the optimal stimulation sites for achieving the desired finger movements. In order to do that, the first step is to define the grid for the anterior and posterior sides of the subject's forearm based on its anatomical measurements, as defined in Section 4.3.

6.1.1 Fixed electrode placement

Since a vast number of possible combinations of electrode placement is possible, the idea is to maintain one of the couple's electrodes in a fixed position, while the other moves along the grid. In order to have consistent placements, the fixed electrodes positioning should be related to the grid, in order to be reproducible between different sessions. Since the grid does not occupy all of the forearm surface, depending on the movement, the fixed electrodes were placed in the regions outside the grid, as shown in Figure 6.1. Precisely, for the thumb extension movement, the fixed electrode is placed in the first region, from radial to ulnar, between the grid and the wrist. As regards the other digits' extension movements, the fixed electrodes are placed in the first three regions (from ulnar to radial) between the grid and the elbow. The same thing is replicated on the anterior side of the forearm for the index, middle, and ring-and-little fingers flexions.
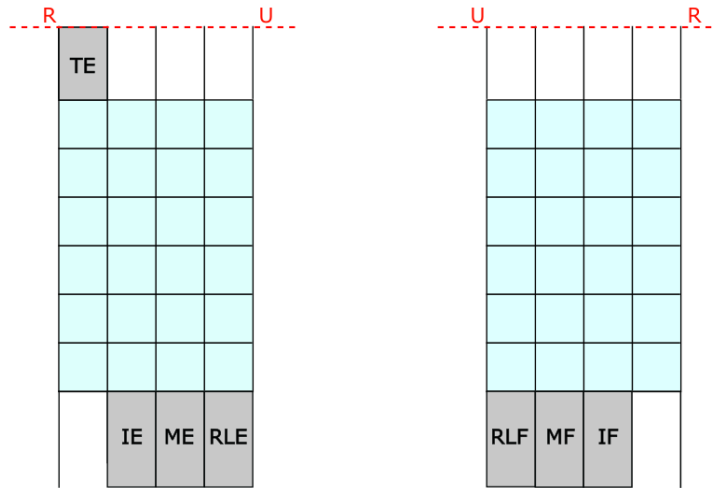
Figure 6.1: Fixed electrodes placement. The figure shows the positioning of the fixed electrodes on the posterior (left) and anterior (right) sides of the forearm, relative to the grid, which is colored in light blue. The red dashed line represents the wrist, with U for ulna and R for radius, assuming a right forearm.

For the thumb opposition, this first phase is not required, as the muscle stimulated is the intrinsic Opponens Pollicis. For this movement, the electrode placement is easier and faster, as shown in Figure 6.2.
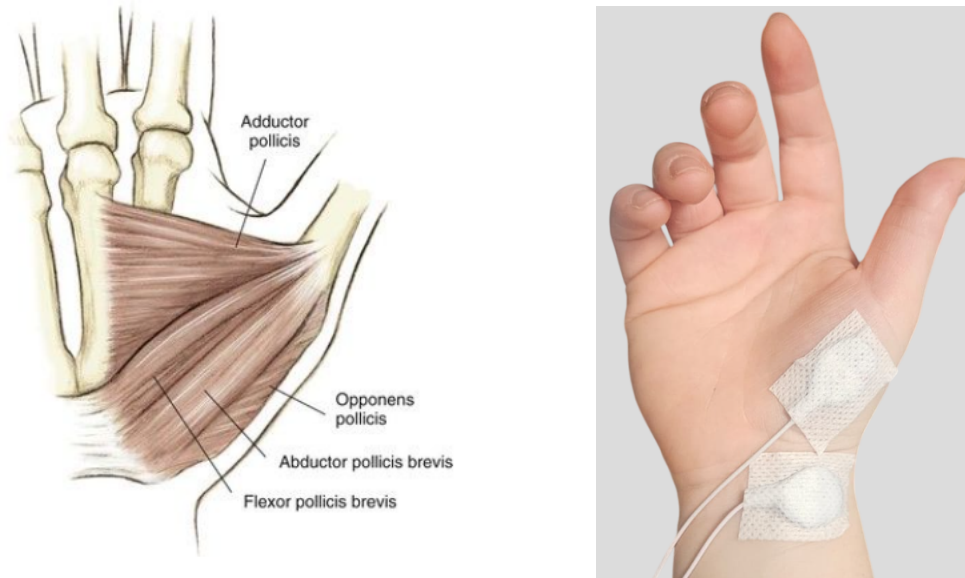
(a) Opponens Pollicis muscle [66].

(b) Thumb opposition electrode placement.

Figure 6.2: Thumb opposition. (a) Illustration of the thenar muscles, including the Opponens Pollicis, which is responsible for thumb opposition. (b) Electrode configuration used to target the Opponens Pollicis muscle.

6.1.2 Stimulation points research

The first phase aims to identify the optimal stimulation points that can elicit the eight desired finger sub-movements. To achieve this, each grid cell is tested using fixed parameters to determine which movement is triggered. If the desired movement is achieved, the process moves to the calibration phase. In this way, calibration is not performed for every grid cell, which helps to maintain a reasonable experiment duration.

Clearly, the fixed parameters in this phase must be high enough to produce a movement. However, due to the high variability between subjects, using the same initial parameters for everyone is not feasible. Therefore, the first step is to determine the initial parameters specific to each subject. To do this, the electrodes are placed in a random configuration, and brief 200 ms stimulations are applied with increasing current intensity and a fixed pulse width of 250 µs. If no movement

is observed at 12 mA, the test is repeated incrementally increasing the pulse width (with 50 µs steps) until a visible movement is detected. The parameters that successfully trigger any visible finger movement are then used in the subsequent search for the optimal stimulation points.

Since flexion movements typically require lower current intensities than extension movements, this procedure is repeated for both the anterior and posterior sides of the forearm. In addition to being necessary for finding the optimal stimulation points, this step also allows the subject to become familiar with the sensation of electrical stimulation.

Once the initial parameters are defined, for each movement one electrode is placed in its appropriate position (based on the desired sub-movement, as described in the previous section), while the other electrode moves along the grid. Each grid cell is tested for 200 ms using the identified initial parameters. During this phase, the subject positions their forearm on a surface in the most comfortable way for them. If the desired movement is successfully triggered, the second phase of the protocol (parameters calibration) will be performed for that specific electrode configuration, as described in the Section 6.2.

6.1.3 Limitations and adaptations to electrode placement

Due to the complexity of the muscle anatomy and the high variability in the subjects' responses to electrical stimulation, different adjustments to the stimulation points research phase were necessary.

Since slight variations in electrode positioning could result in different movements being elicited, a significant limitation of the optimal points identification phase was that it was designed to test only the grid cells, excluding the intermediate positions. To address this, the adaptation involved testing intermediate positions in some cases, based on the movements observed in two adjacent cells: one cell producing no movement and the other eliciting the desired movement not fully isolated. In these situations, the intermediate position was tested in an attempt to achieve the desired isolated movement. Even though this approach did not always lead to the desired result, in certain cases it enable to elicit isolated finger movements that would not have been achievable otherwise.

Another adjustment involved the fixed electrode configurations. As defined above, the fixed electrodes are positioned according to the grid and the target movement in a way that aims to align with the direction of muscle fiber to optimize the stimulation. However, sometimes, a different movement rather than the intended one could be successfully elicited. In such cases, if the movement achieved could not

be obtained with its predefined electrode placement, this alternative configuration was still considered valid. This approach overcame the limitation of the fixed electrode configuration, ensuring that useful movements were not discarded. In addition, the fact that different movements could share the same fixed electrode positioning is not problematic since these areas are larger than individual grid cells, allowing to position more than one electrode.

Lastly, subject's comfort has to be taken into account. If the fixed electrode positioning caused pain or discomfort, it was moved to an adjacent location, even within the grid. For instance, the fixed electrode for thumb opposition, due to its position near the wrist, could cause discomfort. In such cases, this electrode was moved in the nearby grid cell (H1) to improve tolerability while maintaining stimulation effectiveness.

6.2 Stimulation parameters calibration

After determining the optimal stimulation point, the parameters calibration phase begins. This process aims at the customization of the stimulation for the tested subject in order to enhance its efficiency while maximizing the subject's comfort. The calibration of the stimulation parameters is composed of two stages: the current intensity calibration and the pulse width calibration. As in the previous phase, subjects keep their forearm resting on a surface in a comfortable position.

The first stage focuses on identifying the motor threshold needed to achieve the desired movement by gradually increasing the current intensity. As mentioned in Section 5.2.1, this phase follows a stimulation profile of two-second activation phases alternating with four-second rest phases. The process starts with a current intensity of 4 mA, using the pulse width value determined in the previous step, and increases by 2 mA in each subsequent phase. Stimulation continues until the desired movement is achieved or the subject reports discomfort. If the movement is successfully triggered without discomfort, the process moves to the pulse width calibration phase.

The second part of the calibration process is composed of a fixed number of stimulation phases. Specifically, the stimulation profile comprises seven two-second stimulations, each followed by four seconds of rest. During this phase, the current intensity remains fixed at the value that allowed to induce the desired movement in the previous part of the calibration, while the pulse width value, which has been demonstrated to be related to the stimulation depth, is varied in steps of 10%, ranging from -30% to +30% of the initially tested value. Lower pulse width values

are tested to determine whether the desired movement can still be induced with lower stimulation energies. On the other hand, in some cases, an increase in the pulse width may be necessary to target deeper muscles [26, 29], leading to improved movement execution. The stimulation is stopped once the movement is successfully achieved and the calibration phase concludes. The obtained parameters can be saved at this point, as previously illustrated in Section 5.2.2.

6.3   Dexterous gestures stimulation

The stimulation of dexterous gestures represents the final phase of the experimental protocol. Specifically, based on the results found during the calibration phase, the idea is to combine the different sub-movements to achieve a more complex gesture appropriately.

As previously mentioned, this phase is conducted in a separate session from the first two to validate the saved stimulation points and assess the accuracy of the grid. The first step involves constructing the grid on the subjects' forearms. Once the grid is defined, the optimal stimulation points identified during calibration are tested with the previously saved parameters to verify whether the movement can be effectively elicited. Since the grid may vary slightly between sessions, minor adjustments to electrode placement might be necessary to locate the optimal point. Additionally, optimal stimulation parameters may fluctuate between sessions, requiring further fine-tuning.

Once all the saved sub-movements have been tested, hand gesture stimulation begins. The appropriate stimulation patterns (see Section 4.1) are automatically created using the Create Pattern button on the main interface, which allows the selection of the subject and the desired movement. For subjects in whom certain sub-movements were not identified, the first step involved stimulating the available gestures within their restricted range. If the missing movements included finger flexions, an alternative approach proposed by Takahashi [62] was employed. In this case, as displayed in Figure 6.3, a 1.5 cm x 1.9 cm rectangular electrode, obtained by cutting FIAB PG470W electrodes, was placed on the posterior side of the wrist, while an identical electrode was positioned on the dorsal side of the hand to target the lumbrical and interossei intrinsic muscles. However, as expected, the quality of the obtained gestures will be limited, with flexion restricted to the metacarpophalangeal joint.

During this phase, subjects rest their elbow on the surface while keeping their forearm elevated and their wrist in a neutral position, as displayed in Figure 6.4.

Figure 6.3: Example of Takahashi's electrode placement. One electrode is positioned on the dorsal side of the wrist, while the other is placed on the back of the hand to stimulate the interossei and lumbrical muscles. The figure illustrates the electrode placement used to achieve middle finger flexion.

Figure 6.4: Example of forearm position during gesture stimulation.

Chapter 7

Experimental Results and Discussion

In this chapter, the results obtained from the experimental protocol described in Chapter 6 are presented and analyzed.

7.1 Initial parameters for stimulation points identification

As mentioned in the previous chapter, the optimal stimulation points research was performed by testing each grid cell with fixed current amplitude and pulse width parameters. This first phase of the protocol immediately highlighted the necessity to customize stimulation since the parameters could not be maintained fixed for all subjects. Indeed, a fixed current of 10 mA and a pulse width of 250 µs were initially considered; however, for some subjects, these parameters could not elicit any movement, while they were excessively high for others. Therefore, as explained in Section 6.1.2, the first step involved adjusting the initial parameters for each subject before proceeding with the optimal stimulation point identification.

Table 7.1 presents the initial current amplitude and pulse width values used to identify optimal stimulation points for both extension and flexion movements. Additionally, the table reports the Body Mass Index (BMI) and the elbow and wrist circumferences for each subject.

As mentioned above, the initial approach was to maintain fixed parameters for all subjects during the identification of optimal stimulation points. However, due to the high inter-subject variability in response to electrical stimulation, this was not feasible. In fact, these parameters were optimal for both extension and flexion

Table 7.1: Initial parameters values for stimulation points research.

Subject	BMI	Wc[1] (cm)	Ec[2] (cm)	PA[3] (mA)		PW[4] (µs)	
				Ext.	Flex.	Ext.	Flex.
1	24.97	16.0	27.0	10	10	250	250
2	22.49	15.0	25.0	10	8	250	250
3	22.20	15.0	24.5	10	8	250	250
4	25.78	15.5	24.0	10	8	250	250
5	25.50	17.0	29.0	12	10	250	250
6	22.55	16.5	26.0	10	10	250	250
7	25.95	17.0	28.0	12	10	250	300
8	30.12	18.0	29.0	10	10	350	250
9	25.39	14.5	24.5	10	8	250	250
10	27.70	18.0	31.0	10	10	350	300
11	20.83	15.0	22.0	8	8	250	250
12	27.69	15.0	25.0	10	10	400	250
13	37.20	15.0	26.5	10	12	350	250

[1]Wc: Wrist circumference   [2]Ec: Elbow circumference

[3]PA: Pulse Amplitude   [4]PW: Pulse Width

movements only in Subjects 1 and 6. Moreover, while for the extension movements research 46.15% of the subjects required increased stimulation parameters, for the flexion movements only 23.08% required higher charge, while the 38.46% needed a reduction in stimulation parameters, further highlighting the need for a customized stimulation.

In order to compare the stimulation parameters, it is essential to consider both current intensity and pulse width together. A useful parameter for comparing both dimensions is the total charge delivered per second, defined as: $Q_{tot} = PA(mA) \cdot PW(\mu s) \cdot mode \cdot f(Hz)$, where mode depends on the stimulation modality (1 for single, 2 for doublets, and 3 for triplets). However, since the stimulation

frequency and pulse pattern are fixed across all subjects (40 Hz, doublet) and do not contribute to variability, a more practical parameter is the charge per pulse, defined as: $Q = PA(mA) \cdot PW(\mu s)$.

As reported in the table, generally, extension movements require higher stimulation charges per pulse to elicit motion compared to flexion movements. Indeed, on average, the charge per pulse required for flexion was 2.2 µA s, whereas for extension it was 2.9 µA s. Specifically, for 76.92% of participants, the charge required for flexion stimulation points identification was lower than that used for extension movements. However, for Subjects 1, 6, and 11, the stimulation parameters remained unchanged for both flexion and extension across the forearm.

Further considerations can be made regarding BMI, as participants with higher values may require greater stimulation charge per pulse to reach the target muscle, which could be deeper beneath the adipose tissue. However, BMI alone is a limited indicator in this context, as it does not provide information about the distribution of adipose and muscle mass [67]. For this reason, other parameters that have been considered are the wrist and elbow circumferences.

For instance, analyzing extension parameters, six subjects (5, 7, 8, 10, 12, and 13) required higher stimulation parameters compared to those initially considered. Among these, five had BMI values above 27, while Subjects 5 and 7 had BMI values comparable to other participants who did not require increased stimulation. However, observing their anatomical measurements, they were instead more similar to Subjects 8 and 10. These variations suggest that different muscle and adipose tissue distributions are crucial in determining stimulation needs.

A similar consideration can be made observing Subject 13, who had the highest BMI among all participants but exhibited lower anatomical measurements than some subjects with lower BMI values, reinforcing that the body mass index alone provides limited information.

Similarly, for flexion movements, five subjects required lower stimulation charges (Subjects 2, 3, 4, 9, and 11). Between them, three had BMI values below 23, which may explain their lower stimulation needs. However, the other two subjects had higher BMI values but displayed similar forearm measurements, suggesting a relationship between body composition and stimulation energy requirements.

Clearly, a more precise analysis of these stimulation parameters could be obtained by evaluating actual body composition rather than relying solely on BMI and anatomical measurements. Indeed, lean tissues contain large amounts of water and are highly conductive, whereas adipose tissue is a poor conductor [68]. Therefore, assessing body composition through segmental Bioelectrical Impedance Analysis (BIA) could provide a more accurate explanation of these results and facilitate a more precise determination of stimulation parameters.

7.2 Achieved sub-movements

The first phase of the protocol aimed to identify the optimal stimulation points for eliciting the eight finger sub-movements. As expected, not all desired movements could be identified in every subject and the quality of the elicited movements varied considerably, even after the parameter calibration phase: while some subjects exhibited well-isolated and clearly visible movements, others displayed limited or non-isolated responses. To ensure a clear and objective comparison of the elicited movements after the parameter calibration, a four-level evaluation scale was defined:

- Level 3: Well-isolated and clearly visible movement

- Level 2: Fully isolated but limited movement

- Level 1: Not entirely isolated, partial, or barely perceivable movement

- Level 0: No movement achieved

An overview of the elicited movements and their quality is displayed in Figure 7.1.
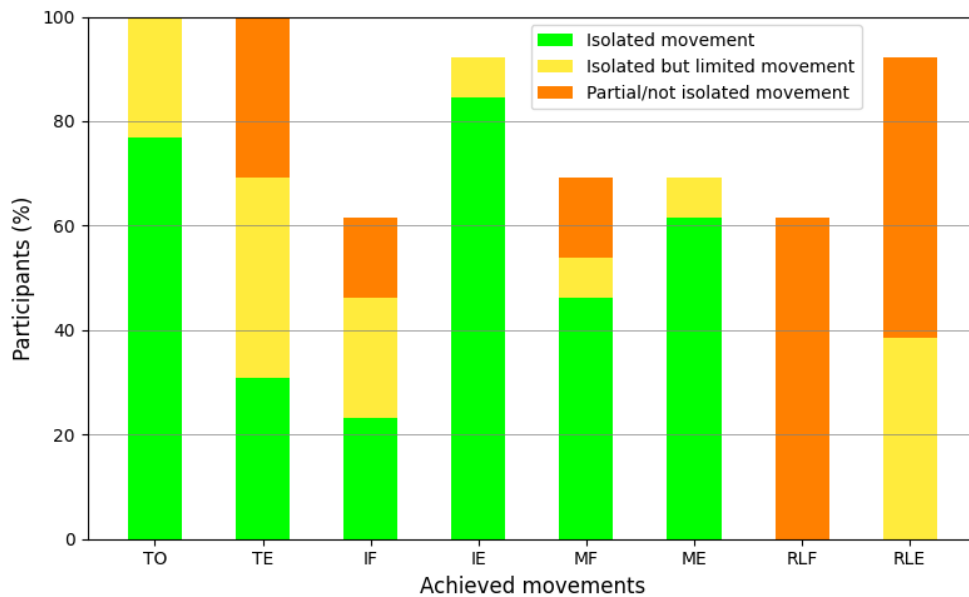
Figure 7.1: Achieved finger movements. The histogram shows the percentage of participants who successfully performed each of the eight defined finger movements. The bars are color-coded based on movement quality: green for Level 3 (well-isolated), yellow for Level 2 (limited but isolated), and orange for Level 1 (partial or non-isolated).

87

As shown in the figure, which presents the percentage of participants who achieved each of the eight finger motions, with the distribution of movement quality represented by different color, with the exception of the thumb, extension movements generally exhibit higher quality than flexion movements. Specifically:

- Thumb: Considering Level 1 motions, both opposition and extension were successfully elicited in all subjects. However, while the opposition movement was consistently of good quality (Level 3 or 2), the extension movements were frequently limited. This discrepancy is likely due to the anatomical characteristics of the muscles involved: the *Opponens Pollicis*, responsible for thumb opposition, is a small intrinsic muscle easy to target, while the *Extensor Pollicis Longus* is a deeper extrinsic muscle. As a result, further tuning of the stimulation parameters may be necessary to improve the precision of the extension movements for the thumb;

- Index finger: While index finger extension was observed in all subjects except one (Subject 8), index finger flexion was more challenging to elicit and, when present, was often limited. This difference can be explained by the fact that a dedicated muscle controls index extension, the *Extensor Indicis*, which allows for a strong and isolated movement. In contrast, index flexion is performed by the *Flexor Digitorum Communis*, which also controls the middle, ring, and little fingers, making isolated activation more difficult;

- Middle finger: Middle finger extension was the least frequently observed extension movement (found in 69.23% of participants), whereas middle finger flexion was the most frequently observed flexion movement. Both middle finger extension and flexion were strong and well-isolated when correctly targeted. The only exceptions were Subjects 12 and 13, where middle finger movement was accompanied by ring finger flexion;

- Ring and little fingers: These movements proved to be the most problematic. Both extension and flexion exhibited the lowest quality. Although ring and little finger extension was often observed, it was frequently accompanied by ulnar deviation, likely due to the activation of the *Extensor Carpi Ulnaris*, located on the posterior side of the forearm. In other cases, the movement was minimal, as increased stimulation parameters led to the wrist motion (Subject 12) or limited to an isolated little finger extension (Subjects 3 and 7). Regarding combined ring and little finger flexion, in 61.54% of participants, the movement was reduced to an isolated ring finger flexion. In the remaining 38.46%, this movement could not be elicited due to unintended wrist flexion activation.

Table 7.2 summarizes the elicited movements for the thirteen participants

involved in the first two phases of the protocol: optimal stimulation point identification and parameter calibration. Each movement is color-coded according to its corresponding level: green for Level 3, yellow for Level 2, orange for Level 1, and red for Level 0 (no movement).

Table 7.2: Evaluation of elicited movements across subjects. Each cell is color-coded based on movement quality and contains a hyperlink to the corresponding video, except for red cells, which indicate no movement was elicited.

Subjects	Finger movements							
	TO	TE	IF	IE	MF	ME	RLF	RLE
1	green	green	red	green	green	green	red	orange
2	green	yellow	green	green	red	green	red	orange
3	green	green	green	green	green	green	orange	orange
4	yellow	yellow	red	yellow	red	red	orange	yellow
5	green	orange	green	green	green	green	red	yellow
6	green	green	orange	green	yellow	green	red	orange
7	green	orange	yellow	green	green	green	orange	orange
8	yellow	orange	red	red	red	yellow	orange	yellow
9	green	green	yellow	green	green	green	orange	orange
10	green	orange	red	green	red	red	orange	yellow
11	green	yellow	red	green	green	green	orange	red
12	yellow	yellow	yellow	green	orange	red	orange	yellow
13	green	yellow	orange	green	orange	red	red	orange

Considering only the best movements i.e., Level 3 and Level 2, 69.23% of the participants exhibited at least five of the eight targeted movements. When including less isolated or very limited movements (Level 1), 76.92% of the participants achieved at least six out of eight movements, with three participants successfully displaying all targeted finger movements (Subjects 3, 7, and 9).

Overall, extension movements were more frequently observed and better isolated than flexion movements. Specifically, when including Level 1 movements, all extension motions were identified in 53.84% of the participants, whereas only

26.67% exhibited all flexion movements. Notably, unintended wrist activation was often observed during flexion stimulation. This is likely due to the anatomical complexity of the *Flexor Digitorum* (Superficialis and Profundus) and *Flexor Carpi* (Ulnaris and Radialis) muscles, which are intricately connected on the anterior side of the forearm. Further calibration of the stimulation parameters may help achieve more selective activation of the digits.

7.3 Stimulation parameters comparison

The high variability between subjects is evident in the stimulation parameters recorded after the calibration phase. Specifically, the current values range from 4 mA to 14 mA, while pulse width values vary between 170 µs and 450 µs. Tables 7.3 and 7.4 report the calibrated current intensity and pulse width values for each subject, respectively.

Table 7.3: Current amplitude values for each movement.

Subjects	Current Amplitude (mA)							
	TO	TE	IF	IE	MF	ME	RLF	RLE
1	6	10	/	8	8	10	/	10
2	6	8	10	8	/	10	/	8
3	6	8	10	8	4	10	6	8
4	6	10	/	10	/	/	10	10
5	8	12	10	10	6	12	/	8
6	8	8	10	10	10	10	/	10
7	8	12	10	10	8	14	10	12
8	6	12	/	/	/	12	8	10
9	4	10	6	8	6	10	6	8
10	10	10	/	10	/	/	8	10
11	4	8	/	6	6	6	6	/
12	10	10	8	10	8	/	10	10
13	6	12	10	8	10	/	/	10

Table 7.4: Pulse width values for each movement.

Subjects	Pulse width (µs)							
	TO	TE	IF	IE	MF	ME	RLF	RLE
1	250	250	/	320	170	200	/	270
2	200	250	250	250	/	220	/	300
3	270	170	220	200	170	220	300	200
4	220	320	/	220	/	/	400	220
5	200	300	220	250	170	200	/	250
6	220	250	250	270	220	220	/	250
7	320	320	320	320	170	250	250	210
8	270	300	/	/	/	320	320	270
9	220	220	300	220	270	200	300	250
10	240	450	/	280	/	/	300	380
11	270	220	/	200	220	250	170	/
12	250	280	200	350	250	/	220	270
13	200	240	250	280	200	/	/	250

The variability in stimulation parameters remains notable even within the same finger movement, as shown in the tables. While pulse width values are generally consistent across sessions, current amplitudes can fluctuate by 2–4 mA, as observed during the final phase of the protocol. Consequently, only limited conclusions can be drawn from the recorded parameters.

As previously observed during the identification of stimulation points, extension movements generally require higher parameters than flexion movements. Among all movements, middle finger extension exhibited the highest average current amplitude (10.44 mA), followed by thumb extension (10.00 mA). In terms of current intensity variability, the extension of the ring and little fingers showed the least fluctuation.

Regarding pulse width, ring and little finger flexion and thumb extension demonstrated the highest average values (282.50 µs and 274.62 µs, respectively). The higher pulse width for thumb extension is likely due to the depth of the Extensor Pollicis Longus muscle. Similarly, the increased pulse width for ring and little

finger movements may be attributed to the anatomical positioning of the involved muscles. However, not all flexion movements required high pulse width values; in fact, middle finger flexion had the lowest average pulse width (204.44 µs).

As shown in Figure 7.2, these trends are further confirmed by the charge per pulse delivered: extension movements, generally, require higher charges than flexions. Thumb extension, on average requiring the highest charge (2.79 µA s), and middle finger flexion, requiring the lowest (1.53 µA s), reflect the patterns seen with current intensity and pulse width.
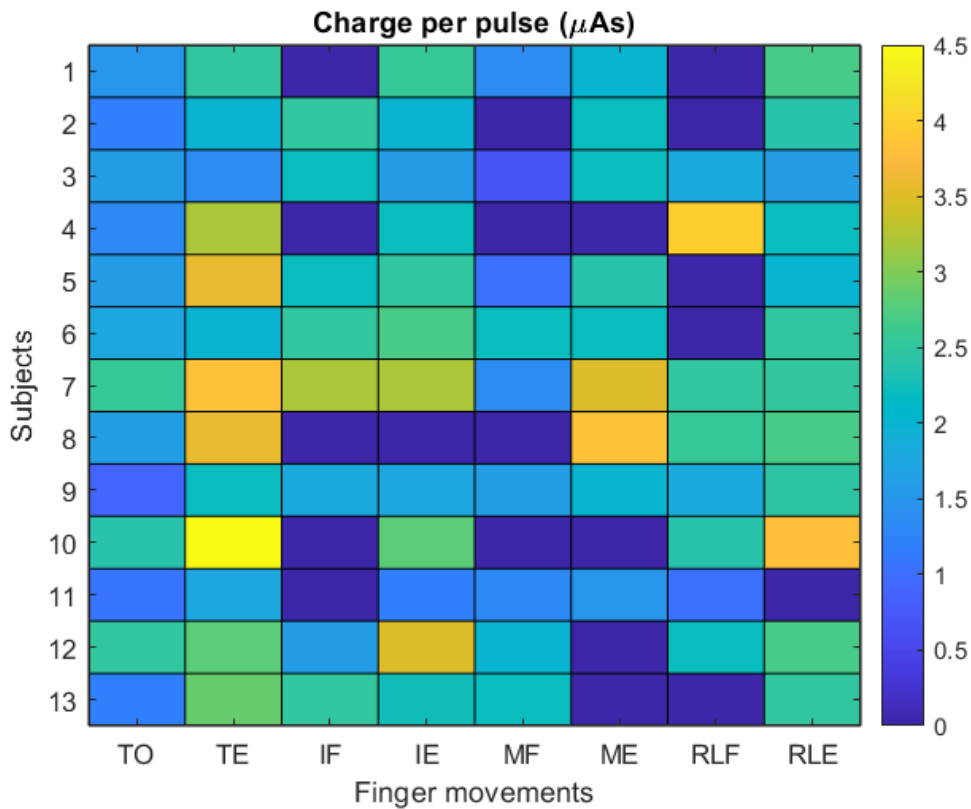
Figure 7.2: Charge per pulse required for each movement. The heatmap represents the charge per pulse, defined as $PA(mA) \cdot PW(\mu s)$, needed to elicit each of the eight finger movements for each subject. Blue cells indicate movements not achieved.

As mentioned in the previous section, a more detailed analysis of stimulation parameters could consider additional factors, such as body composition, to provide a more comprehensive understanding of these variations.

7.4 Electrode placement variability

During the first phase of the protocol, namely the optimal stimulation points research, the need for customized solutions was further emphasized, as shown in Figures 7.3 and 7.4.
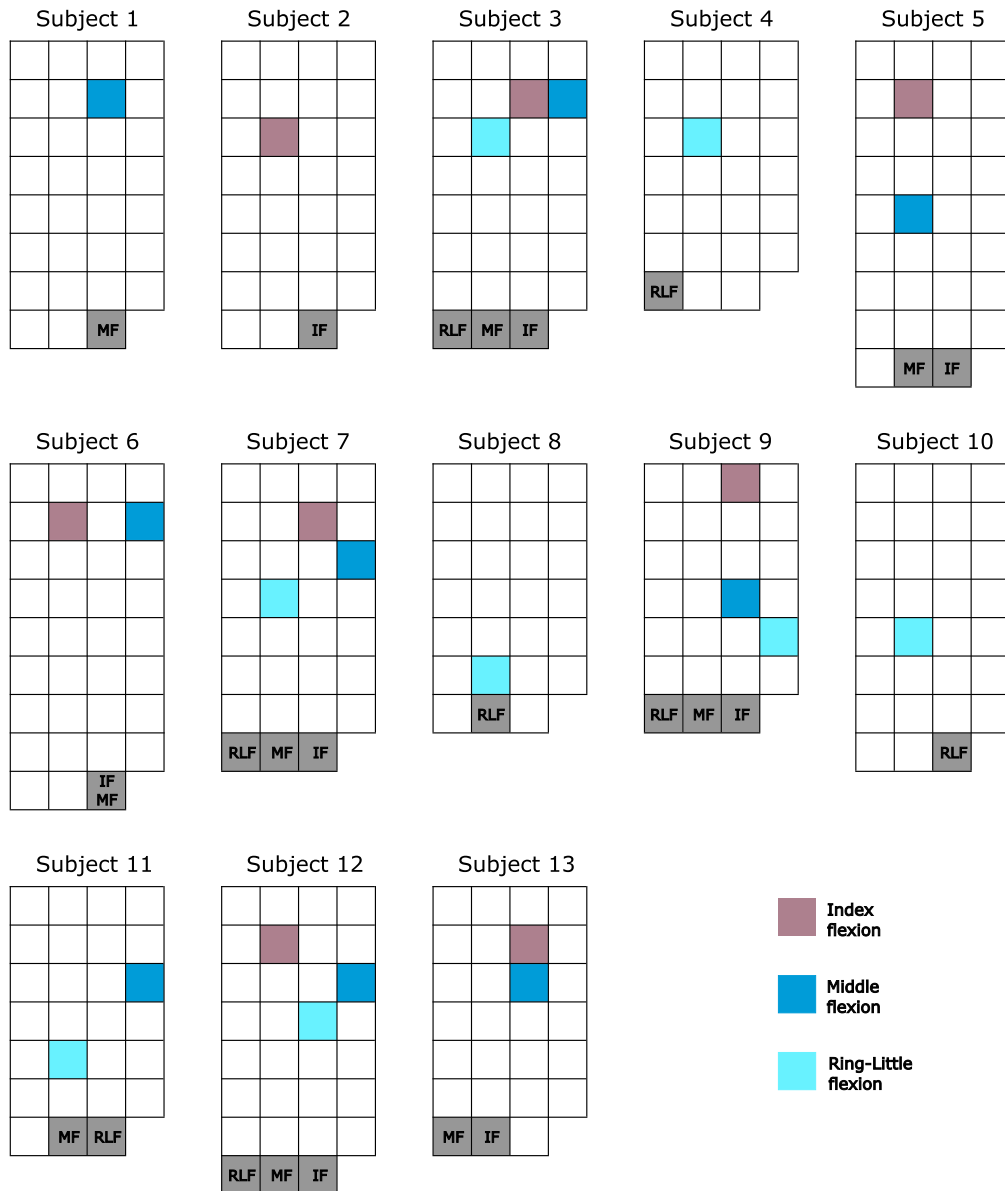
Figure 7.3: Electrode mapping for finger flexions across subjects. Grey cells indicate the fixed electrodes placements.
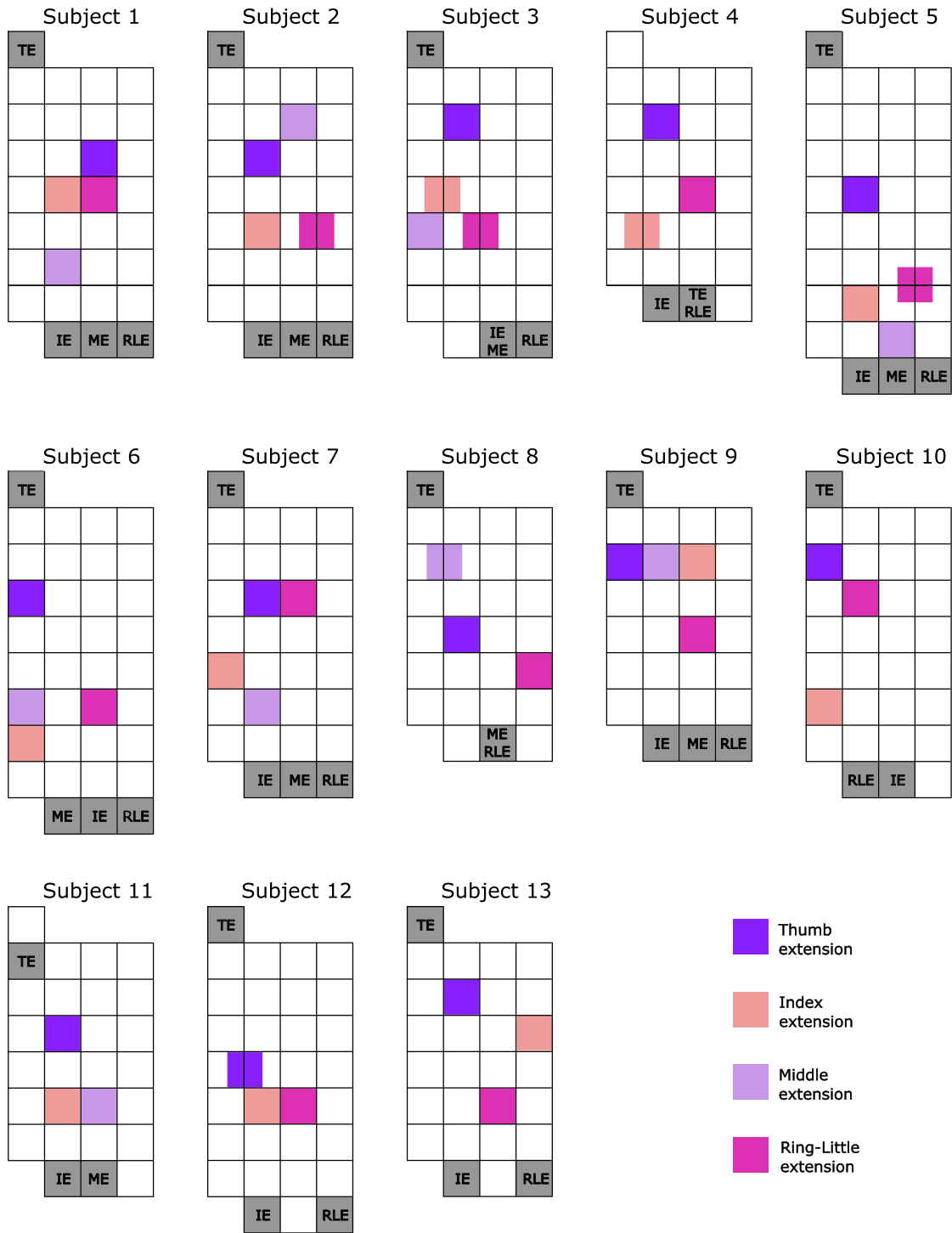
Figure 7.4: Electrode mapping for finger extensions across subjects. Grey cells indicate the fixed electrodes placements.

As depicted in the figures, it is impossible to define the electrode placement for each movement *a priori* due to the intrinsic anatomical variability among subjects. Even for thumb extension, whose muscle is smaller compared to the *Extensor Digitorum Communis*, variability remains high. Moreover, even the fixed electrodes, for which predefined positions were established, may require further adjustments. Therefore, although it is the most time-consuming part of the protocol, the search for optimal stimulation points is an essential phase to ensure the desired response to stimulation.

7.5   Dexterous hand gestures stimulation

The final phase of the protocol aimed to assess the feasibility of stimulating dexterous hand movements by combining the eight predefined finger sub-movements.

As previously mentioned, this phase was conducted separately from the stimulation point identification and parameter calibration. This approach allowed to verify that the predefined grid was sufficiently accurate, as the previously saved electrode placements could be easily relocated, even if the grid was not perfectly identical between sessions. However, as expected, the stimulation parameters showed variations, particularly in terms of current amplitude. Therefore, further fine-tuning of the parameters for each finger sub-movement was necessary before delivering the complete stimulation.

Five of the thirteen subjects tested in the initial phases of the protocol were recalled for this session. Table 7.5 presents the information of the involved subjects, along with the finger movements achieved during the first phase of the protocol.

Table 7.5: Subjects involved in the last part of the protocol.

Subj.	Age	Finger movements							
		TO	TE	IF	IE	MF	ME	RLF	RLE
2	32	green	yellow	green	green	red	green	red	orange
3	26	green	green	green	green	green	green	orange	orange
6	25	green	green	orange	green	yellow	green	red	orange
9	25	green	green	yellow	green	green	green	orange	orange
11	24	green	yellow	red	green	green	green	orange	red

All the selected gestures defined in Section 4.1 were performed for the involved subjects, except for Subject 11. Indeed, unlike Subjects 2 and 6, whose missing

movements were flexions that could still be stimulated using Takahashi's approach, Subject 11 lacked an extension, which could not be elicited through alternative methods. As a result, the *Four* and *Hand Open* gestures could not be performed for this subject.

To evaluate the quality of the complex movements resulting from the combination of finger sub-movements, a new evaluation scale was developed. This scale consists of three levels: the highest level was assigned when all fingers moved as intended, completing the desired movement. The second level was given when one of the four finger sub-movements was either limited or absent. The lowest level was assigned if two or more sub-movements were limited or absent. Additionally, a * symbol was added to gestures that involved wrist movements, and ** was used for gestures where wrist movement was particularly pronounced.

Based on the defined evaluation scale, Table 7.6 presents the quality of the achieved gestures.

Table 7.6: Evaluation of dexterous movements achieved. Each movement is color-coded based on its quality. If wrist movements were present, a * or ** symbol was added, depending on their intensity. For reference, each cell contains a hyperlink to the corresponding video.

▶	Subj.2	Subj.3	Subj.6	Subj.9	Subj.11
One		*			**
Two		**			**
Three	*	*			**
Four	**	**	**	**	
Hand Open	**	**	**	**	
Hand Close					**
Thumb up		**	*		*

As shown in the table, out of 33 total gestures stimulated, 51.52% were categorized as good-quality movements, while only 12.12% fell into the lowest quality category. Typically, the quality of the achieved gesture reflects the quality of the sub-movements involved. In fact, the poorest movements are those requiring finger flexion, which was often stimulated using an alternative approach (Takahashi's method). However, since this technique limits flexion to the metacarpophalangeal joint, the overall movement quality is compromised. For reference, Subject 1, who

lacks middle and combined ring and little finger flexions, performed the lowest-quality movements when both these flexions were required (*One*, *Hand Close*, and *Thumb Up*). On the other hand, Subjects 3 and 9, who exhibited all the expected sub-movements, generally performed the highest-quality complex movements.

From the table, wrist movements were inadvertently elicited in a significant way in 39.40% of cases. These movements were typically observed in gestures involving the extension of more than two fingers, such as *Three*, *Four*, and *Hand Open*. However, for some subjects (notably Subjects 3 and 11), the wrist appeared to be generally easier to stimulate.

7.6 Participants feedback

The first two parts of the protocol took approximately 2 hours per subject, while the final part required about 1.5 hours. At the end of the experiment, participants completed a feedback form to share their experience.

The majority of participants (84.6%) described the sensation of stimulation as a light vibration, while the remaining participants reported a mix of vibration and burning sensation, depending on the area where the electrodes were applied. Regarding discomfort or pain, 30.8% of participants reported experiencing some discomfort. However, when asked to rate the tolerability of the stimulation on a scale from 1 to 5, considering any discomfort, all participants rated it 3 or higher.

No participant reported difficulty in collaborating during the experiment, nor did anyone feel fatigued after completing the tasks. However, 38.5% of participants indicated that they did not feel particularly comfortable during the experiment, rating their comfort level as 3 on a scale from 1 to 5 (where 5 represents maximum comfort), with discomfort being mainly due to the position required for locating the stimulation points during the finger flexion tasks.

Lastly, 7.7% of participants felt that the duration of the first two parts of the experiment was too long.

Chapter 8

Conclusion and Future Perspective

This thesis project proposed an experimental protocol to customize dexterous hand gesture stimulation. Given the high inter-subject variability in response to electrical stimulation, the proposed approach primarily focused on customizing both the stimulation parameters (current intensity and pulse width) and the electrode placement to achieve selective finger movements. The protocol targeted a total of eight finger motions: thumb opposition and extension, as well as flexion and extension of the index, middle, and combined ring and little fingers. Once identified, these movements were appropriately combined in a separate session to stimulate seven selected gestures (*One*, *Two*, *Three*, *Four*, *Hand Open*, *Hand Close*, and *Thumb Up*). The protocol was tested on thirteen subjects during the initial customization phase and five subjects in the final phase. The results were promising: in 76.92% of participants, at least six out of eight finger motions were successfully identified. However, the quality of these movements was not always optimal. When considering only the best-executed motions, 69.23% of participants achieved at least five of eight sub-movements.

In the final phase of the protocol, five participants from the initial group of thirteen were recalled to assess the feasibility of combining isolated finger motions into more complex gestures. Of thirty-three stimulated gestures, 51.52% were classified as good-quality movements, while only 12.12% fell into the lowest-quality category.

8.1 Limitations

Although the results are promising, the proposed approach presents several limitations that, once addressed, could lead to improved outcomes. Moreover, the

protocol was tested exclusively on healthy subjects, meaning its applicability to individuals with motor impairments remains to be investigated.

One of the main limitations concerns the eight finger sub-movements considered. Due to the limited number of channels of the electrical stimulator, not all fingers were stimulated individually. Specifically, the ring and little fingers were coupled for both flexion and extension movements. Finding the optimal electrode placement and stimulation parameters to achieve these two motions combined is inherently more challenging than targeting them individually. Indeed, the results indicate that the quality of these movements was the lowest, as the stimulation often resulted in movement being predominantly limited to one of the two fingers. Separating the movements of these digits could lead to a greater number of distinct, higher-quality movements, thereby enhancing the overall quality when stimulating more complex motions.

Another limitation is represented by unintended wrist motions: the complex anatomy of the forearm muscles can lead to involuntary stimulation of wrist flexion or extension, affecting gesture quality. During the initial phases of the protocol, a more precise tuning of stimulation parameters could prevent this issue. However, in case of more complex gestures stimulation, the combination of multiple stimulation channels often led to a substantial wrist contribution, even when the individual sub-movements did not initially elicit wrist activation. A possible solution is to use one stimulation channel, calibrated in advance, to stabilize the wrist. For instance, when stimulating the Hand Open gesture, a channel dedicated to wrist flexion could counterbalance the unintended extension caused by other stimulation channels.

Regarding stimulation parameters, while the RehaStim2 stimulator offers significant flexibility by allowing customization of both current amplitude and pulse width, one of its main limitations is that the current intensity can only be adjusted in 2 mA increments, rather than smaller steps (e.g., 0.5 mA). Although it is possible to compensate for this limitation by adjusting the pulse width to achieve intermediate charge levels, this approach could alter the stimulation effect. In fact, pulse width influences the depth of stimulation and, consequently, the specific muscles being activated. As a result, even when delivering the same charge per pulse, different parameter configurations can produce distinct movements, affecting the efficiency of the stimulation.

Finally, a limitation lies in the way the protocol was structured. Indeed, the first two phases were conducted separately to reduce the overall duration of the experiment. However, integrating these phases by refining the search for optimal stimulation points while calibrating each grid area could enhance the identification of additional sub-movements. Furthermore, a more flexible electrode configuration

could be explored, avoiding the constraint of fixing one electrode in a predefined position.

8.2   Future developments

This research opens up several potential directions for improvements. Specifically, the following enhancements could refine the proposed protocol:

- Grid Enhancement: A 3D scanner could be utilized to precisely measure the anatomical features of the forearm. Using an appropriate algorithm, a grid could then be generated and visualized directly on the forearm through augmented reality, eliminating the need for manual grid drawing and ensuring consistent positioning across sessions;

- Functional Gesture Stimulation: A key area for future research is the feasibility of stimulating more complex and functional hand movements, such as grasp-and-release and pinching. For grasp-and-release, this could involve a sequence of movements: opening the hand to approach an object, closing it to grasp, and reopening it to simulate the release. While these patterns are more complex, the flexibility of the developed software allows for the creation and integration of such intricate stimulation patterns;

- Customized Solutions: Once optimal electrode placement for the patient has been identified, a personalized sleeve with integrated electrodes could be developed. This would significantly reduce the time required for electrode positioning, improving efficiency.

This research was initiated as a foundational step toward the development of an sEMG-FES system, aimed at enabling hand motor rehabilitation through machine learning-based gesture recognition. The goal is to create a system for use in a patient-therapist setting. On the therapist's forearm, wearable acquisition devices appropriately placed, capture sEMG signals during the execution of various hand gestures. From these signals, a classifier implemented using artificial neural networks recognizes the performed gesture, enabling the delivering of the corresponding customized stimulation pattern to the patient, allowing them to replicate the therapist's movements in real-time.

In this context, the study proposes an experimental protocol for personalizing stimulation patterns for each subject, which could contribute to optimizing hand motor rehabilitation outcomes.

Bibliography

[1] Lynette A. Jones and Susan J. Lederman. *Human Hand Function*. Oxford University Press, May 2006, p. 279. ISBN: 9780199786749. DOI: `https://doi.org/10.1093/acprof:oso/9780195173154.001.0001` (cit. on pp. 1, 4).

[2] World Health Organization. *Spinal Cord Injury*. Accessed: March 10, 2025. URL: `https://www.who.int/news-room/fact-sheets/detail/spinal-cord-injury` (cit. on p. 1).

[3] World Stroke Organization. *Impact of Stroke*. Accessed: March 10, 2025. URL: `https://www.world-stroke.org/world-stroke-day-campaign/about-stroke/impact-of-stroke` (cit. on p. 1).

[4] Bernhard Hirt, Harun Seyhan, Michael Wagner, and Rainer Zumhasch. *Hand and Wrist Anatomy and Biomechanics: A Comprehensive Guide*. Thieme Medical Publishers, Incorporated, Jan. 2017, p. 118. ISBN: 9783132053519. DOI: `10.1055/b-004-135650` (cit. on pp. 2, 5).

[5] Ibrahim Adalbert Kapandji. *The Physiology of the Joints, Volume 1: Upper Limb*. Churchill Livingstone, 1982, p. 293. ISBN: 0 443 02504 5 (cit. on pp. 3, 4, 10).

[6] Henry Gray. *Anatomy of the Human Body*. Philadelphia, Lea & Febiger, 1918, p. 1396. DOI: `https://doi.org/10.5962/bhl.title.20311` (cit. on p. 6).

[7] Visakha K. Nanayakkara, Giuseppe Cotugno, Nikolaos Vitzilaios, Demetrios Venetsanos, Thrishantha Nanayakkara, and M. Necip Sahinkaya. «The Role of Morphology of the Thumb in Anthropomorphic Grasping: A Review». In: *Frontiers in Mechanical Engineering* 3 (2017). DOI: `10.3389/fmech.2017.00005` (cit. on p. 6).

[8] Woohyeok Choi and Yukio Takeda. «Geometric Design and Prototyping of a (2-RRU)-URR Parallel Mechanism for Thumb Rehabilitation Therapy». In: *Machines* 9 (2021), p. 50. DOI: `https://doi.org/10.3390/machines9030050` (cit. on p. 8).

[9] OpenStax College. *Anatomy and Physiology*. Accessed: March 10, 2025. URL: `http://cnx.org/contents/14fb4ad7-39a1-4eee-ab6e-3ef2482e3e22@11.1` (cit. on pp. 12–14, 16, 20).

[10] Dee Unglaub Silverthorn. *Fisiologia Umana: un approccio integrato. Settima edizione.* Pearson, 2017, p. 849. ISBN: 9788891902177B (cit. on pp. 13, 18).

[11] Walter R Frontera and Julien Ochala. «Skeletal Muscle: A Brief Review of Structure and Function». In: *Calcif Tissue International* 96.3 (2015), pp. 183–195. DOI: `10.1007/s00223-014-9915-y` (cit. on pp. 13, 18).

[12] M.A. Cavalcanti Garcia and T.M. M. Vieira. «Surface electromyography: Why, when and how to use it». In: *Revista Andaluza de Medicina del Deporte* 4.1 (2011), pp. 17–28 (cit. on pp. 20, 23–25).

[13] Ketchum, Heather and Bright, Eric. *OU Human Physiology Textbook.* Accessed: March 10, 2025. URL: `https://archive.org/details/cnx-org-col11851/page/n877/mode/2up` (cit. on p. 21).

[14] Roberto Merletti and Dario Farina. «Analysis of intramuscular electromyogram signals». In: *Philosophical Transactions of the Royal Society A: Mathematical, Physical and Engineering Sciences* 367.1887 (2009), pp. 357–368. DOI: `https://doi.org/10.1098/rsta.2008.0235` (cit. on p. 22).

[15] Vladimir Medved, Sara Medved, and Ida Kovač. «Critical Appraisal of Surface Electromyography (sEMG) as a Taught Subject and Clinical Tool in Medicine and Kinesiology». In: *Frontiers in Neurology* 11 (2020), p. 560363. DOI: `10.3389/fneur.2020.560363` (cit. on p. 22).

[16] Douglas Robertson, Graham Caldwell, Joseph Hamill, Gary Kamen, and Saunders Whittlesey. *Research Methods in Biomechanics: Second edition.* Human Kinetics Publishers, Nov. 2013, p. 441. ISBN: 0-7360-8340-0 (cit. on pp. 22, 25, 26).

[17] Anjana Goen and D. Tiwari. «Review of Surface Electromyogram Signals: Its Analysis and Applications». In: *International Journal of Electrical, Computer, Energetic, Electr-onic and Communication Engineering* 7 (2013), pp. 1429–1437 (cit. on p. 23).

[18] Roberto Merletti, Alberto Botter, Amedeo Troiano, Enrico Merlo, and Marco Alessandro Minetto. «Technology and instrumentation for detection and conditioning of the surface electromyographic signal: State of the art». In: *Clinical biomechanics* 24.2 (2009), pp. 122–134. DOI: `10.1016/j.clinbiomech.2008.08.006` (cit. on p. 24).

[19] Michael R. Neuman and et al. «Biopotential electrodes». In: *Medical instrumentation: application and design* 4 (1998), pp. 189–240 (cit. on pp. 24, 25).

[20] Marianne Boyer, Laurent Bouyer, Jean-Sébastien Roy, and Alexandre Campeau-Lecours. «Reducing noise, artifacts and interference in single-channel emg signals: A review». In: *Sensors* 23.6 (2023), p. 2927. DOI: https://doi.org/10.3390/s23062927 (cit. on p. 26).

[21] Fabio Rossi, Paolo Motto Ros, Stefano Sapienza, Paolo Bonato, Emilio Bizzi, and Danilo Demarchi. «Wireless Low Energy System Architecture for Event-Driven Surface Electromyography». In: *Applications in Electronics Pervading Industry, Environment and Society* (2019), pp. 179–185. DOI: 10.1007/978-3-030-11973-7_21 (cit. on pp. 27, 40).

[22] Paolo Motto Ros, Alessandro Sanginario, Marco Crepaldi, and Danilo Demarchi. «Quality-Energy Trade-off and Bio-Inspired Electronic Systems». In: *2018 IEEE International Conference on the Science of Electrical Engineering in Israel (ICSEE).* 2018, pp. 1–5. DOI: 10.1109/ICSEE.2018.8646112 (cit. on p. 27).

[23] Marco Crepaldi, Marco Paleari, Alberto Bonanno, Alessandro Sanginario, Paolo Ariano, Duc Hoa Tran, and Danilo Demarchi. «A Quasi-Digital Radio System for Muscle Force Transmission Based on Event-Driven IR-UWB». In: *2012 IEEE Biomedical Circuits and Systems Conference (BioCAS).* 2012, pp. 116–119. DOI: 10.1109/BioCAS.2012.6418406 (cit. on pp. 27, 40).

[24] Fabio Rossi, Paolo Motto Ros, Ricardo Maximiliano Rosales, and Danilo Demarchi. «Embedded Bio-Mimetic System for Functional Electrical Stimulation Controlled by Event-Driven sEMG». In: *Sensors* 20.5 (2020). DOI: 10.3390/s20051535 (cit. on pp. 28, 40).

[25] Fabio Rossi, Andrea Mongardi, Paolo Motto Ros, Massimo Ruo Roch, Maurizio Martina, and Danilo Demarchi. «Tutorial: A Versatile Bio-Inspired System for Processing and Transmission of Muscular Information». In: *IEEE Sensors Journal* 21.20 (2021), pp. 22285–22303. DOI: 10.1109/JSEN.2021.3103608 (cit. on pp. 28, 39, 41).

[26] Matija Milosevic, Cesar Marquez-Chin, Kei Masani, Masayuki Hirata, Taishin Nomura, Milos R. Popovic, and Kimitaka Nakazawa. «Why brain-controlled neuroprosthetics matter: mechanisms underlying electrical stimulation of muscles and nerves in rehabilitation». In: *Biomedical engineering online* 19.81 (2020). DOI: 10.1186/s12938-020-00824-w (cit. on pp. 29, 32, 82).

[27] Cesar Marquez-Chin and Milos R. Popovic. «Functional electrical stimulation therapy for restoration of motor function after spinal cord injury and stroke: a review». In: *Biomedical engineering online* 19.34 (2020). DOI: 10.1186/s12938-020-00773-4 (cit. on pp. 29, 31).

[28] Shiyu Luo, Haonan Xu, Xiaogang Liu, and Angelo H. All. «A review of functional electrical stimulation treatment in spinal cord injury». In: *NeuroMolecular Medicine* 22 (2020), pp. 447–463. DOI: 10.1007/s12017-019-08589-9 (cit. on p. 29).

[29] Barbara M. Doucet, Amy Lam, and Lisa Griffin. «Neuromuscolar electrical stimulation for skeletal muscle function». In: *The Yale journal of biology and medicine* 85 (2012), pp. 201–215 (cit. on pp. 29, 32, 82).

[30] Alberto Botter, Gianmosè Oprandi, Fabio Lanfranco, Stefano Allasia, Nicola A. Maffiuletti, and Marco Alessandro Minetto. «Atlas of the muscle motor points for the lower limb: implications for electrical stimulation procedures and electrode positioning». In: *European journal of applied physiology* 111 (2011), pp. 2461–2471. DOI: 10.1007/s00421-011-2093-y (cit. on p. 29).

[31] Massimiliano Gobbo, Nicola A. Maffiuletti, Claudio Orizio, and Marco A. Minetto. «Muscle motor point identification is essential for optimizing neuromuscular electrical stimulation use». In: *Journal of NeuroEngineering and Rehabilitation* 11.17 (2014). DOI: 10.1186/1743-0003-11-17 (cit. on p. 30).

[32] Ard J. Westerveld, Alfred C. Schouten, Peter H. Veltink, and Herman van der Kooij. «Selectivity and resolution of surface electrical stimulation for grasp and release». In: *IEEE transactions on neural systems and rehabilitation engineering* 20.1 (2012), pp. 94–101. DOI: 10.1109/TNSRE.2011.2178749 (cit. on pp. 30, 60).

[33] J. Patrick Reilly. *Applied Bioelectricity: From Electrical Stimulation to Electropathology.* Springer, 1998, p. 563. ISBN: 978-1-4612-1664-3 (cit. on p. 30).

[34] Cheryl L. Lynch and Milos R. Popovic. «Functional Electrical Stimulation». In: *IEEE control systems magazine* 28.2 (2008), pp. 40–50. DOI: 10.1109/MCS.2007.914689 (cit. on p. 31).

[35] A.J. Bergquist, J.M. Clair, 0. Lagerquist, C.S. Mang, Y. Okuma, and D.F. Collins. «Neuromuscular electrical stimulation: implications of the electrically evoked sensory volley». In: *European journal of applied physiology* 111 (2011), pp. 2409–2426. DOI: 10.1007/s00421-011-2087-9 (cit. on p. 32).

[36] Stuart Binder-Macleod and Trisha Kesar. «Catchlike property of skeletal muscle: recent findings and clinical implications». In: *Muscle & Nerve* 31 (2005), pp. 681–693. DOI: 10.1002/mus.20290 (cit. on pp. 32, 33).

[37] IBM. *What is machine learning (ML)?* Accessed: March 10, 2025. URL: https://www.ibm.com/topics/machine-learning (cit. on p. 34).

[38] Hewlett Packard Enterprise. *Artificial Intelligence, Enough of the hype! What is it?* Accessed: March 10, 2025. URL: `https://community.hpe.com/t5/hpe-blog-uk-ireland-middle-east/artificial-intelligence-enough-of-the-hype-what-is-it/ba-p/7046672` (cit. on p. 34).

[39] Margherita Grandini, Enrico Bagli, and Giorgio Visani. «Metrics for multi-class classification: an overview». In: *arXiv preprint arXiv:2008.05756* (2020). DOI: `10.48550/arXiv.2008.05756` (cit. on p. 34).

[40] Jason Roell. *From Fiction to Reality: A Beginner's Guide to Artificial Neural Networks.* Accessed: March 10, 2025. URL: `https://towardsdatascience.com/from-fiction-to-reality-a-beginners-guide-to-artificial-neural-networks-d0411777571b` (cit. on p. 35).

[41] Sedat Parlak. *Foundations of Neural Networks.* Accessed: March 10, 2025. URL: `https://medium.com/@sedatparlak1953/foundation-of-neural-networks-a68925aa7e2` (cit. on pp. 35, 36).

[42] Bojan Milosevic, Simone Benatti, and Elisabetta Farella. «Design challenges for wearable EMG applications». In: *Design, Automation & Test in Europe Conference & Exhibition (DATE)*. 2017, pp. 1432–1437. DOI: `10.23919/DATE.2017.7927217` (cit. on p. 38).

[43] Cometa Systems. *Pico Emg.* Accessed: March 10, 2025. URL: `https://www.cometasystems.com/pico-emg/` (cit. on pp. 38, 39).

[44] Delsys. *Trigno Wireless Biofeedback System User's Guide.* Accessed: March 10, 2025. URL: `https://delsys.com/downloads/USERSGUIDE/trigno/wireless-biofeedback-system.pdf` (cit. on pp. 38, 39).

[45] Biometrics Ltd. *Surface EMG sensor.* Accessed: March 10, 2025. URL: `https://www.biometricsltd.com/surface-emg-sensor.htm` (cit. on pp. 38, 39).

[46] Paolo Motto Ros, Marco Paleari, Nicoló Celadon, Alessandro Sanginario, Alberto Bonanno, Marco Crepaldi, Paolo Ariano, and Danilo Demarchi. «A wireless address-event representation system for ATC-based multi-channel force wireless transmission». In: *5th IEEE International Workshop on Advances in Sensors and Interfaces IWASI*. 2013, pp. 51–56. DOI: `10.1109/IWASI.2013.6576061` (cit. on p. 40).

[47] Stefano Sapienza, Marco Crepaldi, Paolo Motto Ros, Alberto Bonanno, and Danilo Demarchi. «On Integration and Validation of a Very Low Complexity ATC UWB System for Muscle Force Transmission». In: *IEEE Transactions on Biomedical Circuits and Systems* 10.2 (2016), pp. 497–506. DOI: `10.1109/TBCAS.2015.2416918` (cit. on p. 40).

[48] David Alejandro Fernandez Guzman, Stefano Sapienza, Bianca Sereni, and Paolo Motto Ros. «Very low power event-based surface EMG acquisition system with off-the-shelf components». In: *2017 IEEE Biomedical Circuits and Systems Conference (BioCAS)*. 2017, pp. 1–4. DOI: 10.1109/BIOCAS.2017.8325152 (cit. on p. 40).

[49] Francesco Tenore, Ander Ramos, Amir Fahmy, Soumyadipta Acharya, Ralph Etienne-Cummings, and Nitish V. Thakor. «Towards the Control of Individual Fingers of a Prosthetic Hand Using Surface EMG Signals». In: *2007 29th Annual International Conference of the IEEE Engineering in Medicine and Biology Society*. 2007, pp. 6145–6148. DOI: 10.1109/IEMBS.2007.4353752 (cit. on p. 41).

[50] Md. R. Ahsan, Muhammad I. Ibrahimy, and Othman O. Khalifa. «Hand motion detection from EMG signals by using ANN based classifier for human computer interaction». In: *2011 Fourth International Conference on Modeling, Simulation and Applied Optimization*. 2011, pp. 1–6. DOI: 10.1109/ICMSAO.2011.5775536 (cit. on p. 41).

[51] Sami Briouza, Hassène Gritli, Nahla Khraief, Safya Belghith, and Dilbag Singh. «An Auto-ANN for EMG Classification for the Motion Recognition of the Human Hand». In: *2022 IEEE Information Technologies Smart Industrial Systems (ITSIS)*. 2022, pp. 1–6. DOI: 10.1109/ITSIS56166.2022.10118372 (cit. on p. 42).

[52] Kyung Hyun Lee, Ji Young Min, and Sangwon Byun. «Electromyogram-Based Classification of Hand and Finger Gestures Using Artificial Neural Networks». In: *Sensors* 22.1 (2022). DOI: 10.3390/s22010225 (cit. on p. 42).

[53] Arthur Prochazka, Michel Gauthier, Marguerite Wieler, and Zoltan Kenwell. «The Bionic Glove. An electrical stimulator garment that provides controlled grasp and hand opening in quadriplegia». In: *Archives of physical medicine and rehabilitation* 78 (1997). DOI: 10.1016/S0003-9993(97)90426-3 (cit. on pp. 42, 43).

[54] Maarten IJzerman, T.S. Stoffers, F.A.C.G. Groen, M.A.P. Klatte, G.J. Snoek, J.H.C. Vorsteveld, R.H. Nathan, and Hermie Hermens. «The NESS Handmaster orthosis: Restoration of hand function in C5 and stroke patients by means of electrical stimulation». In: *Journal of Rehabilitation Sciences* 9 (1996), pp. 86–89 (cit. on p. 43).

[55] G.J. Snoek, M.J. IJzerman, F.A. Groen, T.S. Stoffers, and G. Zilvold. «Use of the NESS Handmaster to restore handfunction in tetraplegia: clinical experiences in ten patients». In: *Spinal Cord* 38.4 (2000), pp. 244–249. DOI: 10.1038/sj.sc.3100980 (cit. on p. 43).

[56] Milos R Popovic, Dejan B Popovic, and Thierry Keller. «Neuroprostheses for grasping». In: *Neurological research* 24.5 (2002), pp. 443–452. DOI: 10.1179/016164102101200311 (cit. on p. 44).

[57] Yu Zhou, Yinfeng Fang, Kai Gui, Kairu Li, Dingguo Zhang, and Honghai Liu. «sEMG Bias-Driven Functional Electrical Stimulation System for Upper-Limb Stroke Rehabilitation». In: *IEEE Sensors Journal* 18.16 (2018), pp. 6812–6821. DOI: 10.1109/JSEN.2018.2848726 (cit. on p. 44).

[58] Enrique Mena Camilo, Jorge Airy Mercado Gutiérrez, Omar Piña Ramírez, Josefina Gutiérrez Martínez, Arturo Vera Hernández, and Lorenzo Leija Salas. «A functional electrical stimulation controller for contralateral hand movements based on EMG signals». In: *2020 17th International Conference on Electrical Engineering, Computing Science and Automatic Control (CCE)*. 2020, pp. 1–6. DOI: 10.1109/CCE50788.2020.9299199 (cit. on p. 44).

[59] Yuyang Chen, Chenyun Dai, and Wei Chen. «A Real-time EMG-controlled Functional Electrical Stimulation System for Mirror Therapy». In: *2019 IEEE Biomedical Circuits and Systems Conference (BioCAS)*. 2019, pp. 1–4. DOI: 10.1109/BIOCAS.2019.8919069 (cit. on p. 44).

[60] Xueliang Bao, Yuxuan Zhou, Yunlong Wang, Jianjun Zhang, Xiaoying Lü, and Zhigong Wang. «Electrode placement on the forearm for selective stimulation of finger extension/flexion». In: *PLOS ONE* 13 (2018). DOI: 10.1371/journal.pone.0190936 (cit. on pp. 44, 45).

[61] Haider Usman, Yu Zhou, Benjamin Metcalfe, and Dingguo Zhang. «A Functional Electrical Stimulation System of High-Density Electrodes With Auto-Calibration for Optimal Selectivity». In: *IEEE Sensors Journal* 20.15 (2020), pp. 8833–8843. DOI: 10.1109/JSEN.2020.2983004 (cit. on pp. 45–47).

[62] Akifumi Takahashi, Jas Brooks, Hiroyuki Kajimoto, and Pedro Lopes. «Increasing Electrical Muscle Stimulation's Dexterity by means of Back of the Hand Actuation». In: *Proceedings of the 2021 CHI Conference on Human Factors in Computing Systems*. 2021, pp. 867–870. DOI: 10.1145/3411764.3445761 (cit. on pp. 47, 48, 82).

[63] Narrendar RaviChandran, Kean C. Aw, and Andrew McDaid. «Characterizing the Motor Points of Forearm Muscles for Dexterous Neuroprostheses». In: *IEEE transactions on bio-medical engineering* 67.1 (2020), pp. 50–59. DOI: 10.1109/TBME.2019.2907926 (cit. on pp. 48, 49).

[64] HASOMED GmbH. *Operation Manual RehaStim 2, RehaMove 2*. 2016. URL: https://static1.squarespace.com/static/5f16af2c5732983b810510ef/t/625445ebc1f33f681fa9ec3e/1649690115682/RehaMove2_User+Manual_2.4._ENG_CM_20170201.pdf (cit. on pp. 50, 51).

107

[65] Bjoern Kuberski. *ScienceMode2. Description and protocol.* 2012. URL: `https://hasomed.de/wp-content/uploads/hasomed-fileadmin/RehaMove/ScienceMode/Science_Mode2_Description_Protocol_20121212.pdf` (cit. on pp. 50, 51, 53).

[66] Anatomy Info. *Hand muscles : Attachment, Nerve Supply Action.* Accessed: March 10, 2025. URL: `https://anatomyinfo.com/hand-muscles/` (cit. on p. 79).

[67] Ministero della Salute. *Calcolo Indice massa corporea - IMC (BMI - Body mass index).* Accessed: March 10, 2025. URL: `https://www.salute.gov.it/portale/nutrizione/dettaglioIMCNutrizione.jsp?area=nutrizione&id=5479&lingua=italiano&menu=vuoto` (cit. on p. 86).

[68] Charlie Beestone. *Bioelectrical Impedance Analysis (BIA).* Accessed: March 10, 2025. URL: `https://www.scienceforsport.com/bioelectrical-impedance-analysis-bia/` (cit. on p. 86).